UNIVERSITE des SCIENCES et TECHONOLOGIES de LILLE

THESE de DOCTORAT EN-COTUTELLE

spécialité: LASERS, MOLECULES, RAYONNEMENT ATMOSPHERIQUE

présentée par Gotard BURDZINSKI

ETUDE DES PROPRIETES PHOTOPHYSIQUES DE THIOCETONES ET LEURS DERIVES EN SOLUTION PAR SPECTROSCOPIES ELECTRONIQUE ET VIBRATIONELLE RESOLUES DANS LE TEMPS.

Soutenue le 25 septembre 2003

Devant le jury composé de:

Dr. R. Naskrecki, Uniwersytet im. A. Mickiewicza, Rapporteur

Dr. J.-C. Mialocq, C.E.A. Saclay, Rapporteur

Dr. G. Buntinx, Université des Sciences et Techonologies de Lille, Co-Directeur de thèse

Prof. A. Maciejewski, Uniwersytet im. A. Mickiewicza, Co-Directeur de thèse

Abstract.

The photophysical properties of a model thioketone molecule, benzopyranthione (BPT), were investigated by transient absorption and emission spectroscopy in various solvents such as hydrocarbons, acetonitrile and water. The properties and reactivity of the long-lived S_2 state were particularly examined. The S_2 state vibrational relaxation and orientational anisotropy decay were studied in hydrocarbon solvents. The latter process was observed for the first time for a molecule in the S_2 state. The nature and mechanism of an intermolecular S_2 state quenching effect occurring in all solvents except in inert perfluorohydrocarbons were also studied. We observed: (i) a shortening by about one order of magnitude of the S_2 state lifetime of BPT in these solvents relative to that in perfluorohydrocarbons, (ii) a notable kinetic isotope effect on the quenching process upon deuteration of the solvent molecule (2.2 to 3.2), and (iii) in hydrocarbons a linear dependence of the S_2 state quenching rate constant on the mean energy of the solvent C-H bonds. In hydrocarbons, the quenching mechanism was described in terms of an aborted hydrogen abstraction or by an ultrafast spin-allowed process of geminate radical cage recombination. In acetonitrile we suggested that two different aborted processes are involved: the formation of a S_2 state exciplex and hydrogen abstraction. The latter process was proposed in order to rationalise the observation of the isotope effect. In water, an aborted formation of the hydrogen-bonded complex was tentatively proposed in order to explain the very high (8.8×10^{11} s^{-1}) quenching rate constant. Structural investigations were also performed for an isomer of BPT, thiocoumarin (TC), in the ground and triplet state by using Raman scattering spectroscopy and *ab initio* calculations. Both states were found to have a planar structure. On going from S_0 to T_1, the benzo moiety is only slightly modified and keeps its aromatic character. Stronger distortions arise in the pyranthione moiety.

Acknowledgements.

Initiated in 1995, collaborations between Dr. Ryszard Naskręcki and Dr. Guy Buntinx, provided the opportunity to perform this thesis between the Uniwersytet im. Adama Mickiewicza (UAM), Poznań, and the Université des Sciences et Technologies de Lille (USTL). I would like to thank them for accepting me into their research laboratories.

It is a great honour to have been directed during this work by Dr. Guy Buntinx (USTL) and Professor Andrzej Maciejewski (UAM). Without their wisdom, this work would not have been completed. I have also had the pleasure to collaborate with Dr. Olivier Poizat, Dr. Christine Lapouge (USTL), Dr. Jerzy Karolczak, Dr. Jacek Kubicki (UAM), Professor Max Glasbeek and Dr. Hong Zhang from the University of Amsterdam (UA). I would like to thank them for the opportunity to undertake this fascinating research project, which involved the use of several time-resolved spectroscopy techniques. I have also appreciated the generous access to the vast experience and knowledge possessed by the above mentioned scientists.

My sincere appreciation is extended to Dr. Daniel Bougeard, director of Laboratoire de Spectrochimie Infrarouge et Raman (USTL) who accepted this research project.

I thank the French government for financial support for this co-directed thesis between France and Poland. I equally acknowledge the European Science Foundation for financial support to carry out research in The Netherlands and also the KBN (Polish State Committee for Scientific Research) for financial support.

I thank Dr. Zdzisław Stryła (UAM) who introduced me to laser spectroscopy methods seven years ago. I would also like to thank many colleagues and friends for their support and encouragement during this work, Krzysztof Dobek, Darek Komar, Adam Łukaszewisz, Marcin Ziółek (UAM), Sarah Foley, Christophe Lemefeux, Laurent Boilet (USTL) and Paul Toele (UA).

I thank Dr. Ryszard Naskręcki (UAM), Dr. Jean-Claude Mialocq (CEA/Saclay), Prof. Max Glasbeek (UA) and Dr. Włodzimierz Jarzęba from the Uniwersytet Jagielloński, Kraków, who have accepted this work for review.

Finally, I thank my family, especially Aleksandra Lubaś for the support and encouragement, I express my deepest love and appreciation.

Table of Contents.

INTRODUCTION.

Scientific discussions concerning thioketones first began at the beginning of the XXth century. More recently, they have attracted interest due to their potential applications in the fields of biology, optical switching and non-linear optics [1 - 5]. Until recently, thioketone research has been mainly studied from a fundamental point of view because they show very different chemical and physical behaviour compared to their widely studied analogues ketones, which play a crucial role in photochemistry. The weaker C=S bond of thiocarbonyl compared to the C=O bond of carbonyls (ca. 430 kJ/mol versus ca. 635 kJ/mol) as well as the difference in the energy of the electronic states can explain the dramatic differences in the photochemistry and photophysics of the two classes of compounds. In particular, the relatively large energy gap between the two lowest excited singlet states, S_1 and S_2, of thioketones leads to a strong decrease of the rate of radiationless decay of the S_2 state. In consequence, the S_2 state of thioketones can be relatively long-lived and therefore fluorescent in violation to Kasha's rule [6]. However, in the gas phase or in inert solvents (perfluorohydrocarbons), the main deactivation pathway of the S_2 state remains radiationless internal conversion to the S_1 state, the rate of which is controlled in part by the magnitude of the $\langle S_2 | S_1 \rangle$ Franck-Condon factor and therefore it is inversely proportional to the exponential of the S_2-S_1 energy gap. In addition to the S_2 state fluorescence, aromatic thioketones generally exhibit phosphorescence from the first excited T_1 state and thermally activated delayed fluorescence from the S_1 state. Some reviews provide a comprehensive picture of the photophysics and photochemistry of thioketones in solution [6, 7]. The main photophysical behaviour of typical rigid aromatic thioketones in inert solvents at room temperature can be summarised as follows:

- The S_2 state decays mainly via radiationless relaxation to the S_1 state. The radiative decay to the ground state (fluorescence) is a minor process. The S_2 state lifetime falls usually in the 80 - 900 ps time range in perfluorohydrocarbon solvents.
- The S_1 state is very short-lived (less than 1 ps) and decays promptly to the T_1 state with near unity efficiency.
- The T_1 state, of microsecond duration, decays by a combination of phosphorescence, intersystem crossing to the ground state and intersystem crossing to the S_1 state. The

proportions of the last two processes depend on the temperature and on the S_1-T_1 and T_1-S_0 energy spacings.

The long lifetime as well as the high energy of the S_2 state of thioketones characterised by the low energy of the π-bond in the thiocarbonyl group enables them to chemically react with most solvents except the chemically inert perfluorohydrocarbons. In all other solvents, including saturated hydrocarbons, a significant shortening of the S_2 state lifetime and a lowering of the S_2 state fluorescence quantum yield are observed due to very efficient intermolecular quenching of the S_2 state of thioketones by the solvents [6, 8]. The S_2 state lifetime is generally reduced by one order of magnitude or even more, suggesting that the quenching by the solvent is the main deactivation pathway of thioketones S_2 state. The efficiency of this quenching process is usually greater than 80 %. Unfortunately, very little is known about the nature and properties of the species formed upon the efficient quenching process of the thioketone S_2 state because most of the studies have been performed using fluorescence spectroscopy, which provides only information about the fluorescent S_2 state. It is therefore necessary to use complementary techniques in order to characterise the non-fluorescent intermediates. Recently, femtosecond transient absorption spectroscopy has been used to study the S_2 state quenching process of xanthione (XT) by acetonitrile [9]. A S_2 state exciplex formation has been proposed to explain the quenching process observed in this solvent.

A detailed understanding of the photophysics of thioketones requires us to not only have a good description of the nature and the dynamics of the various excited states and chemical intermediates involved in the process under study, but also to have a good understanding of the structural and electronic properties of these intermediates. Unfortunately, there are no reports in the literature of structural investigations in the second excited singlet S_2 state or in the first excited triplet T_1 state. Such information can be obtained in solution from the analysis of the vibrational spectra of the transient species generally supported by *ab initio* calculations.

This PhD thesis constitutes part of some fundamental studies of the photophysics and photochemistry of thioketones conducted at the Uniwersytet im. Adama Mickiewicza in Poznań in the group of Professor A. Maciejewski. The topic of this thesis concerns the study of the photophysical properties of thioketones in solution using time-resolved electronic and vibrational spectroscopy. We have chosen a model thioketone molecule, benzopyranthione (BPT), which has been extensively studied by steady-state spectroscopy, but for which a few time-resolved reports have been published. We decided to characterise the mechanism and the

dynamics of intra and intermolecular relaxation of the S_2 state of BPT in three solvents with different properties: hydrocarbons (non polar), acetonitrile (polar aprotic) and water (polar and protic) by using complementary time-resolved electronic spectroscopic techniques. In addition, the structural characterisation of the excited states of thioketones using time-resolved resonance Raman spectroscopy was performed using an isomer of BPT, thiocoumarin (TC), which exhibits improved spectral properties for this purpose.

Chapter 1 gives a review of the current knowledge on the photophysics of thioketones. In particular, one can find in this chapter, the information required for the analysis of the time-resolved results obtained for BPT in this PhD work. Chapter 2 presents three techniques (transient absorption and emission spectroscopy and time-resolved resonance Raman spectroscopy) and five different experimental set-ups used during this thesis. The nanosecond transient absorption set-up, which has been constructed, as part of this thesis, is described in more detail. Chapter 3 concerns the study of the quenching process of the S_2 state of BPT by hydrocarbons, acetonitrile and water. Chapter 4 presents the analysis of the vibrational relaxation and the orientational anisotropy decay of BPT S_2 state in hydrocarbon solvents. Chapter 5 concerns the time-resolved resonance Raman as well as *ab initio* calculations analysis of the structure of the T_1 state of thiocoumarin. Finally, a summary of the main results obtained during this thesis and some perspectives about this topic are presented in the conclusion.

References:

1. M. Borges, A. Romão, O. Matos, C. Marzano, S. Caffieri, R. S. Becker, A. L. Maçanita, *Photochem. Photobiol.*, 75 (2002) 97.
2. R. F. Bradford, G. B. Schuster, *J. Org. Chem.*, 68 (2003) 1075.
3. U. Eckart, M. P. Fülscher, and L. Serrano-Andrés, A. J. Sadlej, *J. Chem. Phys.*, 113 (2000) 6235.
4. L. Serrano-Andrés, R. Pou-Amérigo, M. P. Fülscher, A. C. Borin, *J. Chem. Phys.*, 117 (2002) 1649.
5. P. Munshi, T. N. G. Row, *Acta Cryst.*, B58 (2002) 1011.
6. A. Maciejewski, R. P. Steer, *Chem. Rev.*, 93 (1993) 67.
7. R. P. Steer, V. Ramamurthy, *Acc. Chem. Res.*, 21 (1988) 380.
8. J. Kubicki, A. Maciejewski, M. Milewski, T. Wrozowa, R. P. Steer, *Phys. Chem. Chem. Phys.*, 4 (2002) 173.
9. M. Lorenc, A. Maciejewski, M. Ziolek, R. Naskrecki, J. Karolczak, J. Kubicki, B. Ciesielska, *Chem. Phys. Lett.*, 346 (2001) 224.

CHAPTER 1.

Photophysical properties of thioketones in solution.

1.1. Introduction.

The photophysical and photochemical properties of ketones have been extensively investigated due to the key role they play in photochemistry. However, relatively little is known about their analogues thioketones, which contains the thiocarbonyl group >C=S instead of the carbonyl group >C=O. The C=S π bond is formed by the overlap of the 2 p carbon orbital and the 3 p sulphur orbital (versus 2 p orbital for oxygen in carbonyls). Thus, the lowest energy electronic transitions of thioketones are shifted in the visible range to significantly lower energies than those of the ketones. Since benzopyranthione (BPT) is considered as a model compound to study the photophysics of thioketones, examples illustrating the thioketones properties will be given mainly for this molecule. Fig.1.1 presents the schematic representation of aromatic thioketones, BPT, its butyl derivative ($BPTC_4$) and the thiocoumarin (TC) studied in this thesis. Fig.1.1 also shows the structures of pyranthione (PT), xanthione (XT) and thioxanthione (TXT), which are cited in this thesis.

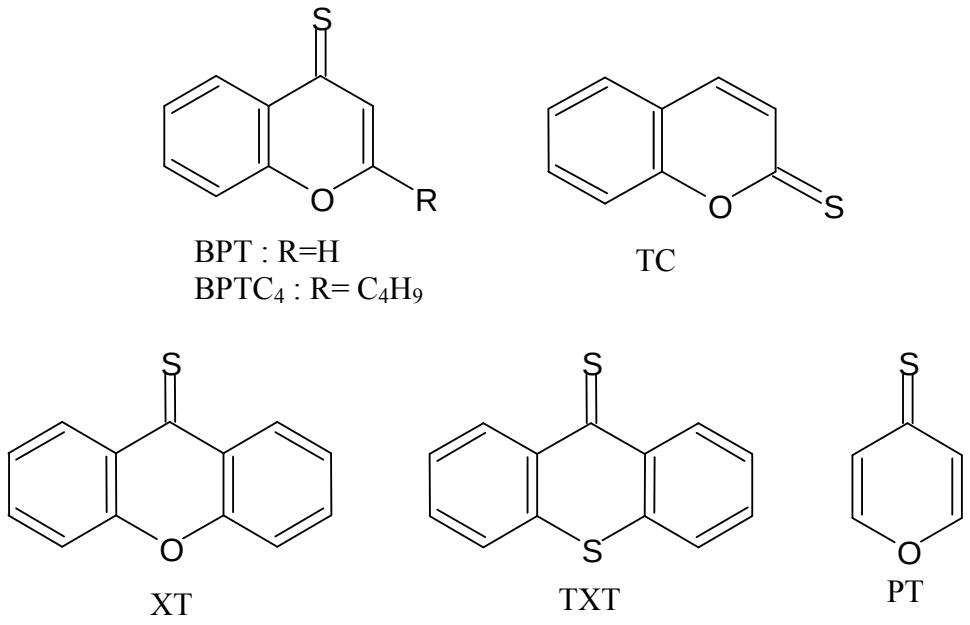

Figure 1.1. Schematic representation of various thioketones: BPT, 4H-1-benzopyrane-4-thione; $BPTC_4$, 2-butyl-4H-1-benzopyrane-4-thione; TC, thiocoumarin; XT, xanthione; TXT, thioxanthione; PT, 4*H*-pyrane-4-thione.

1.2. General photophysical properties.

Many spectral, photophysical and photochemical properties of thioketones have been reviewed by Maciejewski and Steer [1]. The ground state absorption spectrum of thioketones is generally well resolved and clearly shows the electronic transitions from the ground state to the singlet excited states and to the lowest excited triplet T_1 state. A weak absorption band corresponding to the orbitally forbidden transition to the $S_1(n,\pi^*)$ state is usually observed in the red (absorption extinction coefficient ε_{max} of 10 - 30 $M^{-1}cm^{-1}$). The band corresponding to the strongly allowed transition to the $S_2(\pi,\pi^*)$ state localised mainly on the >C=S chromophore of typical ε_{max} values ranging from 9000 $M^{-1}cm^{-1}$ to 17000 $M^{-1}cm^{-1}$, appears in the blue or UV. This transition induces a decrease of the electric dipole moment of thioketones in the S_2 state compared to the S_0 state, as evidenced for pyranthione and xanthione by electro-optic method [2]. As an example, the absorption spectrum of BPT in 3-methylpentane is presented in Fig.1.2. This spectrum is representative of what is generally observed for aromatic thioketones in solution.

Note that in Fig.1.2 the $S_0 \rightarrow T_1$ absorption transition shows a well resolved 0-0 band peaking at 630 nm, which is well separated from the 0-0 band of the $S_0 \rightarrow S_1$ transition peaking at 590 nm. The $S_0 \rightarrow S_2$ absorption band in Fig.1.2 (about 370 nm) is spectrally well resolved from the $S_0 \rightarrow S_n$ (n≥3) ones.

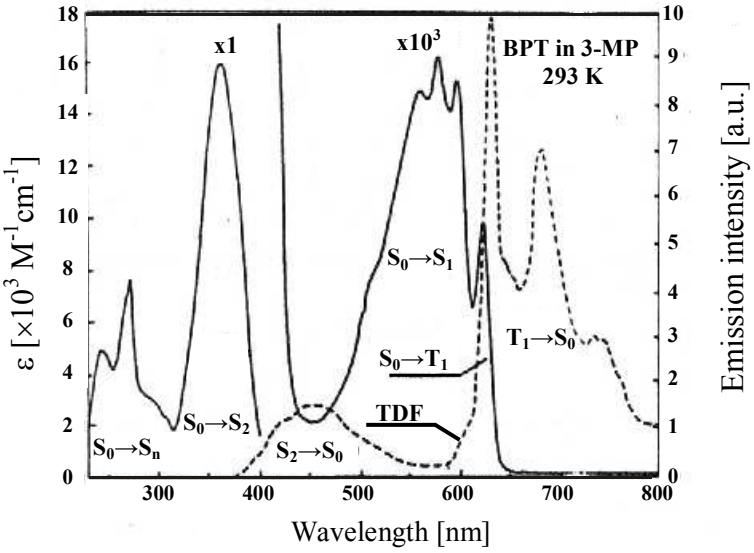

Figure 1.2. Steady-state absorption of BPT in 3-methylpentane: $S_0 \rightarrow T_1$, $S_0 \rightarrow S_1$, $S_0 \rightarrow S_2$, $S_0 \rightarrow S_n$ (n≥3), and emission spectra: fluorescence $S_2 \rightarrow S_0$ and phosphorescence $T_1 \rightarrow S_0$ [1]. TDF refers to thermally activated delayed $S_1 \rightarrow S_0$ fluorescence.

As mentioned above, the S_1 state of thioketones has a n,π* character, however, the nature of lowest excited triplet state T_1 usually depends on the solvent polarity. An inversion of the $^3(n,\pi^*)$ and $^3(\pi,\pi^*)$ states on going from non-polar to polar solvents has been evidenced by Maciejewski and co-authors for BPT, PT and XT by [3]. The difference in the lowest excited triplet state electronic configuration of thioketones in solvents of various polarities usually manifests itself in the shape of the phosphorescence spectrum. Thioketones usually exhibit phosphorescence even at room temperature due to their high phosphorescence rate constant of 10^4 s^{-1}, rarely met among other molecules [4]. A remarkable example of thioketone showing a high phosphorescence quantum yield Φ_P is pyranthione (PT in Fig.1.1). Its Φ_P of 0.47 measured in perfluorohydrocarbons by direct $S_0 \rightarrow T_1$ excitation has been reported by Maciejewski and co-authors [5]. Another typical characteristic of thioketones is the $S_2 \rightarrow S_0$ fluorescence in violation of Kasha's rule. The fluorescence of xanthione $S_2 \rightarrow S_0$ was first reported in 1975 [6]. The electronic energy gap between the second excited S_2 state and the lowest excited S_1 states is large enough to inhibit the radiationless process $S_2 \sim> S_1$, due to a weak S_2-S_1 vibrational wave functions overlap. Thus, the lifetime of thioketones in the S_2 state is long enough to detect the $S_2 \rightarrow S_0$ fluorescence (typical radiative rate constant of 10^8 s^{-1}) [1]. The fluorescence spectrum of BPT shows a maximum at around 460 nm in Fig.1.2. Thioketones generally do not exhibit fluorescence from the first excited $S_1(n,\pi^*)$ state, due to the low fluorescence rate constant (10^5 s^{-1}) and the high $S_1 \sim> T_1$ intersystem crossing rate constant k_{ISC} (10^{12} s^{-1}) as a result of an increase of the spin-orbit coupling compared to ketones [7]. Only in thioxanthione has the short-lived S_1 state of thioketones in solution been directly observed by Tittelbach-Helmrich and Steer ($\tau_{S1} \approx 0.5$ ps in acetonitrile, acetone and 1-octanol) [7]. The quantum yield of the $S_1 \sim> T_1$ intersystem crossing of thioketones is close to unity. Maciejewski and co-authors have shown for PT, BPT, XT and TXT, that the quantum yield $\Phi_p(S_1)$ of phosphorescence obtained from steady-state excitation to the S_1 state is only slightly smaller than that of $\Phi_p(T_1)$ obtained by the direct excitation to the T_1 state [8]. For instance, $\Phi_{ISC} = 1$ for BPT in perfluorohydrocarbons [9]. For many thioketones, the intersystem crossing process $S_1 <\sim T_1$ leads to a thermally activated fluorescence $S_1 \rightarrow S_0$, due to the relatively small electronic energy gap between the S_1 and the T_1 states [10]. For example, the value of this energy gap $\Delta E(S_1\text{-}T_1)$ is about 700 cm^{-1} for BPT, PT and XT in perfluorohydrocarbons [10]. Thus, at room temperature the population of molecules in the triplet state possessing an excess of vibrational energy can be significant. For

example, the thermally activated delayed fluorescence of BPT can be distinguished in Fig.1.2 as a shoulder on the blue edge of the $T_1 \rightarrow S_0$ phosphorescence spectrum (marked as TDF).

Time-resolved spectroscopic studies (transient absorption and emission measurements) show that the decay rates of thioketones in the S_2 state and especially in the T_1 state are strongly influenced by the self-quenching process resulting from the collision of an excited thioketone molecule with another one in the ground state [1, 11]. The self-quenching process is diffusion controlled with a rate constant of $k_{sq} \sim 10^{10}$ $M^{-1}s^{-1}$. For many thioketones even at concentrations as low as 10^{-5} M, the self-quenching process affects the T_1 state lifetime τ. It is possible to determine the triplet state lifetime τ_{T1}^{0} in the absence of self-quenching by extrapolating the measured lifetime τ to infinite thioketone dilution using a Stern-Volmer plot:

$$\frac{1}{\tau} = \frac{1}{\tau_{T1}^{0}} + k_{sq}[thioketone]. \qquad (1.1)$$

An example of Stern–Volmer plot showing the lifetime of the T_1 state of BPT at room temperature in deoxygenated perfluoro-1,3-dimethylcyclohexane versus concentration is presented in Fig.1.3. The best fitted function gives a self-quenching rate constant of $k_{sq} = 6.9 \times 10^{9}$ $M^{-1}s^{-1}$ and a τ_{T1}^{0} value of 16 μs.

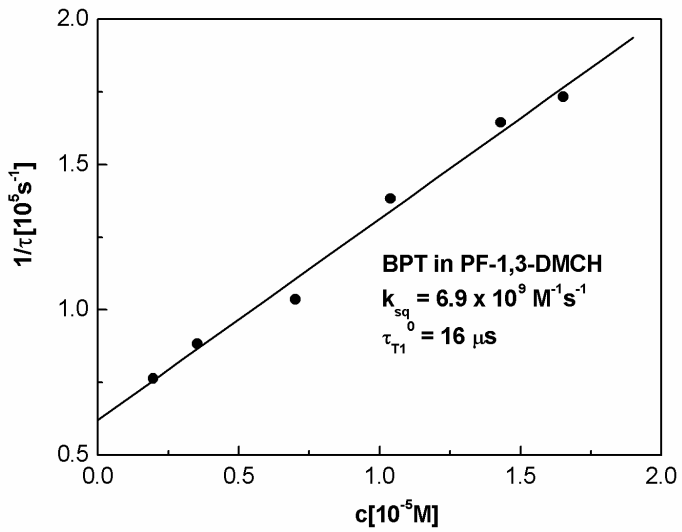

Figure 1.3. Stern–Volmer plot showing the lifetime of the T_1 state of BPT in deoxygenated perfluoro-1,3-dimethylcyclohexane versus the ground state BPT concentration at room temperature (from reference [12]). The excitation source was a Nd:YAG laser, 1 mJ, 10 ns, 355 nm. The phosphorescence was monitored at 620 nm.

Thioketones in the excited states can also be quenched by oxygen. Both T_1 and S_2 states are quenched with a diffusion controlled rate (for BPT S_2 state in perfluoro-n-hexane the rate constant is $k_{O2} = 2.3\times10^{10}$ $M^{-1}s^{-1}$ [12]). The triplet state lifetime is strongly affected by the presence of oxygen. The S_2 state lifetime is only slightly shortened by the presence of oxygen because the sum of the other deactivation rates is much higher [12]. The quenching process by oxygen can be cancelled by performing the experiments in deoxygenated solutions.

High concentration of thioketones in the triplet state can induce delayed fluorescence from the S_2 state due to triplet–triplet annihilation ($T_1+T_1 \sim> S_2+S_0$). This phenomenon has been seen for BPT in perfluoro-1,3-dimethylcyclohexane by Nickel and co-authors [13].

1.3. Thioketones intramolecular S_2 state deactivation.

Since thioketones in the S_2 state are highly reactive, the study of the intramolecular relaxation processes for the S_2 state requires the use of inert solvents. For this purpose, the best solvents are perfluorohydrocarbons (PFs), due to their very weak interactions with the solute molecules [14]. The high dissociation energy of the C-F bonds (129 kcal/mol compared to 90 - 100 kcal/mol for C-H bond in hydrocarbons) and of the C-C bonds (96.5 kcal/mol) explains the inert nature of PFs. PFs are also characterised by a high ionisation potential (13 - 16.5 eV), a low refraction index (n ~ 1.23 - 1.3) and a low polarisability. The photophysical properties of solutes in PFs are comparable with those obtained in the gas phase. However, PFs play an additional role of that of efficient vibrational thermalisers, which act as an inert heat bath, and which can accept an excess of energy from hot excited solutes. PFs do not emit or absorb any light down to 200 nm. For all these reasons PFs solvents are well adapted for an investigation on the intramolecular relaxation processes of the thioketones S_2 state.

Steer and co-workers have shown that, for thioketones, the radiationless processes play the most important role in the S_2 state deactivation ($S_2 \sim> S_1$ transition) and that the radiationless rate constant obeys the Energy Gap Law [4, 12, 15]. According to the well-established principles of radiationless transition theory, Eq.1.2 represents the expression of the rate constant of the radiationless transition k_{nr} between two electronic states [16, 17]:

$$k_{nr} = \frac{2\pi}{h} B^2 \rho F, \qquad (1.2)$$

where B is the electronic coupling matrix element between the two states, ρ is the effective

density of the vibrational states in the electronic S_1 state equienergetic with the vibrationally relaxed S_2 state, and F is the Franck-Condon factor. A linear relation between F and $exp(-\Delta E(S_2\text{-}S_1))$ has been reported for thioketones, where $\Delta E(S_2\text{-}S_1)$ is the energy difference between the relaxed vibrational states of the two involved electronic states [4, 12, 15]. The proportionality between lnk_{nr} and ΔE is known as the Energy Gap Law. This law has been verified not only for thioketones, but also for azulene and its derivatives (S_2~>S_1 transition) and for aromatic hydrocarbons (T_1~>S_0 transition), under the assumption, that B and ρ do not differ substantially within a group of structurally similar compounds [18 - 20]. The results obtained for rigid thioketones presented in Fig.1.4 are consistent with the Energy Gap Law [12].

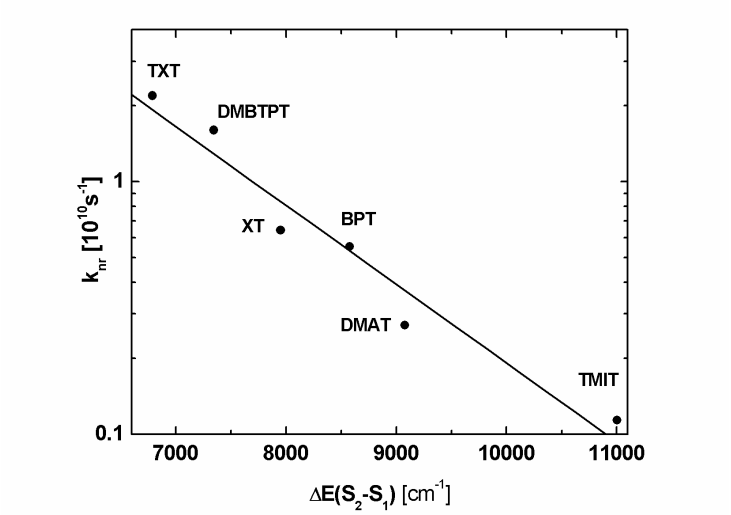

Figure 1.4. Semilogarithmic plots of $log(k_{nr})$ versus the energy gap, $\Delta E(S_2–S_1)$ for aromatic thioketones in PF-1,3-DMCH at room temperature [12]. The solid line shows the best fitted function according to the Energy Gap Law. DMBTPT, 2,6-dimethyl-4H-1-benzopyran-4-thione; DMAT, 9,9-dimethylanthranthione; TMIT, 2,2,3,3-tetramethylindanethione.

The energy gap values plotted in Fig.1.4 have been determined on the basis of steady-state absorption and emission measurements [12]. The k_{nr} values have been calculated using the following formula:

$$\tau_{S2} = \frac{1}{k_{nr} + k_r} \qquad (1.3)$$

where: τ_{S2} is the lifetime of the S_2 state (obtained from time-resolved emission studies), k_r is the radiative rate constant equal to the ratio of the emission Φ_{fl} quantum yield (obtained from steady-state measurements) to the lifetime τ_{S2}.

In thioketones, the radiationless transition $S_2 \sim > S_0$, can usually be neglected because of the large energy gap $\Delta(S_2–S_0)$ and the small $<S_2 | S_0>$ Franck-Condon factors [15].

The main deactivation pathway of thioketones S_2 state in perfluorohydrocarbons is the $S_2 \sim > S_1$ internal conversion [9, 12].

1.4. Thioketones intermolecular S_2 state quenching.

The deactivation processes of the upper excited singlet states (S_n, $n \geq 2$) of most of the molecules are generally intramolecular irrespective of the solvent used. However, the thioketones S_2 state is known to be extremely reactive because of the existence of efficient intermolecular quenching by all solvents except perfluorohydrocarbons. For example, Table 1.1 presents the photophysical properties of the S_2 state of BPT in different solvents: perfluoro-tetradecahydrophenanthrene (PFTDHP), n-hexane, acetonitrile, carbon tetrachloride, methanol and water. Table 1.1 shows a long lifetime τ_{S2} (177 ps) and a high fluorescence quantum yield Φ_{fl} (0.025) for BPT in PFTDHP compared to other solvents.

Table 1.1. Photophysical properties of the S_2 state of BPT in different solvents. The lifetimes were determined by femtosecond fluorescence up-conversion spectroscopy [a] (author results) and TCSPC method [b,c].

Solvent	PFTDHP[f]	n-Hexane	Acetonitrile	CCl_4	Methanol	Water
τ_{S2} [ps]	177.0±2.0[b]	20.2±0.5[a,b]	14.9±0.5[a]	30±2[a]	7±1[a,c]	1.0±0.1[a]
Φ_{fl} [$\times 10^{-3}$][d]	25.0	2.2	1.7	3.4	0.62	0.09
k_r [$\times 10^8$ s^{-1}]	1.5	1.1	1.1	1.2	0.9	0.9
$\Delta E(S_2–S_1)$ [cm^{-1}]	8590	8330	7150	7620[d]	6370	4220[d]
k_{nr} [$\times 10^{10}$ s^{-1}]	0.54	0.64	1.5	1.1	2.6	12.2
k_q [$\times 10^{10}$ s^{-1}]	<0.001	4.5	5.2	2.2	11.7	88
Quenching[e] [%]	-	87	78	68	82	88

[b] Ref. [12], [c] Ref. [21], [d] Ref. [22], [e] $quenching = 100 \times k_q/(k_r+k_{nr}+k_q)$,

[f] PFTDHP - perfluoro-tetradecahydrophenanthrene.

The change to non-perfluorohydrocarbon solvents results in the shortening of lifetime τ_{S2} and in the decreasing of the quantum yield of fluorescence Φ_{fl} due to a quenching process. In general, the lifetime τ_{S2} of thioketones in the S_2 state (that can be determined by time-resolved spectroscopy), can be expressed by:

$$\tau_{S2} = \frac{1}{k_{nr} + k_r + k_q}, \qquad (1.4)$$

where: k_q is the quenching rate constant of the S_2 state by the solvent molecules,

k_r is the radiative rate constant, that can be calculated from $k_r = \Phi_{fl}/\tau_{S2}$, if the lifetime τ_{S2} and the quantum yield Φ_{fl} of fluorescence are determined,

k_{nr} is the radiationless rate constant, that can be estimated from the linear relation presented in Fig.1.4, when the value of the thioketone energy gap $\Delta E(S_2–S_1)$ is known.

Eq.1.4 allows us to determine the quenching rate constant k_q of thioketones S_2 states by the solvent molecules.

Table 1.1 also presents the efficiency $100 \times k_q/(k_r+k_{nr}+k_q)$ [%] of intermolecular quenching of BPT S_2 state confirming the exceptionally high reactivity of thioketones S_2 state in all solvents expect perfluorohydrocarbons. Even hydrocarbon solvents, considered as non-polar and unreactive, and acetonitrile that is usually considered as chemically inert, efficiently quench the thioketones S_2 state. Moreover, the quantum yield Φ_D of the net photochemical consumption of the thioketone is less than 0.001 (for BPT). A photochemical quenching process leading to a net consumption of thioketone can thus be disregarded. That means that the quenching process finally leads to the ground state S_0 of thioketone.

Within this thesis, BPT is chosen as a model compound for studying the intermolecular quenching process of thioketones in the S_2 state, and thus a better characterisation of BPT in the excited states is given in the next paragraph.

1.5. Characterisation of the excited states of benzopyranthione.

The changes of the electron density distribution due to the photoexcitation of thioketones can be an important aspect to consider in evaluating the solute-solvent interactions. For example hydrogen bond formation between thioketone in the ground or excited state and hydrogen bonding solvents (water, alcohol) is important. It has been mentioned that the nature of the triplet T_1 state of BPT depends on the solvent polarity: in

non-polar solvents the lowest excited triplet state T_1 has a n,π* character while in polar solvent a π,π* character. This is due to an inversion between the two lowest triplet states [3].

The electronic nature of BPT in the excited states: $S_1(n,\pi^*)$, $S_2(\pi,\pi^*)$, $T_1(\pi,\pi^*)$, $T_2(n,\pi^*)$ has also been confirmed by INDO/S CI-1 calculations (performed by J. Koput). The calculated electronic $S_0 \rightarrow S_n$ transitions are compared to the BPT absorption spectrum measured in n-hexane (293 K) in Fig.1.5. Note that the absorption spectrum of BPT in n-hexane is similar to those obtained in the gas phase or in perfluorohydrocarbons. Theoretical calculations give only a tentative value. However, a good agreement between experimental results and theoretical calculations can be seen in Fig.1.5. The strong absorption band with a maximum at 365 nm is clearly related to the strongly allowed $S_0 \rightarrow S_2$ $\pi \rightarrow \pi^*$ transition (oscillator strength of 0.52). A wide energy range can be used to excite BPT in the S_2 state, because transitions to other singlet states ($S_0 \rightarrow S_n$ for $n \geq 3$) are much higher in energy. The $S_0 \rightarrow S_2$ transition corresponds mainly to an electron excitation from the orbital $\pi_{C\text{-}S}$ localised primarily on the sulphur atom to the orbital $\pi^*_{C\text{-}S}$ localised on the carbon atom of the thiocarbonyl group. Table 1.2 gives the calculated electron density distribution for different atoms and for the benzo moiety of BPT in the ground state S_0, as well as in various excited states. In the ground state S_0 of BPT there is an excess of electron density on the sulphur atom (~0.4 e relative to the 6 electrons (1σ, 1π, 4n) expected for sulphur).

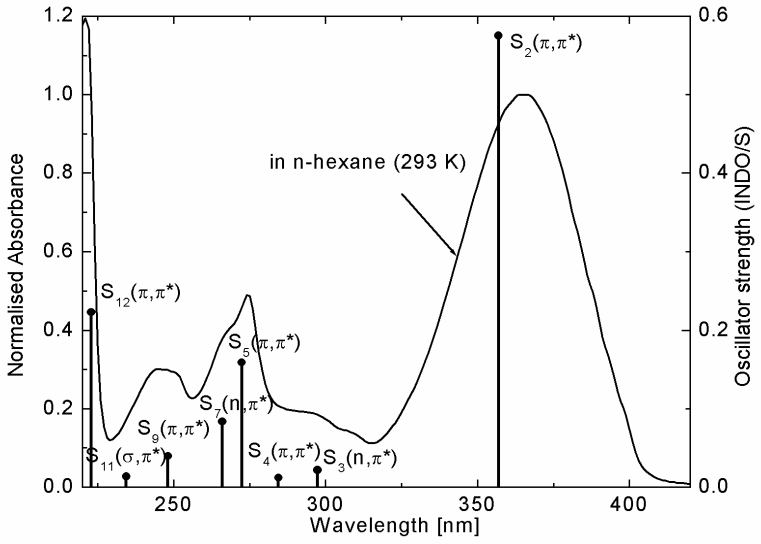

Figure 1.5. Experimental and theoretical (calculated with INDO/S CI-1 method) electronic absorption spectrum of BPT. Calculations have been performed by J. Koput (unpublished results).

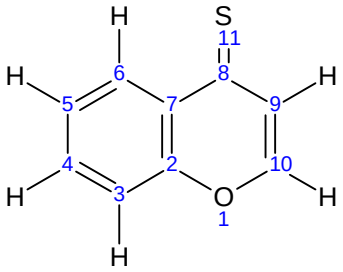

Figure 1.6. Numbering of atoms of BPT (benzopyranthione).

In parallel, a deficiency in the electron density on the adjacent carbon atom (~0.15 e) is observed. This is consistent with the electronegativity of the sulphur and carbon atoms. In the excited states, the electron density is shifted from the sulphur atom toward other atoms - mainly towards the neighbouring carbon atom (~0.7 e and ~0.4 e for $n\rightarrow\pi^*$ and $\pi\rightarrow\pi^*$ transitions respectively). Such large changes in the electron density are responsible for the different properties in the excited states (S_1, S_2, T_1 and T_2) compared to that in the ground state. In consequence, the affinity for a hydrogen bond formation by the thiocarbonyl group of BPT in the S_2 state with water or alcohol molecules can be lower than in the ground state. With the charge transfer associated with the $S_0\rightarrow S_2$ transition a decrease of the dipole moment can be expected [2]. Table 1.2 also shows that the BPT oxygen does not undergo a significant change in its electron density distribution.

Table 1.2. Changes in electron density for different atoms and for the benzo moiety of BPT calculated by the INDO/S CI-1 method. Atoms were numbered according to Fig.1.6 The electron density is expressed in [e]. Calculations have been performed by J. Koput (unpublished results).

State	O(1)	C(2)	C(7)	C(8)	C(9)	C(10)	S(11)	Benzo moiety
S_0	-6.215	-3.845	-3.985	-3.852	-4.041	-3.849	-6.411	-23.897
Change of electron density due to excitation								
$S_1(n,\pi^*)$	-0.039	-0.044	0.009	-0.473	0.0011	-0.134	0.753	-0.123
$S_2(\pi,\pi^*)$	0.028	0.012	0.068	-0.348	0.045	-0.119	0.429	-0.033
$T_1(\pi,\pi^*)$	0.006	-0.021	0.024	-0.337	0.055	-0.087	0.409	-0.046
$T_2(n,\pi^*)$	-0.038	-0.031	0.012	-0.469	0.012	-0.101	0.691	-0.097

The calculations show a very high spin-orbit coupling constant between $S_1(n,\pi^*)$ and $T_1(\pi,\pi^*)$ (~25 cm^{-1}) and $S_2(\pi,\pi^*)$ and $T_2(n,\pi^*)$ (~23 cm^{-1}) states. Despite strong spin-orbit coupling constants between the S_2 and T_2 states, only the $S_1(n,\pi^*) \rightarrow T_1(\pi,\pi^*)$ transition is expected to be efficient. The large energy gap $\Delta E(S_2(\pi,\pi^*)\text{-}T_2(n,\pi^*)) > 8000$ cm^{-1} (in perfluorohydrocarbons) limits the efficiency of the $S_2(\pi,\pi^*) \rightarrow T_2(n,\pi^*)$ transition. This is consistent with the long lifetime observed in perfluorohydrocarbons for BPT in the S_2 state (see Table 1.1). Very low values of spin-orbit coupling constants between $S_1(n,\pi^*)$ and $T_2(n,\pi^*)$ (~0.043 cm^{-1}), $S_2(\pi,\pi^*)$ and $T_1(\pi,\pi^*)$ (~0.006 cm^{-1}), $S_2(\pi,\pi^*)$ and $T_3(\pi,\pi^*)$ (~0.067 cm^{-1}), have also been determined. Note that very similar results have been published for a BPT isomer, the thiocoumarin [23].

1.6. References.

1. A. Maciejewski, R. P. Steer, *Chem. Rev.*, 93 (1993) 67.
2. H. K. Sinha, O. K. Abou-Zied, R. P. Steer, *Chem. Phys. Lett.,* 201 (1993) 433.
3. A. Maciejewski, M. Szymanski, R. P. Steer, *Chem. Phys. Lett.*, 143 (1988) 559.
4. M. Szymanski, A. Maciejewski, R. P. Steer, *Chem. Phys.*, 124 (1988) 143.
5. M. Szymanski, R. P. Steer, A. Maciejewski, *Chem. Phys. Lett.*, 135 (1987) 243.
6. J. R. Huber, M. Mahaney, *Chem. Phys. Lett.*, 30 (1975), 410.
7. D. Tittelbach-Helmrich, R. P. Steer, *Chem. Phys. Lett.*, 262 (1996), 369.
8. A. Maciejewski, M. Szymanski, R. P. Steer, *J. Phys. Chem.*, 92 (1988) 2485.
9. B. Nickel, H. Eisenberger, M. T. Wick, R. P. Steer, *J. Chem. Soc., Faraday Trans.,* 92 (1996), 1101.
10. A. Maciejewski, M. Szymanski, R. P. Steer, *J. Phys. Chem.*, 90 (1986) 6314.
11. J. Kozlowski, A. Maciejewski, M. Szymanski, *J. Chem. Soc. Faraday Trans*, 88 (1992) 557.
12. J. Kubicki, A. Maciejewski, M. Milewski, T. Wrozowa, R. P. Steer, *Phys. Chem. Chem. Phys.*, 4 (2002) 173.
13. H. Eisenberger, B. Nickel, A. A. Ruth and R. P. Steer, *J. Chem. Soc., Faraday Trans.*, 92 (1996) 741.
14. A. Maciejewski, *J. Photochem. Photobiol., A: Chem.*, 51 (1990) 87.
15. A. Maciejewski, A. Safarzadeh-Amiri, R. E. Verrall, R. P. Steer, *Chem. Phys.*, 87 (1984) 295.
16. K. F. Freed, *Acc. Chem. Res.*, 11 (1978) 74.
17. P. Avouris, W. M. Gelbart, M. A. El-Sayed, *Chem. Rev.*, 77 (1977) 796.
18. B. D. Wagner, D. Tittelbach-Helmrich, R. P. Steer, *J. Phys. Chem.*, 96 (1992) 7904.
19. N. Tétreault, R. S. Muthyala, R. S. H. Liu, R. P. Steer, *J. Phys. Chem. A*, 103 (1999) 2524.
20. W. Siebrand, *J. Chem. Phys.*, 44 (1966) 4055.
21. M. Milewski, J. Baksalary, P. Antkowiak, W. Augustyniak, M. Binkowski, J. Karolczak, D. Komar, A. Maciejewski, M. Szymanski, W. Urjasz, *J. Fluoresc.*, 10 (2000) 89.
22. M. Milewski, PhD-thesis: *Spectral, photophysical, photochemical properties of 4H-1-benzopyran-thione and its derivatives in solution and micro-organised systems*, Adam Mickiewicz University, 1998, Poznan.
23. M. Szymanski, A. Maciejewski, J. Kozlowski, J. Koput, *J. Phys. Chem. A*, 102 (1998) 677.

CHAPTER 2.

Time-resolved electronic and vibrational spectroscopic techniques.

2.1. Introduction.

The real time characterisation of photochemical reactions and photophysical processes requires the use of time-resolved spectroscopic methods. These methods can provide information about the nature of the transient species involved in the reaction all along the reaction pathway (excited states, exciplexes, radicals, ions,...) which can generally be identified by their spectral signature. If the time resolution of the utilised technique is high compared to their lifetimes, they can also provide information about the dynamics of these transient species. Among all the spectroscopic techniques that can be used to characterise photochemical intermediates, the most common ones are the electronic spectroscopies (absorption and emission) [1 - 3]. Excited states can be characterised by fluorescence or phosphorescence spectroscopies while ground state transient species are often characterised by transient absorption spectroscopy. Additional structural information about the photochemical intermediates can be obtained by using time-resolved vibrational spectroscopies. The design of the time-resolved experimental set-up depends on the kind of spectroscopic method used, the time resolution needed and the kind of information required (spectral or temporal)... In this thesis, both electronic and vibrational spectroscopies (Raman) were used and experiments performed using five different experimental set-ups.

Time-resolved emission measurements were performed using time-correlated single photon counting (TCSPC) and up-conversion methods. The TCSPC method provides a high sensitivity and a time resolution of few picoseconds while the up-conversion method gives access to the femtosecond time-scale but presents a much lower sensitivity.

Transient absorption spectroscopy was used to characterise the "dark" intermediates, which do not emit light. Two different experimental set-ups were used, one with a 100 fs time resolution and the other with a 10 ns time resolution. Phosphorescence emission measurements were made on the same set-up as that for nanosecond transient absorption measurements using the same 10 ns time resolution.

Time-resolved resonance Raman studies were performed only on the nanosecond time-scale. The experimental set-up utilised had a time resolution of about 10 ns.

Since some of the above mentioned set-ups are based on the pump-probe method, its principle is summarised below. This method requires the use of at least two light pulses. The first one, the so-called pump pulse perturbs the sample at time t=0. The second one delayed

by Δt with respect to the pump pulse crosses the perturbed sample and acts as a probe. The action of the pump pulse on the sample can be analysed in two different ways:

- by comparing the probe pulse characteristics crossing the sample before and after the action of the pump pulse (absorption for instance),
- by observing new effects created by the probe itself before and after the action of the pump pulse (Raman scattering for instance).

Fig.2.1 presents the principle of the pump-probe technique applied to the analysis of a transient species by absorption, stimulated emission and resonance Raman spectroscopies. It is important to note that both pump and probe pulses have to be tuned to specific electronic transitions: a ground state electronic transition for the pump pulse and a transient species electronic transition for the probe pulse.

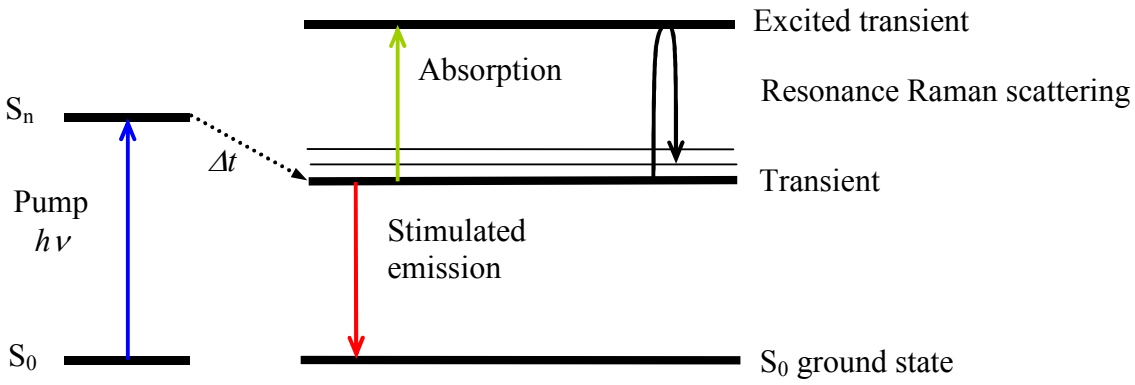

Figure 2.1. Principle of the pump-probe method. The pump pulse with energy $h\nu$ induces an electronic transition ($S_0 \rightarrow S_n$ for instance), while after a time delay Δt the transient species are analysed by the probe pulse through stimulated emission, transient absorption or resonance Raman scattering.

In this chapter, we will describe the five experimental set-ups used by the author at Uniwersytet im. Adama Mickiewicza, Université des Sciences et Technologies de Lille and University of Amsterdam. The nanosecond transient absorption set-up has been developed by the author during his PhD thesis and therefore will be described in more detail. The experimental procedure is also briefly discussed for each technique.

2.2. Picosecond time-correlated single photon counting.

Time-Correlated Single Photon Counting (TCSPC) is a statistical method, which allows us to investigate the dynamics of fluorescent excited-states by the construction of a histogram of the number of fluorescence photons counted versus time [2].

2.2.1. Experimental set-up.

TCSPC experiments were performed using the set-up located at the Adam Mickiewicz University (Centre for Ultrafast Laser Spectroscopy headed by Prof. A. Maciejewski). This system allows the characterisation of the excited states with lifetimes in the order of a few ps with high reliability and reproducibility (time-precision of about Δt=1 ps) [4, 5]. The basic scheme of the set-up is presented in Fig.2.2. A solid-state Ti:sapphire laser *Spectra-Physics Tsunami* with a second harmonic generator was used for generating the linearly polarised exciting pulses with a time-width of about 1 ps, wavelengths ranging from 360 to 500 nm and a repetition rate of 4 MHz. The excitation beam photoexcites the sample and the fluorescence of a small volume of solution is collected at 90º by the collecting lens and sent to the entrance slit of the monochromator. The polarisation of the fluorescence is selected by a polariser placed between the collecting lens and the monochromator. In our experiments, we only used the magic angle configuration (54.7º between the polarisation of the pump and the analysed fluorescence). The fluorescence signal is detected by a multichannel plate photomultiplier.

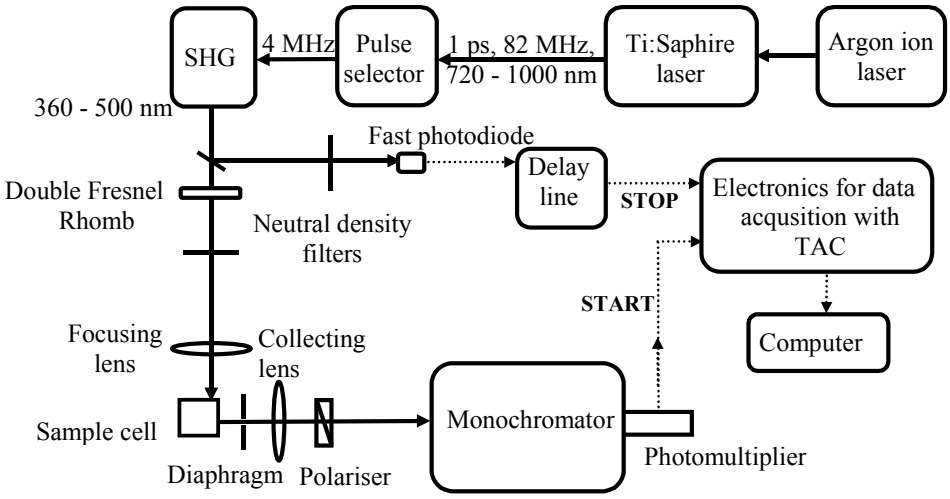

Figure 2.2. Schematic diagram for emission detection used in picosecond TCSP system, with 90° geometry (the exciting beam is perpendicular to the fluorescence beam).

The principle of the measurement is as follow. The exciting pulse is split into 2 parts. One is sent to the sample and the other one to a photodiode. When one photon from the excited sample is detected by the photomultiplier it delivers an appropriate signal, called a START pulse, which reaches the input of the time-to-amplitude converter (TAC) and initiates the charging of a capacitor. This process is stopped by a STOP pulse, which is delivered by the photodiode and properly delayed by the electronics. At this moment the TAC generates a pulse, whose amplitude is proportional to the charge accumulated in the capacitor, and in consequence, to the time difference between the START and STOP pulses. When this procedure is repeated a great number of times, one can build a histogram of photon counts versus time *t*. This histogram represents the decay curve of the fluorescence emission. In the case when an exciting pulse leads to more than one photon, a pile-up effect occurs which means that the electronics counts only one event related to the first photon. This effect can be eliminated by adjusting the system in a way, that only one over 200 successive exciting pulses leads to the detection of a single emission photon.

2.2.2. Data processing.

The decay of the measured emission signal $D(\lambda_{exc},\lambda_{em},t)$ is the convolution of the real decay of fluorescence $I(t)$ with the instrument response function $IRF(\lambda_{exc},\lambda_{em},t)$ [2],

$$D\left(\lambda_{exc},\lambda_{em},t\right) = I\left(t\right) \otimes IRF\left(\lambda_{exc},\lambda_{em},t\right), \qquad (2.1)$$

where: λ_{exc} is the excitation wavelength, λ_{em} is the emission wavelength. Our experimental system is characterised by a reproducible time-width of *IRF* of about 30 ps (FWHM) obtained by using scattered laser light. However *IRF* depends on several factors such as excitation wavelength, emission wavelength, sample refractive index *n*, difference of optical paths for emission photons passing through the monochromator to reach the microchannel plate photomultiplier, the time-response of electronics, the time-width of the exciting laser pulses. Thus accurate direct determination of $IRF(\lambda_{exc},\lambda_{em},t)$ is not possible. This can be achieved by use of a Delta Function Convolution Method (DFCM) [6], which allows us to determine the lifetime τ from a time-dependence $I(t)$ function. DFCM takes into account the *IRF*, but leaves out its direct determination. In this method, within the same experimental conditions, one has to measure not one, but two fluorescence decays D^S and D^R for the sample (*S*) and the reference (*R*), respectively. The reference should emit and absorb in the same spectral range as the sample. The solvents used for *S* and *R* must also be characterised by similar refractive

indices *n* to avoid a time dispersion effect between the *S* and *R* measurements. The expected relation between lifetimes must be $\tau_S > \tau_R$. The analysis of data is based on a fitting procedure of the theoretical decay function $D^T(\lambda_{exc},\lambda_{em},t)$ to the measured decay D^S. $D^T(\lambda_{exc},\lambda_{em},t)$ is presented in the following form :

$$D^T\left(\lambda_{exc},\lambda_{em},t\right) = D^R\left(\lambda_{exc},\lambda_{em},t\right) \otimes \left[I^T\left(t\right)\delta\left(0\right) + \frac{d}{dt} I^T\left(t\right) + \frac{1}{\tau_R} I^T\left(t\right) \right], \qquad (2.2)$$

where: $\delta(0)$ is the delta Dirac function for time zero.

The fitting procedure directly provides the lifetime τ_S from the time-dependence $I^T(t)$ function. The $I^T(t)$ function can be a single exponential decay, but even more complex forms of $I^T(t)$ can be expected according to which kinetics model of reaction is considered. When the lifetime τ_R is known, its value is set as a fixed parameter during the fitting procedure. In the case where the lifetime τ_R is unknown, τ_R can be also treated as a variable parameter to determine its proper value.

The fitting procedure is performed using the Simplex algorithm [7], which seems to be better than that proposed by Maquardt [8], due to the fact that the latter is characterised by its higher tendency to stop in local minimum (instead of the real one) during the minimisation procedure of the chi-square parameter χ^2 defined as:

$$\chi^2 = \frac{1}{N-n} \sum_{i=1}^{N} \left[\frac{D^S(t_i) - D^T(t_i)}{\sigma(t_i)} \right]^2, \qquad (2.3)$$

where: t_i is a value of time related to the i^{th}-channel of the time-axis in the TCSPC method, $D^S(t_i)$ and $D^T(t_i)$ are the number of measured counts and the value of the fitted function, respectively, σ_i is the standard deviation of the observed $D^S(t_i)$, N is the number of fitted experimental points and n the number of fitted parameters.

The validity of the fitted function $D^T(\lambda_{exc},\lambda_{em},t)$, can be easily checked by calculating the weighted residuals function $WR(t)$, expressed by:

$$WR(t_i) = \frac{D^S(t_i) - D^T(t_i)}{\sigma(t_i)}, \qquad (2.4)$$

where: $\sigma(t_i)$ is the standard deviation determined for t_i.

The values of $WR(t)$ must be randomly distributed in the range (-3, 3).

The determination of the autocorrelation function of the weighted residuals can be very useful too, because the values of this function must be randomly distributed. If not, the autocorrelation function can determine some correlations between the weighted residuals *WR* in short or longer time-scale:

$$AC_j = \frac{\frac{1}{m}\sum_{i=1}^{m} WR(t_i)WR(t_{i+j})}{\frac{1}{N}\sum_{i=1}^{N} WR(t_i)^2}, \qquad (2.5)$$

where: $m=N/2$, $0 \le j \le m$, t_i is a value of time related to i^{th}-channel of the time-axis in the TCSPC method.

The mentioned data processing and the TCSPC set-up characterised by a stable shape and width of the *IRF* ensures us of the accuracy and precision of the fluorescence lifetimes τ_S.

2.3. Femtosecond fluorescence up-conversion.

The up-conversion technique is an optical sampling technique, which can be used to measure fluorescence decays with a femtosecond time resolution.

2.3.1. Principle of the fluorescence up-conversion method.

This technique is based on the use of two synchronised femtosecond laser pulses: the exciting and the gating pulses. The fluorescence of the sample induced by the exciting pulse is collected and focused on a nonlinear crystal (e.g. β-barium borate, BBO). The gating pulse is delayed by τ by means of an optical delay line and is also focused on the nonlinear crystal (see Fig.2.3a). The simultaneous presence within the crystal of the fluorescence signal and of the gating pulse yields an up-conversion signal whose frequency ω_{up} depends on the frequencies of the incoming pulses [1, 9]. The frequency ω_{up} can be expressed by:

$$\frac{1}{\lambda_{up}} = \frac{1}{\lambda_{fluo}} + \frac{1}{\lambda_{gating}}, \qquad (2.6)$$

implying,

$$\omega_{up} = \omega_{fluo} + \omega_{gating}. \qquad (2.7)$$

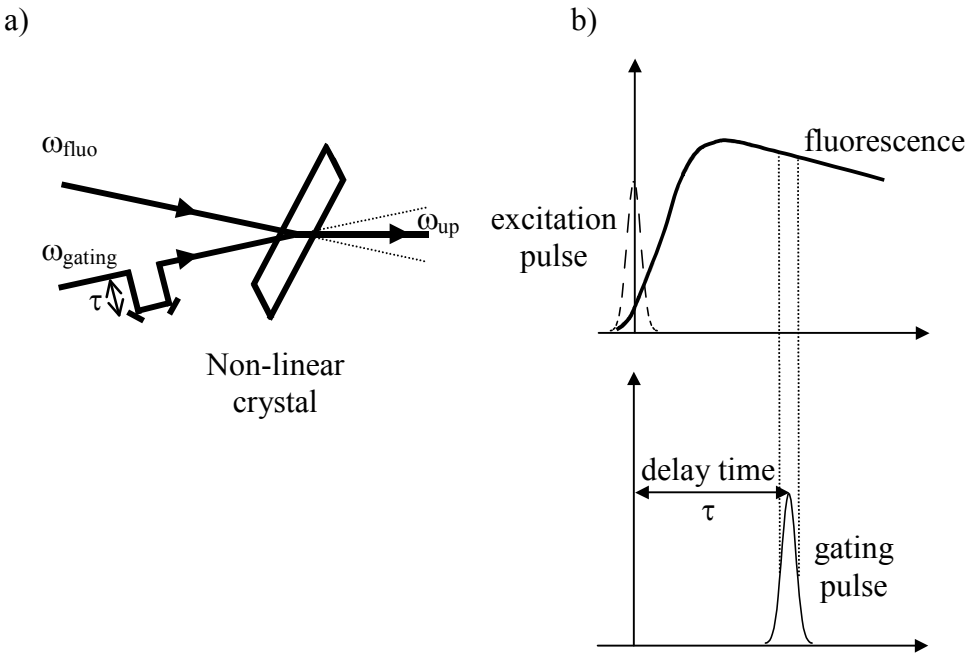

Figure 2.3. Principle of spectral (a) and temporal (b) sampling of the fluorescence signal by the up-conversion technique [1].

In order to be efficient, the frequency mixing process in the crystal must fulfil the phase-matching conditions (wave vector conservation rule $\vec{k}_{up} = \vec{k}_{fluo} + \vec{k}_{gating}$). The intensity of the up-conversion signal is given by the formula:

$$I_{up}(\tau) \propto \int_{-\infty}^{\infty} I_{fluo}(t) I_{gating}(t-\tau) dt, \qquad (2.8)$$

where $I_{fluo}(t)$ is the fluorescence intensity and $I_{gating}(t-\tau)$ is the gating pulse intensity. Thus, the nonlinear crystal acts as an optical gate, which is opened only when the gating pulse is present in the crystal. Finally, to obtain the fluorescence intensity versus time, the delay time τ between the gating pulse and the excitation pulses is scanned and the time dependent intensity of the up-converted signal $I_{up}(\tau)$ is measured (Fig.2.3b).

2.3.2. Experimental set-up.

The author used the femtosecond fluorescence up-conversion system located at the University of Amsterdam (group headed by Prof. M. Glasbeek in the Laboratory for Physical Chemistry). The details of this experimental set-up have been described previously [10, 11]. This set-up is based on a 1 kHz amplified Ti:saphire laser (Fig.2.4).

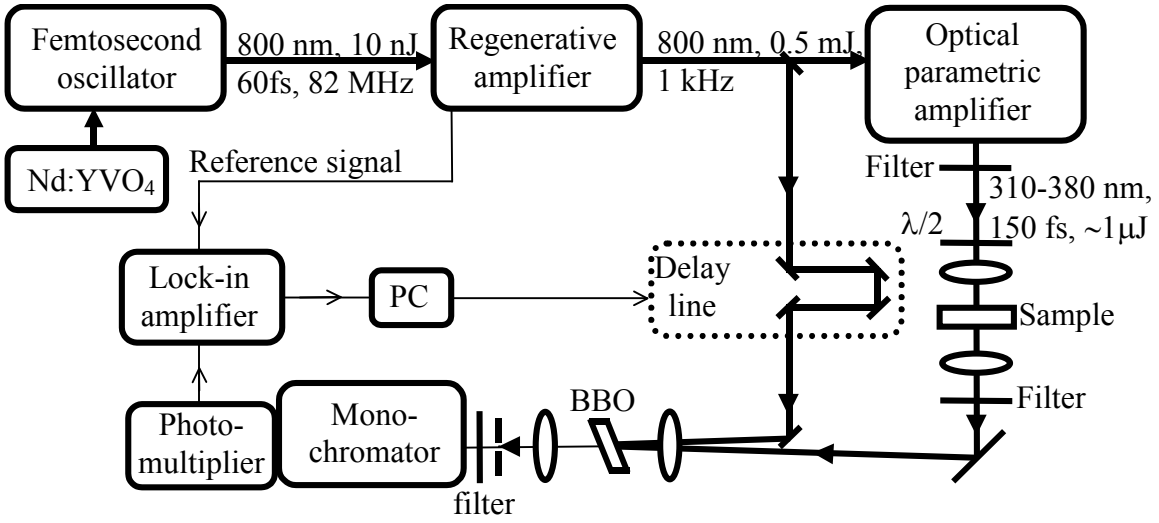

Figure 2.4. Experimental set-up for femtosecond fluorescence up-conversion measurements (➔ and → are related to optical and electrical paths respectively).

The femtosecond oscillator (see Fig.2.4) is a mode-locked *Tsunami* Ti:sapphire laser optically pumped by a *Spectra-Physics Millennia X* Nd:YVO_4 CW diode pumped laser. It produces 800 nm, 60 fs (fwhm) and 10 nJ pulses at a repetition rate of 82 MHz. The amplification system is a *Quantronix* regenerative amplifier, which generates 800 nm, 0.5 mJ pulses at a 1 kHz repetition rate. A beam splitter is used to produce two beams: the excitation and the gating beams.

The excitation beam is led to an optical parametric amplifier system (*TOPAS Light Conversion Ltd.*) based on BBO crystals. The *TOPAS* system also uses the second and third harmonic generation steps in order to produce the wavelength-tunable excitation beam (310 - 380 nm). A 2 mm thick *Schott DUG 11* optical filter is used to block other residual wavelengths. Typically, the sample is excited by 150 fs, 1 μJ pulses. The sample is contained in a 1 mm thick quartz cell, moving in a plane perpendicular to the excitation beam in order to minimise as much as possible the overheating of the solution. A 410 nm cut-off filter is placed behind the sample to reject the scattered laser and/or Raman light and allows pass the visible fluorescence wavelength to pass.

The gate beam (800 nm) is overlapped noncollinearly (cross angle $<5^0$) with the fluorescence in a 1 mm thick BBO crystal to allow generation of the up-converted signal. The up-converted light is produced by a type I sum frequency generation (O+O→E) meaning that the gating pulse (of vertical polarisation) is mixed only with the fluorescence signal having the same linear polarisation. In the set-up a half-wave plate placed on the pump beam is used to vary the polarisation of the pump with respect to the gate beam in order to perform

fluorescence measurements using the parallel, perpendicular and magic angle configurations. After the up-converting crystal, a variable iris aperture spatially separates the up-converted signal from the residual gating beam. A UV band-pass filter (*Schott UG 11*) is also used to remove the background signals generated in the mixing crystal: the second harmonic (~400 nm) and third harmonic (~266 nm) of the gate beam. The up-converted signal is focused on the entrance slit of a monochromator (spectral resolution of 10 nm) and detected by an *EMI 9863 QB/350* photomultiplier. The electric signal from the photomultiplier, as well as, a reference signal (1 kHz) is set at the inputs of the lock-in amplifier (*Stanford Research System SR830DSP)*. The data from the lock-in amplifier are transferred to a personal computer to be digitally stored and analysed. A stepping motor driven optical delay stage is used to control the time delay τ and which is controlled by computer. The up-conversion signals are accumulated for 1 s for each time-delay step of the translational stage. The change in the monitored fluorescence wavelength occurs through the rotation of the up-conversion crystal angle (to fulfil the phase-matching conditions) and the selection by the monochromator of the appropriate wavelength (see Eq.2.7).

2.3.3. Data processing.

To take into account the finite temporal resolution of the apparatus, a deconvolution procedure is needed [3, 12]. The instruments response function *IRF* represents the signal from the instrument related to an instantaneous sample response. *IRF* was estimated to be about 300 fs (fwhm) with a shape close to Gaussian function. *IRF* can be measured by different signal mixing in the up-converting crystal:

- The residual excitation pulse (wavelength selected in the 315 - 380 nm spectral range) with the gating pulse (800 nm).
- The Raman line of neat solvent samples with the gating pulse (e.g. cyclohexane).
- The white light continuum with the gating pulse. White light continuum was generated in a neat solvent sample (e.g. cyclohexane).

The measured up-converted emission signal decay $I_{up}(\tau)$ is a convolution of the real decay of fluorescence $I_{fluo}(t)$ with the instrument response function $IRF(t)$ [3]:

$$I_{up}(\tau) = \int_{-\infty}^{\tau} I_{fluo}(t) IRF(\tau - t) dt = I_{fluo} \otimes IRF. \qquad (2.9)$$

Thus, a fitting procedure (simplex method) of the observed up-converted emission signal $I_{up}(\tau)$ to a convoluted form $I_{fluo} \otimes IRF$ is used to establish the best parameters for the function $I_{fluo}(t)$. For our set-up, the time resolution after the deconvolution procedure is about 150 fs.

2.4. Femtosecond transient absorption spectroscopy.

Transient absorption spectroscopy with femtosecond time resolution is a very good pump-probe method used to investigate spectral and kinetic evolution related to ultrafast photophysical or photochemical phenomena.

2.4.1. Principles.

In a fs transient absorption experiment, the pump pulse (ultrashort, quasi-monochromatic and relatively intensive) excites the sample at $t=0$ leading to the formation of transient species (excited states, radicals, ions,...). These transients species are analysed by measuring the absorption of a probe pulse (ultrashort, low energy) at time $t+\Delta t$. The dynamics of the processes are obtained by changing the delay time Δt between the pump and probe. Femtosecond absorption spectrometers can be operated in two different ways:

- The "monochannel way" in which a quasi monochromatic pulse at a selected wavelength λ is used as the probe and is detected by a photodiode. The sensitivity of this method is usually high since silicon photodiodes provide low noise level and high quantum efficiency (≥40 %) in a broad spectral range (300 - 1050 nm). This sensitivity can be increased by modulating the pump beam and by using a lock-in amplifier. Time-resolved absorption spectra can be reconstructed from the kinetics recorded at various wavelengths [13, 14]. In this way, a great number of recorded kinetics results in good spectral resolution of the reconstructed spectra.
- The "multichannel way" in which a broad band white light continuum is used as the probe. In this case, the absorption spectrum, for all the wavelengths covered by the continuum is simultaneously recorded by a multichannel analyser (CCD camera). This method is very convenient to directly follow the time-evolution of the complete transient spectra [1]. However, it also enables the reconstruction of kinetic traces for a great number of selected wavelengths from a set spectra recorded at various delay times Δt.

2.4.2. Experimental set-up.

The femtosecond spectrometer operating in the multichannel mode was used in the Laboratoire de Spectrochimie Infrarouge et Raman at Université des Sciences et Technologies de Lille in the group headed by Dr. G. Buntinx. This apparatus is characterised by a high sensitivity, which is necessary, when weak transient absorption changes have to be measured.

The laser system used for the generation of the pump and probe pulses is presented in Fig.2.5. It is an amplified Ti:sapphire laser. The oscillator is a *Coherent MIRA 900D* pumped by a 10 W cw argon laser (*INNOVA 310, Coherent*). The oscillator delivers pulses characterised by time-duration of 100 fs (FWHM), energy of 10 nJ, repetition rate of 76 MHz and wavelengths tunable in the 690 - 1050 nm spectral range. These pulses are amplified in a regenerative amplifier (*ALPHA 1000, BM Industries*) using the chirped pulse amplification method. The amplifier is pumped by a 13 W, 1 kHz intracavity frequency-doubled Nd:YLF laser (*621D, BM Industries*) [15 - 17]. Each amplified pulse has the following parameters: energy of 1 mJ, time duration of 80 fs (FWHM) determined by autocorrelation and 750 - 850 nm tunability. The majority of the energy of the fundamental beam is frequency doubled by the second harmonic generation (SHG) in a 0.3 mm thick BBO crystal to generate pump pulses at wavelengths chosen from 375 to 425 nm [1, 18]. The remaining energy (a few microjoules) is used to generate a white light continuum in a 1 mm thick CaF_2 plate using non-linear processes [19 - 22]. White light continuum pulses (probe pulses) are characterised by a broad spectral range (from UV to IR). Only the 350 - 750 nm spectral range was considered in our measurements.

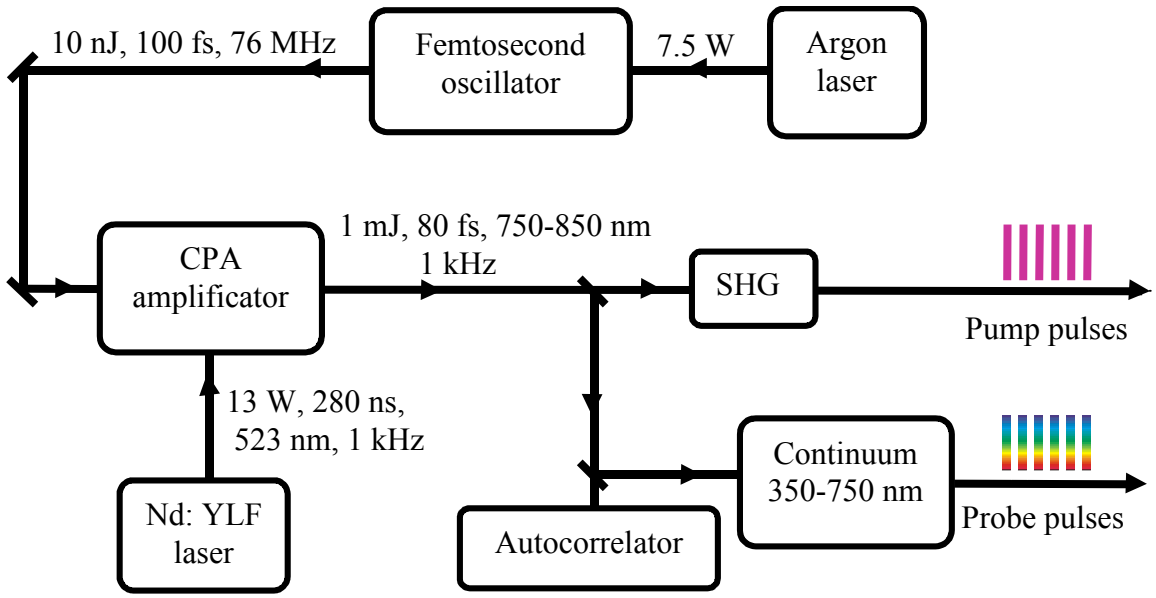

Figure 2.5. Generation of femtosecond pump and probe pulses.

The probe polarisation is set to one of the following configurations: parallel, perpendicular and the magic angle (54.7°) related to the pump beam polarisation. The pump beam and the white light continuum beam can be switched on or off by computer controlled shutters, and chopped by the synchronised choppers 1 and 2 as shown in Fig.2.6. The white light continuum probe pulses are time-delayed from 0 ps to 1500 ps relative to the pump pulse by using a stepping motor driven translation stage equipped with a hollow corner cube as a retroreflector. The continuum is split into two parallel probe and reference beams and then directed into the sample cell. The probe beam is overlapped in the sample cell with the excitation beam. The reference beam passes through a non-excited volume of the sample. Probe and reference beams are directed onto the entrance slit of a polychromator at two different heights and detected by a nitrogen cooled CCD camera (*LN/CCD-1340/400- EB/1 Princeton Instruments*). The CCD camera has a high dynamic range (up to 65536 counts), a high sensitivity (quantum yield better than 0.5 in 300 - 750 nm spectral range and more than 0.9 at the maximum), a low noise level (shot-noise-limited) and a spatial resolution of 1340×400 pixels^2. The chip surface of the CCD camera can be software divided into two areas of 1340×200 pixels^2 each. Therefore, both the probe and the reference spectra can be simultaneously and separately detected and recorded. Integrated intensities of the probe beam (I^{probe}) and corresponding reference beam (I^{ref}) are acquired at a repetition rate of 65 Hz. The readout of the CCD camera is properly synchronised with the chopper 2. A good signal-to-noise ratio is obtained thanks to the high data acquisition rate, 65 Hz, and due to the modulation of the pump beam at half the frequency of the probe beam, 32.5 Hz (kind of multichannel "lock-in" technique).

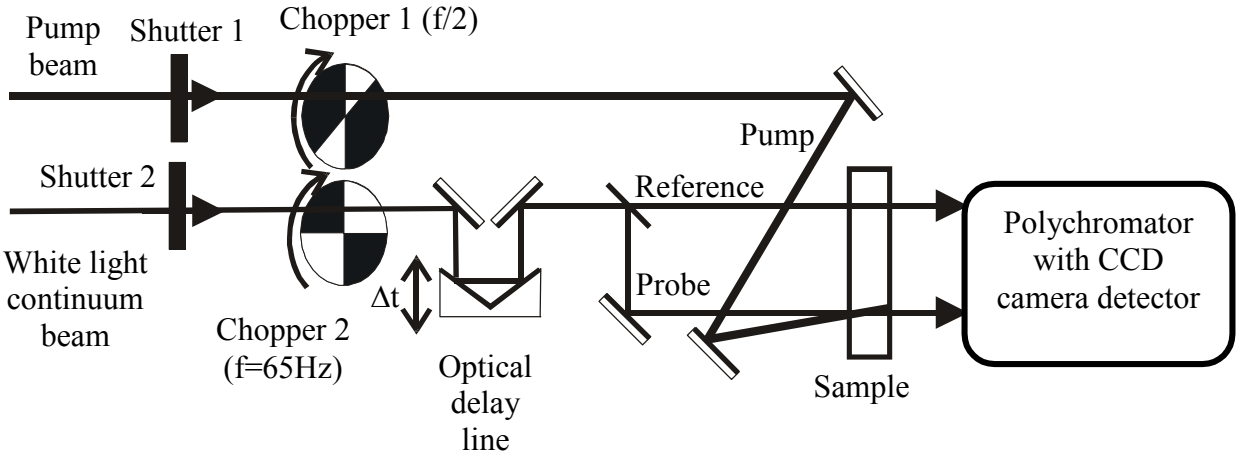

Figure 2.6. Sensitive dual beams (probe and reference) technique for measuring transient absorption spectra.

In order to minimise the influence of the long term laser intensity fluctuation as well as the possible photodegradation of the sample caused by long data acquisition times, the transient absorption spectra recorded at the chosen delay times were averaged by moving the optical delay stage alternatively forward and backward.

2.4.3. Data processing.

The spectral variation of the optical density for a delay time Δt is given by the following formula:

$$\Delta OD(\lambda,\Delta t) = log\left[\frac{I_0^{probe}(\lambda) - I^{stray}(\lambda)}{I_0^{ref}(\lambda) - I^{stray}(\lambda)} \cdot \frac{I_{pump}^{ref}(\lambda) - I^{em}(\lambda)}{I_{pump}^{probe}(\lambda,\Delta t) - I^{em}(\lambda)}\right], \qquad (2.10)$$

where:

- I_0^{probe} and I_0^{ref} represent the intensity of the probe and reference beams respectively, when the pump is off (the pump beam is blocked by chopper 1),
- I_{pump}^{probe} and I_{pump}^{ref} represent the intensity of the probe and reference beam respectively, when the pump is on (the pump beam passes through chopper 1),
- I^{stray} represents the dark noise (negligible), the straylight and the offset of the detection (shutters 1 and 2 are closed),
- I^{em} represents the spontaneous emission of the sample induced by the pump beam when the continuum is blocked by the shutter 2 (I^{em} contains also I^{stray}).

The I^{stray} and I^{em} are recorded prior to each experiment. The data acquisition procedure is totally controlled by *Winspec 32* software (*Princeton Instruments*). The calculated transient absorption signal is properly related to the variation of the sample properties induced by the pump, since other changes of the continuum spectral distribution along the different optical paths are suppressed. A very high signal-to-noise ratio can be obtained with this set-up. In 1 minute acquisition time, the noise level is better than ΔOD=0.0005.

As already mentioned assembling spectral data from several different time-delays is needed to reconstruct the transient absorption kinetic traces at selected wavelengths. To analyse these traces, a kinetic model describing the observed processes should be assumed. In consequence, an adequate theoretical function $\Delta OD_\lambda^{fit}(t)$ is fitted to the measured kinetics $\Delta OD_\lambda(t)$ to determine the different time-constants. If one of these time-constants is close to the apparatus function (about 130 fs for our set-up), the fitting procedure should also take into

account a convolution integral: the theoretical function $\Delta OD_{\lambda}^{fit}(t)$ with the cross-correlation $C(t)$ function between probe and pump pulses:

$$C(t) \otimes \Delta OD_{\lambda}^{fit}(t) = \int_{0}^{t} C(\tau)\Delta OD_{\lambda}^{fit}(t-\tau)d\tau. \qquad (2.11)$$

The cross-correlation function can be determined by measuring some instantaneous processes (for example the two photon (pump + probe) absorption from the solvent). Usually, a Levenberg-Marquardt algorithm is used to perform nonlinear least squares fitting. When a good agreement is found between the fitted function and the experimental data, we can state that the assumed kinetic model and the calculated time-constants are correct. In this thesis we limit our investigation to time delays greater than 1 ps. Consequently, the convolution procedure was not applied.

2.4.4. Measurements and artifacts.

Femtosecond transient absorption measurements can be disturbed by the group-velocity dispersion effect (GVD) of the probe (continuum) and of the pump (quasi-monochromatic) pulses. GVD reflects the dependence of group velocity on wavelengths resulting in an increase in the time duration of the pulses passing through the different media. In consequence, the "red" portion of the pulse arrives earlier than the "blue" one. Therefore, in the set-up only reflecting optics are used in order to minimise the influence of GVD effects on the measurements. In the case of transient absorption spectra measurements in the subpicosecond time-scale, a procedure of GVD correction (time-zero correction) must be used to obtain all kinetics $\Delta OD_{\lambda}(t)$ in the equivalent time-scale. In the picosecond time-scale the GVD effect can be neglected because the time dispersion of the continuum over the 350 - 750 nm spectral range is only 0.7 ps as measured from the two-photon absorption signal of neat n-hexane [22]. The time resolution of the transient absorption spectrometer (FWHM of the pump-probe intensity cross-correlation) is estimated to be about 130 fs from the two-photon absorption rise time observed for a very thin (150 μm) BK7 optical glass plate.

The sample is circulating in a 2 mm optical path length flow cell equipped with thin CaF_2 windows (~ 0.2 mm thick). The energy of a single pump pulse is about 15 μJ (~2.0 mJ/cm^2), which ensures one-photon absorption of the sample. As already mentioned, in this thesis the transient absorption spectra below 1 ps are left out of consideration since they might be obscured by different photophysical side-effects, such as [23]:

- Two photon absorption: the solvent (or the cell window) can simultaneously absorbs two photons: one from the pump and the second from the probe leading to a positive band that can affect the transient absorption spectra.
- Stimulated Raman scattering: solvent vibrational modes (for example CH stretching mode of n-hexane) can be excited by pump and probe photons that lead to a negative or positive band in the transient absorption spectra.
- Cross-phase modulation in the solvent or in the cell window: intense pump pulses can time-dependently modify the index refraction n of the medium, which yields to spectral distribution changes of the continuum probe pulses [24]. The resulting transient absorption spectrum is affected because the reference pulses are free from cross-phase modulation.

These side-effects occurring when pump and probe pulses overlap in space and time, should be taken into account and subtracted when very fast processes (<1 ps) are investigated.

2.5. Nanosecond transient absorption spectroscopy.

Photophysical and photochemical processes induced by ultrashort laser pump pulse are not usually completed within the picosecond time-scale. The femtosecond transient absorption spectrometer described previously allows us to perform studies within the 0 - 1500 ps time-window. This limitation can be overcome by using a nanosecond transient absorption spectrometer to investigate the photophysical and photochemical processes in the nano/microsecond time-domain. One of the goals of this PhD was to construct and perform experiments using a nanosecond transient absorption spectrometer. The project was undertaken at the Centrum Ultraszybkiej Spektroskopii Laserowej (directed by Prof. A. Maciejewski) using commercially available components. This spectrometer was also designed for the purpose of phosphorescence emission measurements and thus this set-up will be described in detail.

The most recent review concerning nanosecond transient spectroscopy can be found in Bonneau and co-workers technical report [25]. Nanosecond transient absorption spectrometers typically use a single monitoring beam and can operate in:

- "The kinetics mode": a ns laser pulse (pump) excites the sample, at a selected wavelength λ_{pump}. The time-dependent absorption changes at a given wavelength are

monitored by a probe light, which can be CW (continuous-wave) or pulsed. In the later case, the probe pulse is much longer than the pump pulse. The probe light is usually generated by a xenon lamp or a laser diode, and finally it is detected by a photomultiplier or a photodiode, respectively. The signal delivered by the detector is sampled in real-time by a digital oscilloscope [26 - 30]. In this technique, the time resolution is mainly dependent on the detector response time constant and on the pump pulse duration.

- "The spectral mode": a ns laser pulse (pump) excites the sample, at a selected wavelength. At a chosen delay time Δt the absorption changes are monitored by a broadband probe pulse, the wavelengths of which are simultaneously detected by a gated intensified multichannel analyser (ICCD camera or photodiode array) [31, 32]. An image intensifier enhances the intensity of the monitoring light and acts as a shutter with a 1 ns rise time and a minimum open-time of about 5 ns. The later limits the time resolution of this method. The kinetics can be obtained by changing the delay Δt and repeating the experiment.

A spectrometer operating in "spectral mode" is very convenient to follow directly the time-evolution of transient absorption spectra. It is less common than the "kinetic mode" due to the lower signal-to-noise ratio of the data obtained by this method and also due to the expense of the detection system (ICCD camera coupled with an electronic pulse generator) [33]. The use of a streak camera in the detection system allows us to measure simultaneously time and spectrally resolved changes in optical density, but with a poor signal-to-noise ratio [34]. Thus we have chosen to build up a set-up based on the "kinetic mode" which for a reasonable cost allows a sensitivity of $\Delta OD<0.001$.

2.5.1. Description of the transient absorption set-up developed in Poznań.

The UV-visible absorption set-up with nanosecond time-resolution is shown in Fig.2.7. The transient species are produced by irradiating the sample at a repetition rate of 0.5 Hz with 8 ns pulses (FWHM) generated by a flashlamp pumped Q-switched Nd:YAG laser (*Continuum Surelite II*). Time profile and spatial distribution of the laser pulse are presented in Fig.2.8. The crossbeam energy profile of the laser beam (Fig.2.8b) is characterised by a diameter of 6 mm (FWHM). We generally used the third harmonic (355 nm) of this laser. The maximum available energy per pulse at this wavelength is 200 mJ and the linewidth is 1.5 cm^{-1}.

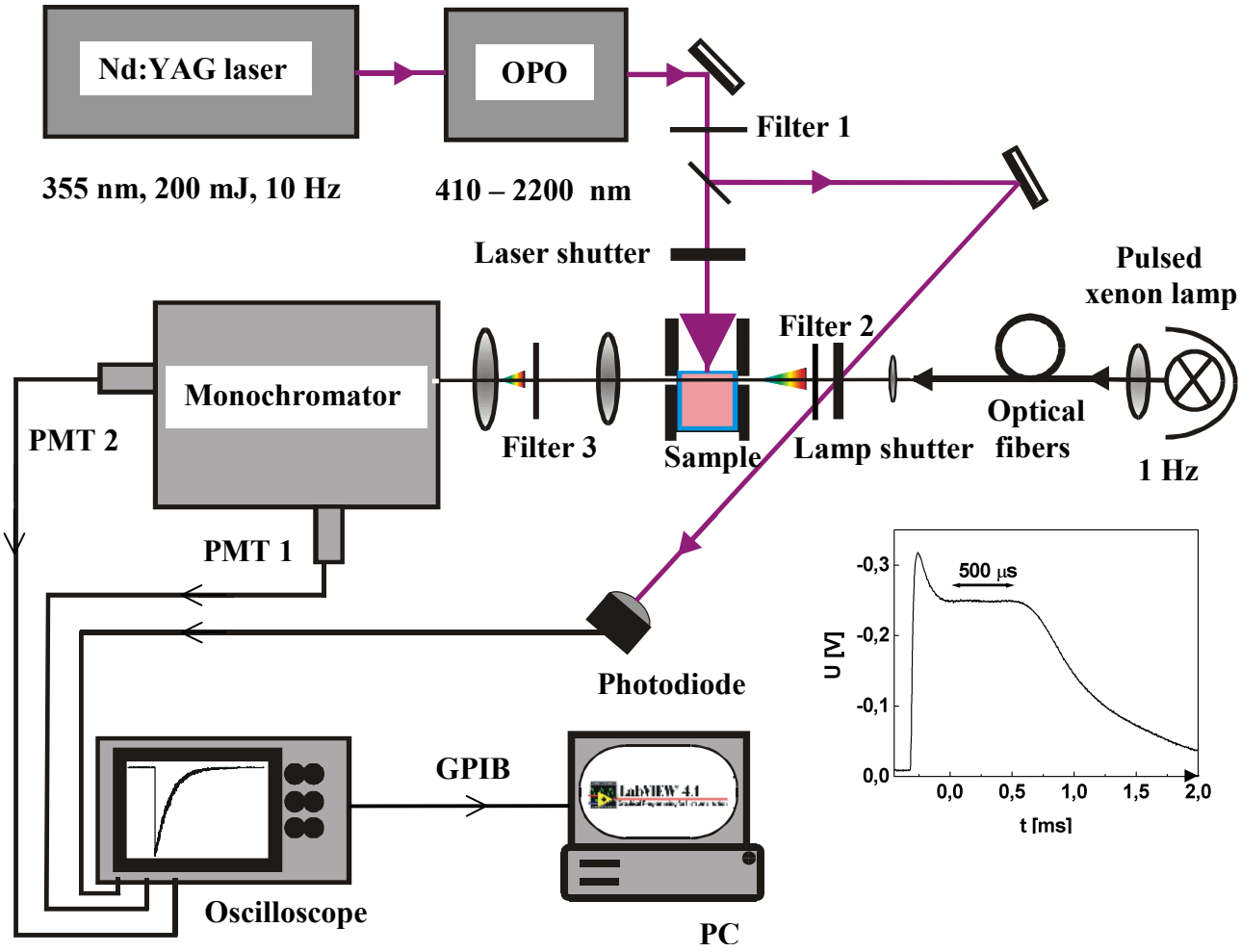

Figure 2.7. Nanosecond transient absorption spectrometer. The lamp intensity time-profile characterised by a 500 µs monitoring plateau is shown in the inset.

However, experimental conditions often require much lower pump energies (for thioketones about 1 mJ per pulse) in order to limit the concentration of excited molecules and thus avoid unwanted processes such a triplet-triplet annihilation. A *Continuum Surelite* OPO (Optical Parametric Oscillator) based on a β-barium borate (BBO) crystal pumped by the Nd:YAG laser can be used to provide excitation wavelengths ranging from 410 to 2200 nm [35]. In the case when a 355 nm pump excitation is used (third harmonic of Nd:YAG), an additional dichroic mirror removes the unwanted residual photons from the second harmonic generation process (532 nm). The colour glass filter 1 is used to lower the laser pulse energy. A *Molectron* pyroelectric joulemeter equipped with a *J25* head measures the energy of each pump pulse reaching the sample. The analysing (probing) light source is a 150 watt xenon arc lamp (*Applied Photophysics*), which is used in the pulsed mode with a 1 Hz repetition rate.

a) b)

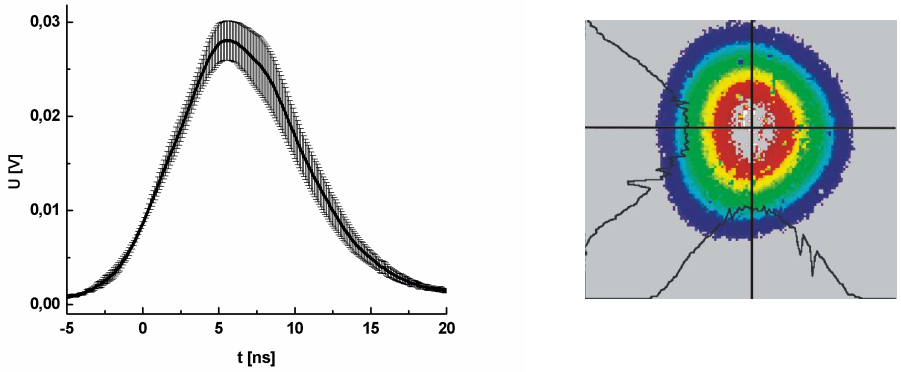

Figure 2.8. Characterisation of 355 nm laser pulses. Average time-profile of 20 laser pulses detected by a photodiode (*S1722-02 Hamamatsu*) and digitised by an oscilloscope. The envelope is the total error caused by pulse-to-pulse amplitude jitter. The measured time duration (FWHM) is 8 ns obtained from gaussian fitting function (a). Gaussian cross-section of the laser beam detected by a CCD camera (pulse energy of 0.1 mJ) (b).

The lamp pulsing causes a significant increase in the emitted photon flux during the period of the pulse: 50 times in the visible region and about 200 times in the UV. The emission plateau usable for data recording is about 500 µs. An intense lamp pulse reduces the shot noise (random fluctuation in the signal intensity that arises from the finite number of photons detected in short time intervals) and provides a better signal to noise ratio. On a longer time-scale (>500 µs) lamp pulsing is disabled and continuous light is used. In order to reduce the exposure of the sample and of the detection system to the radiation of the lamp and of the laser, two shutters are used. These two electronically driven *VS25 Vincent Associates* shutters (diameter of 25 mm) are equipped with $AlMgF_2$ high reflective coating blades resistant to laser pulses in the milijoule range and to the xenon lamp light irradiation. The laser beam shutter and lamp beam shutter operate at repetition rates of 0.5 Hz and 1 Hz, respectively. Appropriate time-synchronisation of these devices will be described later in details. The terminal of a spectrosil light guide with an accepting light active area of 7×1 mm^2 is optically coupled to the arc of the xenon lamp. The second end of spectrosil light guide is circular. A planoconvex lens positioned 30 mm from the circular end of the fibre, collimates the light in order to pass it efficiently through the sample (quartz cell 1×1 cm^2). A long pass filter (filter 2) absorbing wavelengths shorter than 285 nm is placed between the lamp shutter and the sample. The diameter of the probed cylindrical volume (about 2 mm) is determined by variable iris apertures positioned on either side of the sample. The laser beam is at 90° with

respect to the monitoring beam. The pump beam reaching the sample is not focused and is limited by a rectangular aperture (2.5×10 mm^2). In this way, the volume of the exciting solution completely overlaps the cylindrical volume analysed by the probe light. For transient absorption measurements at wavelengths longer than 500 nm, a colour glass filter (filter 3) absorbing wavelengths shorter than 450 nm is placed between the two lenses which focuses the probe beam onto the entrance slit of the monochromator. The filter 3 prevents the ultraviolet light (lamp and scattered laser pulses) being detected at the output of the monochromator via the second order dispersion of the grating. The probe light enters the *SpectraPro-300i Acton Research* monochromator, which is controlled by computer via a RS232 interface. The monochromator is equipped with a 300 g/mm grating (with 500 nm blaze wavelength) that possesses a wide spectral response, ranging from 290 nm to 900 nm. The entrance and exit slits are variable (from 10 μm to 3 mm), but slit width of 0.5 mm is usually used (corresponding to a 6 nm (FWHM) spectral resolution at 532 nm). The monochromator is equipped with two photomultipliers: PMT1 for transient absorption measurements and PMT2 for emission detection. For transient absorption measurements a *R928 Hamamatsu* photomultiplier was chosen because of its wide spectral response, ranging from 200 to 800 nm and its high current amplification. The photomultiplier is supplied with a *PS 325 Stanford Research System* power supply, which delivers stable high voltage. To increase the signal to noise ratio, mostly limited by the shot noise, an intense probing light source and minimum losses in the optical paths are required. The high analysing photon flux is detected by the photocathode of the photomultiplier. Due to this high level of signal, the amplification of the photoelectrons in the photomultiplier is performed using only five dynodes (home-built 5-stage circuit based on *Applied Photophysics* scheme) resulting in a high anode currents and a fast time response (ca. 2 ns). Test measurements have ensured a linear operation with currents up to 6 mA (equivalent to -300 mV signal for a load resistance of 50 Ω), which is in agreement with that determined by Bebelaar [27]. A short cable is used to connect the output of the photomultiplier to the signal input of the digital oscilloscope *Tektronix TDS 680 C*. The oscilloscope operates as a transient digitiser characterised by a maximum sampling rate of 5 GS/s, thus the minimum time between each data point is 200 ps. The oscilloscope has a maximal bandwidth of 1 GHz. The number of recorded points can be varied from 500 to 15000 points. The oscilloscope is triggered by a small portion of the laser pulse passing through the lamp shutter and detected by a *S1722-02 Hamamatsu* photodiode. The output from this fast photodiode (1ns rise time) acts as a zero time trigger for our data

collection channel. For pre-trigger data acquisition (10 % of the record) an adequate function of the digital oscilloscope is used. An offset of about 250 mV is added to the PMT signal in order that the level of the plateau is close to 0 mV. In this way, one can increase the sensitivity of the input of the oscilloscope and thus obtain a high dynamic for the digitalisation of the transient signal. Digitised data (containing PMT signal voltage as a function of time) are transferred via a GPIB interface from the oscilloscope to a *Pentium IV PC* computer. The optical density changes versus time are derived from two alternating data measurements:

- Signal $I_{signal}(t)$. The laser is on and reaches the sample.
- Reference $I_{reference}(t)$. The laser is off, since the pump pulse is blocked by the laser shutter.

Each pair of data sets is used to calculate the changes in optical density $\Delta OD_{\lambda}(t)$ using Eq.2.12 at the analysed wavelength λ (see Fig.2.9).

$$\Delta OD_{\lambda}(t) = log \frac{I_{reference}(t)}{I_{signal}(t)}. \qquad (2.12)$$

Using this equation, the variation of the amplitude of the lamp plateau versus time (see Fig.2.9) and other reproductive "noises" (for example electromagnetic interference induced by the Pockel's cell of the laser) are eliminated. The correctness of this method is based on the high (better than 1%) pulse-to-pulse amplitude and shape reproducibility of the lamp pulses.

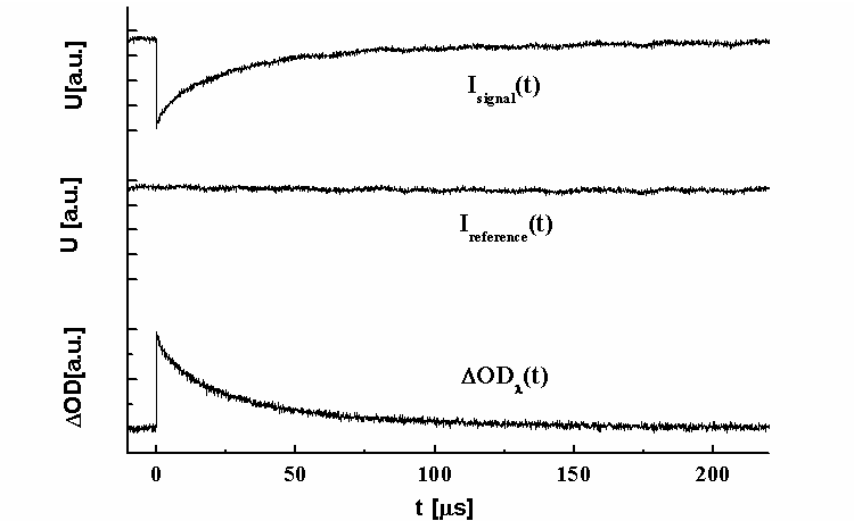

Figure 2.9. An example of time-dependent intensities $I_{signal}(t)$ and $I_{reference}(t)$, and calculated changes in optical density $\Delta OD_{\lambda}(t)$ according to Eq.2.12.

Care must be taken with respect to the presence of phosphorescence, fluorescence and scattered laser light, which can distort the kinetics $\Delta OD_\lambda(t)$ [26, 36]. This can be performed by recording a correction signal $I_{corr}(t)$ with the pump beam on and the probe beam off, all other experimental parameters being kept identical. In this case, $I_{signal}(t)$-$I_{corr}(t)$ replaces $I_{signal}(t)$ in the Eq.2.12.

In order to detect weak transient absorption signals ($\Delta OD_\lambda(t)$ of about 0.002) an average of ten measurements is taken in order to improve the signal-to-noise ratio. This ratio increases as the square root of the accumulation number. The transient absorption spectrometer can be operated in the 290 - 800 nm spectral range. However, this wide measuring range is generally reduced due to the strong ground state absorption of the sample, which prevents the probing light from passing through the sample. The time-resolution of the transient absorption spectrometer can be determined easily by measuring an instantaneous phenomenon (for example the laser photons scattered by the sample cell filled with water results in negative signals of $\Delta OD_{\lambda laser}(t)$, see Fig.2.10). The test measurements show that the 9 ns time-resolution of our set-up is mainly limited to the time-width of the exciting laser pulses (~8 ns FWHM, see Fig.2.8a).

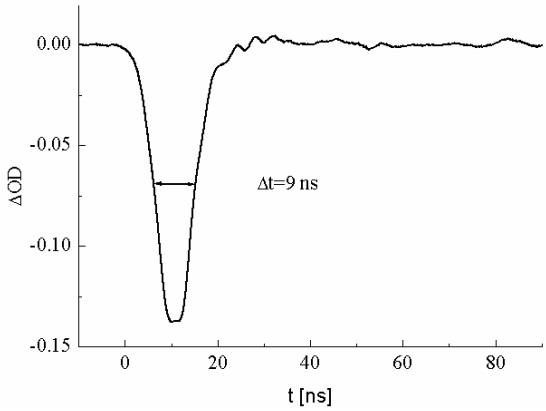

Figure 2.10. Instrument response function measured at 355 nm. The negative signal is due to scattered laser photons (355 nm) superposed on probing light (100-fold accumulation).

2.5.2. Data processing.

The analysis of the kinetic traces can be done assuming a kinetic model, which describes the observed processes. Therefore, an adequate theoretical function $\Delta OD_\lambda^{fit}(t)$ is fitted to the measured kinetics $\Delta OD_\lambda(t)$, in order to determine the time-constant of the various processes. Usually a Levenberg-Marquardt algorithm is chosen to perform the nonlinear least

squares fitting. In the case where the theoretical function is found to fit perfectly to the data, we can state that the assumed kinetic model is correct. The accuracy of the determined time constant τ is usually about 5 % in the case of a single-exponential function.

It is often useful to study not only the kinetics but also the spectral properties of the transient species. The assembling of the data from the kinetics recorded for several different wavelengths enables the reconstruction of the transient absorption spectra ($\Delta OD_t(\lambda)$). To do that, all kinetics traces $\Delta OD_\lambda(t)$ must be consequently measured within the same time-window while changing the analysing wavelength λ. In consequence, all the obtained kinetics $\Delta OD_\lambda(t)$ form a two-dimensional array of data $\Delta OD(\lambda,t)$. The corresponding array $\Delta OD^{fit}(\lambda,t)$ of the best fitted functions is the base used to plot the transient absorption spectra at various time delays.

2.5.3. Synchronisation.

Whereas in the femtosecond absorption set-up the pump and probe pulses are derived from the same initial laser pulse, on nanosecond time-scale, the pump and probe pulses are generally created separately by a laser and a pulsed lamp, respectively. In this case, an electronic synchronisation is needed. The control-program, written by the author in *LabView 4.1*, controls the timing of TTL signals necessary for the synchronisation of the different elements involved in the set-up via an input output card, enabling the dialog between the PC and the oscilloscope and which performs the ΔOD calculations and data fitting. The controlled card (*PCI-MIO-16XE-10 National Instruments*) generates the synchronised TTL pulses sequence to trigger the laser, the lamp pulser and the shutters (see Fig.2.11). The laser is triggered by the falling edge of the TTL pulses at a constant repetition rate of 10 Hz (see channel 1 on Fig.2.11b). At this rate the shot-to-shot intensity variation is much lower than in a single shot laser operation. Energy stability is important for the reliable determination of amplitudes in transient absorption measurements. The rate of the pump pulses reaching the sample is set to 0.5 Hz by the laser shutter, which is adequately triggered by TTL pulses (channel 2 in Fig.2.11b). TTL pulses triggering the laser are delayed by 10 ms compared to those triggering the shutters in order to take into account the opening time of the shutters. The shutters are opened for 40 ms in order to pass one laser or lamp pulse. The lamp shutter and lamp pulser are triggered with a 1 Hz repetition rate according to the data acquisition procedure: alternatively the signal (laser on) and reference (laser off) data are measured.

a)

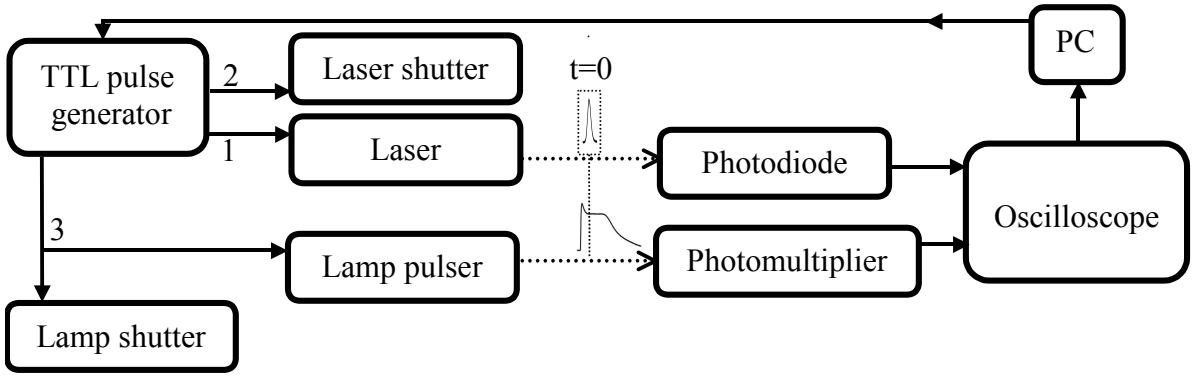

b)

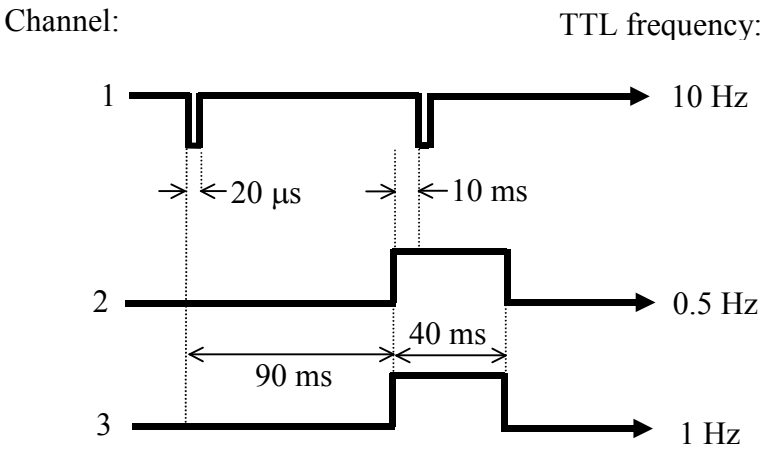

Figure 2.11. Principle of the synchronisation used in the nanosecond transient absorption spectrometer (electric paths and optic paths are presented by solid and dotted lines, respectively) (a) and TTL timing sequence (b).

An internal delay time of 10 ms in the lamp pulser ensures that the laser pulses are set at the beginning of the plateau region of the lamp pulse (see Fig.2.11) in order to maximise the available recording time window (up to 500 µs).

2.5.4. Emission spectrometer with nanosecond time-resolution.

The excited states of molecules exhibiting emission (fluorescence or phosphorescence) in the nano/microsecond time-domain can be investigated with the same experimental set-up. Only small modifications are required. The analysing lamp light is no longer necessary and is blocked. The laser induced emission is detected by the PMT2 photomultiplier shown in Fig.2.7. A metal package photomultiplier (*H5783-01 Hamamatsu*) was chosen for the emission experiments, because of its high sensitivity and wide spectral response ranging from

300 to 820 nm as well as its fast time-response (0.65 ns). A linear operation of this photomultiplier in the 0 - 10 μs is obtained for voltages down to -200 mV with a 50 Ω load resistance. The signal is digitised by the oscilloscope. To improve collection of the emission light and thus the signal-to-noise ratio, the iris placed between the sample and the monochromator is completely open. The time synchronisation diagram presented in Fig.2.11 is kept identical, so only every second record contains the emission signal *I(t)*. Usually a ten-fold accumulation of the emission signal *I(t)* is used to improve the signal-to-noise ratio. The same fitting procedure is applied to the emission data as that which is used to treat transient absorption data. The lifetime τ accuracy is usually about 2 %. The time-resolution of the set-up is determined by measuring a picosecond fluorescence signal. An 8 ns time-resolution was found which is limited by the laser pulse width (see Fig.2.8a).

2.6. Nanosecond time-resolved resonance Raman spectroscopy.

Since time-resolved Raman spectroscopy is a less common technique than that of time-resolved electronic spectroscopies, some basic principles of this technique are recalled.

2.6.1. Principle of Raman spectroscopy.

Irradiating a molecule by a monochromatic light at frequency ν_0 can result in inelastically scattered photons at frequencies $\nu = \nu_0 \pm \nu_r$ related to Stokes ($\nu < \nu_0$) or anti-Stokes ($\nu > \nu_0$) Raman scattering, where ν_r are the vibrational frequencies of the molecule (see Fig.2.12).

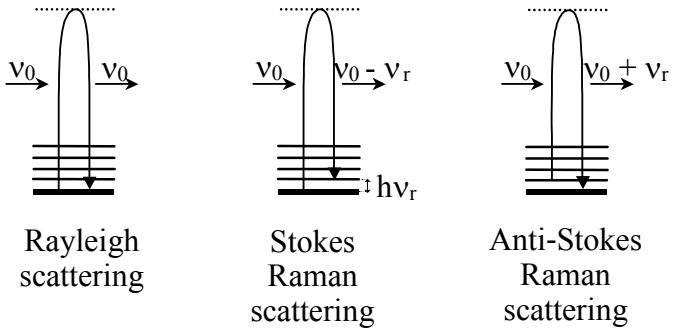

Figure 2.12. Schematic representation of spontaneous Rayleigh, Stokes and Anti-Stokes Raman scattering.

The Raman intensity I can be approximately expressed by the following formula [37 - 39]:

$$I = k \cdot I_0 \cdot (\nu_0 - \nu_{if})^4 \sum_{\rho\sigma} \left| (\alpha_{\rho\sigma})_{if} \right|^2, \qquad (2.13)$$

where k is a constant, ν_0 is the frequency of the incident light with an intensity I_0, ν_{if} is a transition frequency between two vibrational states: initial i and final f, $\alpha_{\rho\sigma}$ is the ρth, σth element of the polarisability tensor, ρ and σ are the x, y, or z components. A quantum mechanical treatment provides the following expression for the element of the polarisability tensor:

$$(\alpha_{\rho\sigma})_{if} = \sum_k \left[\frac{< f|\mu_\rho|k >< k|\mu_\sigma|i >}{(\nu_{ik} - \nu_0 + i\Gamma_k)} + \frac{< f|\mu_\sigma|k >< k|\mu_\rho|i >}{(\nu_{kf} + \nu_0 + i\Gamma_k)} \right], \qquad (2.14)$$

where $|i\rangle$ and $|f\rangle$ are the initial- and final-state wave functions, and μ_ρ and μ_σ are the dipole moment operators. The wave function of an intermediate state is $|k\rangle$, ν_{ik} and ν_{kf} are the transition frequencies from the i to k-state and from the k to f-state, respectively and $i\Gamma_k$ is a damping factor (in wavenumbers units) inversely proportional to the lifetime of the k-state. When $\nu_0 \approx \nu_{ik}$, both terms in Eq.2.14 give comparable contributions. As ν_0 approaches ν_{ik}, the first term of the Eq.2.14 dominates and it is this which is responsible for the resonance Raman effect. In the case of resonance with a strongly allowed electronic transition (from i to k-state), the Raman lines observed in the spectrum which are involved in this electronic transition are the vibrational modes i.e. the totally symmetric vibrational modes.

For a given molecule, there are *3N* degrees of freedom (*N* is the number of atoms), six of which involve molecular rotations and translations. The remaining, *3N-6*, degrees of freedom are the normal vibrational modes of the molecule. Each mode of vibration has a characteristic vibrational frequency that depends on interatomic force constants, atomic masses and coupling of motion between adjacent and distant atoms. The observed experimental Raman spectrum is defined by the intensity I of the scattered light versus the Raman shift $(\nu_0 - \nu)$.

2.6.2. Time-resolved resonance Raman spectroscopy.

Time-resolved resonance Raman spectroscopy (TRRRS) is a complementary method to transient absorption spectroscopy. The former provides structural information on the transient species while the latter is a very good method used to characterise the dynamics of

the photoinduced processes. The time-resolved resonance Raman technique is a pump-probe method [40 - 45]. The sample is excited at time t=0 by a pump pulse tuned to an absorption band of the ground state molecule. After a time delay Δt, the probe pulse at frequency ν_0 is sent onto sample and is inelastically scattered into other frequencies ν. The low concentration of the transient species produced by the pump requires resonance conditions to enhance the Raman intensity. The resonance condition is satisfied if the wavelength of the probe pulse is tuned to a strong absorption band of the transient species to be analysed. This means that one has to use transient absorption spectroscopy prior to time-resolved Raman measurements if the transient absorption spectrum of that species under investigation is not known. One of the main advantages of TRRRS compared to transient absorption spectroscopy is its selectivity. In the case of a chemical in solution involving several transient species, the absorption spectra are generally composed of superimposed broad bands, which make the analysis difficult. In contrast, TRRRS provides well resolved spectra that can be more easily analysed. Moreover, we can enhance the Raman spectrum of a specific transient species by changing the probe wavelength. However, sensitivity of this technique is low, despite the resonance effect. Thus, such experiments are usually performed for relatively high concentrations (10^{-2} - 10^{-3} M) of the sample, as well as, with the use of tightly focussed pump and probe beams in the sample. As a result, care must be taken to avoid multiphoton excitation of the molecules, photochemical decomposition, photoionisation and triplet-triplet annihilation. Note, that the application of the time-resolved resonance Raman method can be limited in the case of samples, which exhibit strong emission signal that may completely hide the Raman signal.

Time-resolved resonance Raman studies are usually supported by steady-state Raman measurements. The differences between these Raman spectra can be due to structural changes induced on going from the ground state to the transient species. Characterisation of the structure of the transient species, as well as, the assignment of the vibrational bands can be supported by appropriate quantitative modelling methods such as structure optimisation and *ab initio* molecular orbital calculations. Progress in computer calculations has strongly increased the role of theory for predicting Raman spectra to which experimental results can be directly compared.

2.6.3. Experimental set-up.

A nanosecond time-resolved resonance Raman set-up must contain: a laser system to produce the monochromatic pump and probe pulses, a system of synchronisation of these

pulses in order to obtain a proper pump-probe delay time and a detection system consisting of a polychromator combined with a multichannel detector. Fig.2.13 represents the spectrometer operating in the nano/microsecond time scale, used in the Laboratoire de Spectrochimie Infrarouge et Raman by the group headed by Dr. G. Buntinx at the Université des Sciences et Technologies de Lille. A diode pumped Nd:YAG laser *Diva II Thales* generates 10 ns pump pulses at 355 nm (or 266 nm), with an energy of 4.0 mJ per pulse at a repetition rate of 20 Hz. The probe beam is produced by an optical parametric oscillator OPO (*Vega BM Industries*), which is pumped by a single longitudinal mode Nd:YAG laser (*5000 BM Industries*). This source ensures the generation of 6 ns, 0.3 cm^{-1}, pulses tunable in the 240 - 2200 nm spectral range, at a repetition rate of 20 Hz. Both, the pump and probe beams are focussed on the sample by using 300 mm focal length lenses. The time delay Δt between the probe and pump pulses is set by using a pulse generator *DG535 Stanford Research Sys.*, which triggers both lasers (see Fig.2.13). The scattered light is collected at 90° by an 80 mm focal length achromatic lens. The intense Rayleigh light (at wavelength of the probe, see Fig.2.12) is removed by using a holographic Notch filter. A 250 mm focal length focuses the scattered Raman light onto the polychromator entrance slit. This homemade 500 mm, focal length polychromator is equipped with a 1200 g/mm grating. A thermoelectrically cooled intensified photodiode array PDA (*DILOR*) is used as the multichannel detector.

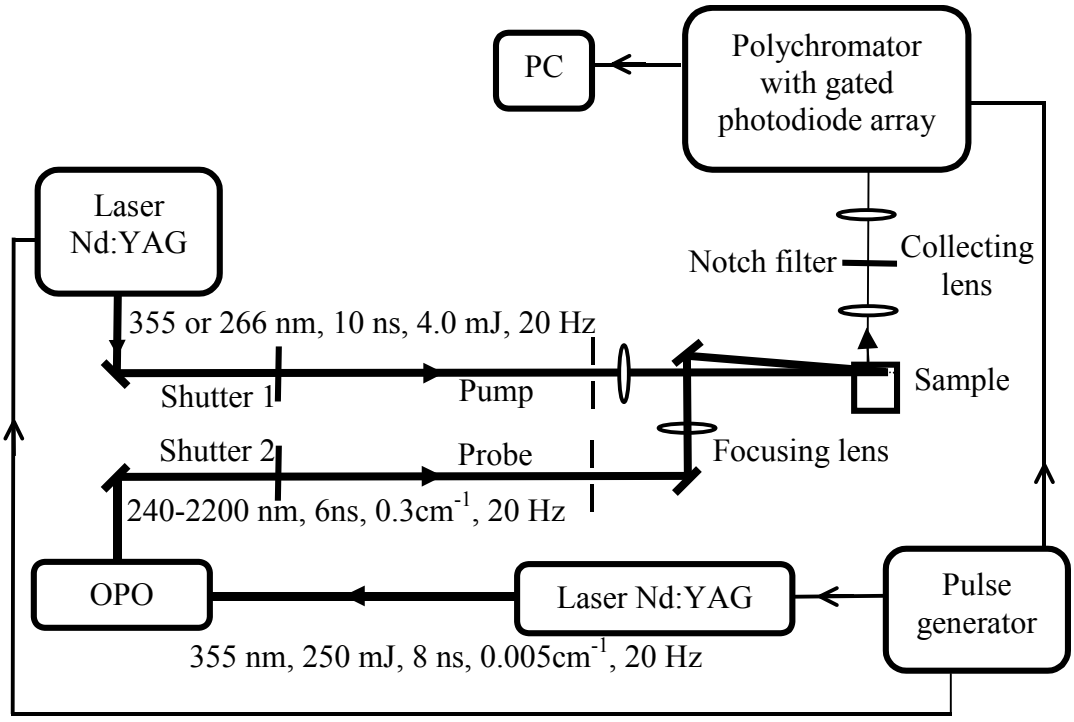

Figure 2.13. Experimental set-up used for nanosecond time-resolved resonance Raman spectroscopy.

The image intensifier enhances the intensity of the Raman spectrum and also acts as a shutter. The 20 ns shutter gate is temporarily centred on the probe pulse in order to allow all the Raman photons (present only during the probe pulse) to be detected by the PDA detector. When the shutter gate is closed, other photons coming from the fluorescence emission induced by the pump or from the phosphorescence emission lasting tens of microsecond are strongly rejected. This enables a large increase in the Raman spectra signal to noise ratio. The timing of the gate of the detector is controlled by the same *DG535* pulse generator to ensure a synchronised operation with the probe pulses. Data are transferred to a PC computer for processing. The spectral and temporal resolutions of the spectrometer are about 5 cm^{-1} and 10 ns, respectively. 5000 pump-probe pulse pairs are typically used to obtain one time-resolved resonance Raman spectrum.

The transient species resonance Raman spectrum result from two measurements:

- A spectrum recorded with the pump off and the probe on which corresponds to the solvent spectrum.
- A spectrum recorded with pump and probe on which contains the transient species spectrum plus the solvent spectrum.

The pure transient Raman spectrum is then calculated by an adequate subtraction of the first spectrum from the second one. The results can be distorted by some superposed straylight emissions. Usually emissions have a broad spectral distribution on which sharp Raman lines are superimposed, so a base-line correction can be used to subtract the emission spectrum from the transient species Raman spectrum. A more correct approach consists of recording a third spectrum with the pump on and the probe off. In this case we obtain only the emission spectrum, which can be subtracted from the spectrum resulting from the previous data treatment. Note, that in our case only the first method was applied.

2.7. Material and methods.

The aromatic thioketones under study (BPT, n-butyl derivative $BPTC_4$ and TC) were synthesised as previously described [46 - 48] and were purified by high-performance liquid chromatography (HPLC). For the time-resolved studies all spectroscopic grade solvents (Aldrich, Merck Uvasol,..) were used as received. Bidistilled water quality was employed. No impurities were detectable in the absorption and emission spectra of neat solvents.

Dimerisation and other aggregation of solutes were not observed for concentration up to 10^{-3} M.

For femtosecond transient absorption measurements a large volume of solution was used in order to avoid as much as possible the influence of photochemical consumption that occurs during the long accumulation time of the experiment. Usually, 50 ml of solution was prepared. The absorbance measured in a 2 mm thick cell was adjusted to about 0.2 at the excitation wavelength, which corresponds to a concentration of $10^{-4} \div 10^{-3}$ M. During the experiments, the solution was circulated in a 2 mm thick flow cell equipped with thin CaF_2 windows. The cell was routinely inspected to prevent bubbles or product formation on the windows, which may modify the transient absorption spectra.

Femtosecond fluorescence up-conversion measurements were performed in a 1 mm thick cell moving in a plane perpendicular to the excitation beam in order to minimise the solution from heating. To rule out the influence of photochemical consumption the sample was renewed after every single scan. Thioketones concentration were approximately 3×10^{-4} M.

For picosecond emission measurements, a quartz cell (1 mm × 1 cm) containing 1 ml of solution was used. The thioketone concentration was taken to be similar to that used in femtosecond transient absorption measurements for the sake of comparison.

Nanosecond transient absorption and emission experiments were performed for samples containing 4 ml of solution in a quartz cell (1cm × 1cm). The lifetime of the triplet T_1 state can be easily shortened by several orders of magnitude due to the quenching by oxygen, so the solution was deaerated by bubbling high purity nitrogen (or deoxygenated with helium that passed through a hot copper column to remove traces of O_2) for about 15 min prior to each experiment. An absorbance of about 1 at the laser excitation wavelength was generally used, which corresponds to approximately 1×10^{-4} M of thioketone.

For transient resonance Raman measurements higher concentrations of thioketone (about 0.5×10^{-3} M) were used to ensure a sufficient scattered photon flux containing signal. The solution was also placed in a quartz cell (1cm × 1cm).

All measurements were made at room temperature. After each time-resolved measurements, the quantum yield of net photochemical consumption of thioketone, was determined by measuring the absorbance changes of the solutions.

2.8. References.

1. C. Rullière, *Femtosecond Laser Pulses*, Springer-Verlag Berlin Heidelberg (1998).
2. J. R. Lakowicz, *Principles fluorescence spectroscopy-second edition*, Kluwer Academic / Plenum Publishers, New York, 1999.
3. J. N. Demas, *Excited-State Lifetime Measurements*, Academic Press: New York, 1983.
4. J. Karolczak, D. Komar, J. Kubicki, T. Wróżowa, K. Dobek, B. Ciesielska, A. Maciejewski, *Chem. Phys. Lett.*, 344 (2001)154.
5. J. Karolczak, D. Komar, J. Kubicki, M. Szymański, T. Wróżowa, A. Maciejewski, *Bull. Pol. Acad. Sci. Chem.*, 47 (1999) 361.
6. M. Van Der Zegel, N. Boens, D. Deams, F. C. De Schryver, *Chem. Phys.*, 101 (1986) 311.
7. F. H. Walters, S. L. Morgan, L. R. Parker, S. N. Deming, *Sequential simplex optimisation*, CRC Press LLC, 1991.
8. D. W. Marquardt, *J. Soc. Ind. Appl. Math.*, 11 (1963) 86.
9. M. A. Kahlow, W. Jarzeba, T. P. DuBruil, P. F. Barabra, *Rev. Sci. Instrum.*, 59 (1988) 1098.
10. P. Prosposito, D. Marks, H. Zhang, M. Glasbeek, *J. Phys. Chem. A*, 102 (1998) 8894.
11. P. Toele, H. Zhang, M. Glasbeek, *J. Phys. Chem. A*, 106 (2002) 3651.
12. M. L. Horng, J. A. Gardecki, A. Papazyan, M. Maroncelli, *J. Phys. Chem.*, 99 (1995) 17311.
13. V. I. Klimov, D. W. McBranch, *Opt. Lett.*, 23 (1998) 277.
14. I. Martini, G. V. Hartland, *Chem. Phys. Lett.*, 258 (1996), 180.
15. D. Strickland, G. Mourou, *Optics Comm.*, 56 (1985) 219.
16. K. Yamakawa, A. Magana, P. H. Chiu, *Appl. Phys. B*, 58 (1994) 323.
17. F. Salin, J. Squier, G. Mourou, G. Vaillancourt, *Ultrafast Phenomena VIII*, Springer-Verlag (1993).
18. D. Eimerl, L. Davis, S. Velsko, E. K. Graham, A. Zalkin, *J. Appl. Phys.*, 62 (1987) 1968.
19. R. R. Alfano, *The Supercontinuum Laser Source*, Springer-Verlag New York Inc. (1989).
20. R. L. Fork, C. V. Shank, C. Hirlimann, R. Yen, W. J. Tomlinson, *Opt. Lett.*, 8 (1983) 1.
21. R. R. Alfano, S. L. Shapiro, *Phys. Rev. Lett.*, 24 (1970) 592.
22. G. Buntinx, R. Naskręcki, O. Poizat, *J. Phys. Chem. A*, 100 (1996) 19380.
23. M. Lorenc, M. Ziolek, R. Naskrecki, J. Karolczak, J. Kubicki, A. Maciejewski, *Appl. Phys. B*, 74 (2002) 19.
24. K. Ekvall, P. van der Meulen, C. Dhollannde, L.-E. Berg, S. Pommeret, R. Naskrecki, J-C. Mialocq, *J. Appl. Phys.*, 87 (2000) 2340.

25. R. Bonneau, J. Wirz, A. D. Zuberbühler, *Pure & Appl. Chem.*, 69 (1997) 979.
26. L. M. Hadel, *CRC Handbook of Organic Photochemistry*, J. C. Scaiano ed., Vol. 1, CRS Press, Boca Raton, p. 279.
27. D. Bebelaar, *Chem. Phys.*, 3 (1974) 205.
28. F. van Mieghem, K. Brettel, B. Hillmann, /a. Kamlowski, A. W. Rutherford, E. Schlodder, *Biochemistry*, 34 (1995) 4798.
29. J. von Sonntag, *J. Photochem. Photobiol. A: Chemistry*, 126 (1999) 1.
30. J. A. Cline, C. D. Jonah, D. M. Bartles, *Rev. Sci. Instrum.*, 73 (2002) 3908.
31. K. Ushida, T. Nakayama, T. Nakazawa, K. Hamannoue, T. Nagamura, A. Mugishima, S. Sakimukai, *Rev. Sci. Instrum.*, 60 (1989) 617.
32. G. Baldachicino, B. Hickel, *Rev. Sci. Instrum.*, 69 (1998) 1605.
33. C. J. Kleverlaan, D. J. Stufkens, *J. Photochem. Photobiol. A: Chemistry*, 116 (1998) 109.
34. M. Koeberg, M. H. V. Werts, H. J. van Ramesdonk, J. W. Verhoeven, *EPA Newsletter*, 71 (2001) 21.
35. J. X. Zhou, X. Hou, K. X. Yang, S.-J. J. Tsai, R. G. Michel, *Appl. Spectroscopy*, 52 (1998) 176.
36. K. A. Hodgkinson, I. H. Munro, *J. Phys. B: Atom. Molec. Phys.*, 6 (1973) 1582.
37. A. C. Albrecht, *J. Chem. Phys.*, 34 (1961) 1476.
38. T. G. Spiro, P. Stein, *Ann. Rev. Phys. Chem.*, 28 (1977) 501.
39. R. J. H. Clark, T. J. Dines, *Molec. Phys.*, 45 (1982) 1153.
40. G. H. Atkinson, J. B. Pallix, T. B. Freedman, D. A. Gilmore, R. Wilbrandt, *J. Am. Chem. Soc.*, 103 (1981) 5069.
41. R. Rossetti, S. M. Beck, L. E. Brus, *J. Phys. Chem.*, 87 (1983) 3058.
42. H. Hamaguchi, 1987, Ed. J. R. Durig, *Vibrational Spectra and Structure*, Elsevier, Amsterdam, Vol. 16, 227.
43. M. R. Ondrias, M. C. Simpson, R. W. Larsen, *Modern Techniques in Raman Spectroscopy*, Chap. 9, p. 343, J. J. Laserna Ed., J. Wiley & Sons, 1996.
44. O. Poizat, G. Buntinx, *Revue de L`Institut Français du Pétrole,* 48 (1993) 287.
45. G. Buntinx, C. Lapouge, O. Poizat, *L`Actualité Chimique, Février 2001*.
46. A. Maciejewski, M. Szymanski, R. P. Steer, *J. Phys. Chem.*, 92 (1988) 6939.
47. M. Milewski, W. Urjasz, A. Maciejewski, W. Augustiniak, *Pol. J. Chem.*, 72 (1998) 2405.
48. M. Szymanski, A. Maciejewski, J. Kozlowski, J. Koput, *J. Phys. Chem. A*, 102 (1998) 677.

CHAPTER 3.

Photophysics of benzopyranthione and S_2 state quenching processes in solution.

3.1. Introduction.

The S_2 state of thioketones is known to be extremely reactive in solution due to the existence of an efficient intermolecular quenching processes by most of the solvents including saturated hydrocarbons and acetonitrile [1 - 6]. The S_2 state deactivation is exclusively intramolecular only in perfluorohydrocarbons (PFs) [1, 4 - 6]. A significant shortening of the S_2 state lifetime of thioketones (about one order of magnitude) is observed on going from PFs to acetonitrile or hydrocarbon solvents [4, 5]. The nature and mechanism of the solvent-induced thioketone S_2 state quenching processes are not fully understood. This chapter deals with the study of the quenching processes by hydrocarbons, acetonitrile and water of the model thioketone, 4H-1-benzopyrane-4-thione (BPT). Before going into the results, we present below a brief review of the actual knowledge of the quenching mechanism of thioketones by hydrocarbons, acetonitrile and water.

All the results published hitherto led to the conclusion that in hydrocarbons the S_2 state quenching of thioketones results from a hydrogen atom abstraction process from the solvent. De Mayo and co-authors have proposed such a reaction for aliphatic thioketones [7 - 9]. In the case of aromatic thioketones, the study of xanthione (XT) by picosecond time-correlated single photon counting method in hydrocarbons has demonstrated that the XT S_2 state quenching rate constant depends on the energy of the C-H bond and consequently on the number of primary, secondary and tertiary C-H bonds in the hydrocarbon molecule [6]. A kinetic isotope effect on the quenching rate constant ($k_H/k_D \approx 2$) has been observed upon deuteration of the quencher [10]. Recently, a hydrogen atom abstraction process has also been proposed as the quenching process of BPT by n-hexane [5]. In these studies, no short-lived species other than the emissive S_2 state of thioketones has been investigated since only fluorescence spectroscopy has been applied.

Acetonitrile has also been found to be an efficient quencher of the S_2 state of the XT from femtosecond transient absorption and picosecond time-correlated emission measurements [3, 4]. The formation of a S_2 state solute-solvent exciplex has been suggested as the intermolecular interaction responsible for the XT S_2 state quenching process. A very weak residual transient absorption signal, observed after subtraction of the S_2 and T_1 absorption bands, has been attributed to this exciplex. However, the low amplitude of this signal makes the assignment debatable [4]. One purpose of the present work will be to determine if the formation of such an exciplex can be identified in the case of BPT. The

isotope effect on the quenching rate constant was not checked in the case of XT. We will examine this point carefully for BPT.

Water has never been used as a solvent for time-resolved spectroscopic studies of thioketones. The main reason being their low solubility in water. Among all the thioketones, BPT is a good candidate for such measurements because of its relatively high solubility in water.

We have chosen to address the problem of BPT S_2 state quenching by hydrocarbons, acetonitrile and water by using different time-resolved spectroscopic techniques. Femtosecond fluorescence and picosecond time-correlated single photon counting techniques have been used to provide specific information on the BPT S_2 state while femtosecond transient absorption spectroscopy has been applied to characterise the non emissive short lived species. The ultrafast experiments have been completed with steady-state absorption and fluorescence as well as nanosecond transient absorption and phosphorescence measurements. The results obtained in hydrocarbon solvents have already been partially published by the author and by Maciejewski, Buntinx, Poizat and Lefumeux [11].

3.2. Hydrocarbon solvents [11].

3.2.1. Steady-state measurements.

Previous steady-state spectroscopic studies of BPT have concerned themselves with absorption, S_2 state fluorescence and T_1 state phosphorescence in various PFs, n-hexane and 3-methylpentane [1, 5]. The spectral properties were found to be similar in all solvents. Fig.3.1 presents the absorption and the fluorescence spectra of BPT in n-hexane at room temperature. The strong absorption band with a maximum at 365 nm (ε = 16060 $M^{-1}cm^{-1}$) has been interpreted as the strongly allowed $S_0 \rightarrow S_2$ ($\pi \rightarrow \pi^*$) transition. The shorter wavelength absorption bands correspond to $S_0 \rightarrow S_n$ transitions ($n \geq 3$). The fluorescence spectrum peaking around 450 nm has been assigned to the $S_2 \rightarrow S_0$ transition. The absence of direct fluorescence from the S_1 state is explained as result of its short lifetime $\tau_{S1} \approx 10^{-12}$ s due to an ultrafast $S_1 \rightarrow T_1$ intersystem crossing process and a small radiative rate constant of about 10^5 s^{-1} [12]. Although BPT at high concentration is known to form dimers in solution, an analysis of the shape and intensity of the absorption and emission spectra indicates that no aggregation of BPT occurs for concentrations up to 10^{-3} M. Thus, we assume that our time-resolved measurements performed in the 10^{-5} - 10^{-3} M concentration range are not affected by dimer formation. This point is important as it allows us to neglect the very efficient process of static self-quenching of the BPT S_2 state by BPT in the S_0 state that would certainly occur within dimeric entities. On the other hand, diffusional self-quenching is unlikely on the picosecond time scale of our measurements.

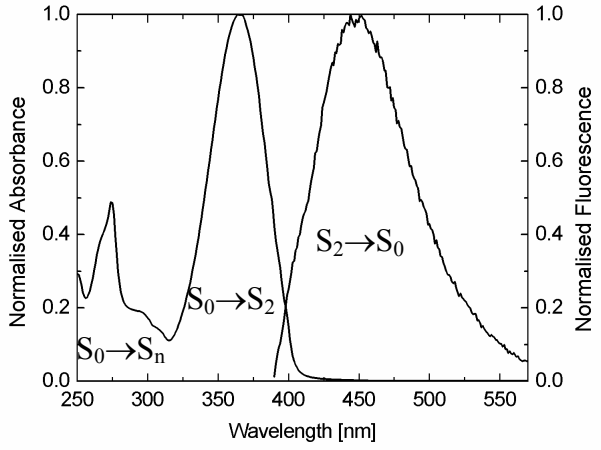

Figure 3.1. Steady-state absorption and emission (λ_{exc} = 370 nm) spectra of BPT in n-hexane.

Similarly, the influence of diffusional quenching of the BPT S_2 state by oxygen at atmospheric pressure (rate constant $k_{02} = 2.3\times10^{10}$ $M^{-1}s^{-1}$) can also be neglected in this time domain [5]. Two different pump excitation wavelengths of 380 nm and 403 nm were chosen for femtosecond transient absorption studies in order to estimate the influence of the vibrational relaxation in the observed S_2 state dynamics. Such a process was also investigated by femtosecond fluorescence up-conversion spectroscopy with excitation wavelengths of 330, 350 and 380 nm. As can be seen in Fig.3.1, the mentioned excitation wavelengths ensured a selective excitation of the S_2 state of BPT, because the energy difference between the vibrationally relaxed S_3 and S_2 states is about 7000 cm^{-1}. The longest excitation wavelength (403 nm) is situated at the low-energy edge of the $S_0\rightarrow S_2$ absorption band, which ensures a photoexcitation of BPT in the S_2-state without any excess of vibrational energy. For nano/microsecond transient absorption measurements a 355 nm pump wavelength was chosen.

3.2.2. Time-resolved fluorescence measurements.

Picosecond time-correlated single photon counting (TSCPC) and femtosecond fluorescence up-conversion (FFUC) are well suited techniques to investigate the dynamics of the fluorescent excited S_2 state of thioketones. Fig.3.2 presents the decay of the S_2 state fluorescence measured by TCSPC for BPT in cyclohexane-d_{12} and cyclohexane-h_{12} excited at 403 nm. Emission at 465 nm was observed close to the steady-state fluorescence maximum. The obtained lifetimes can be ascribed purely to the S_2 state lifetimes, τ_{S2}, without any contribution from vibrational relaxation processes (403 nm excitation) nor from molecular rotational diffusion effects (fluorescence was collected at the magic angle). Moreover, the random distribution along the axes of weighted residuals and autocorrelation function respectively, confirm the expected purely monoexponential decay of the BPT S_2 state population. The accuracy of the results is presented in Table 3.1, showing a high reproducibility of the calculated BPT S_2 state lifetimes τ_{S2} (32.9 ± 1.0 ps and 11.6 ± 1.0 ps for cyclohexane-d_{12} and cyclohexane-h_{12}, respectively). The S_2 state fluorescence decay was also measured at 530 nm. The results are summarised in Table 3.2. Table 3.2 shows that τ_{S2} lifetimes obtained for BPT in various solvents at two different emission wavelengths (465 and 530 nm) are identical within experimental error. The BPT S_2 state lifetimes in cyclohexane and cyclohexane-d_{12} were obtained by the author.

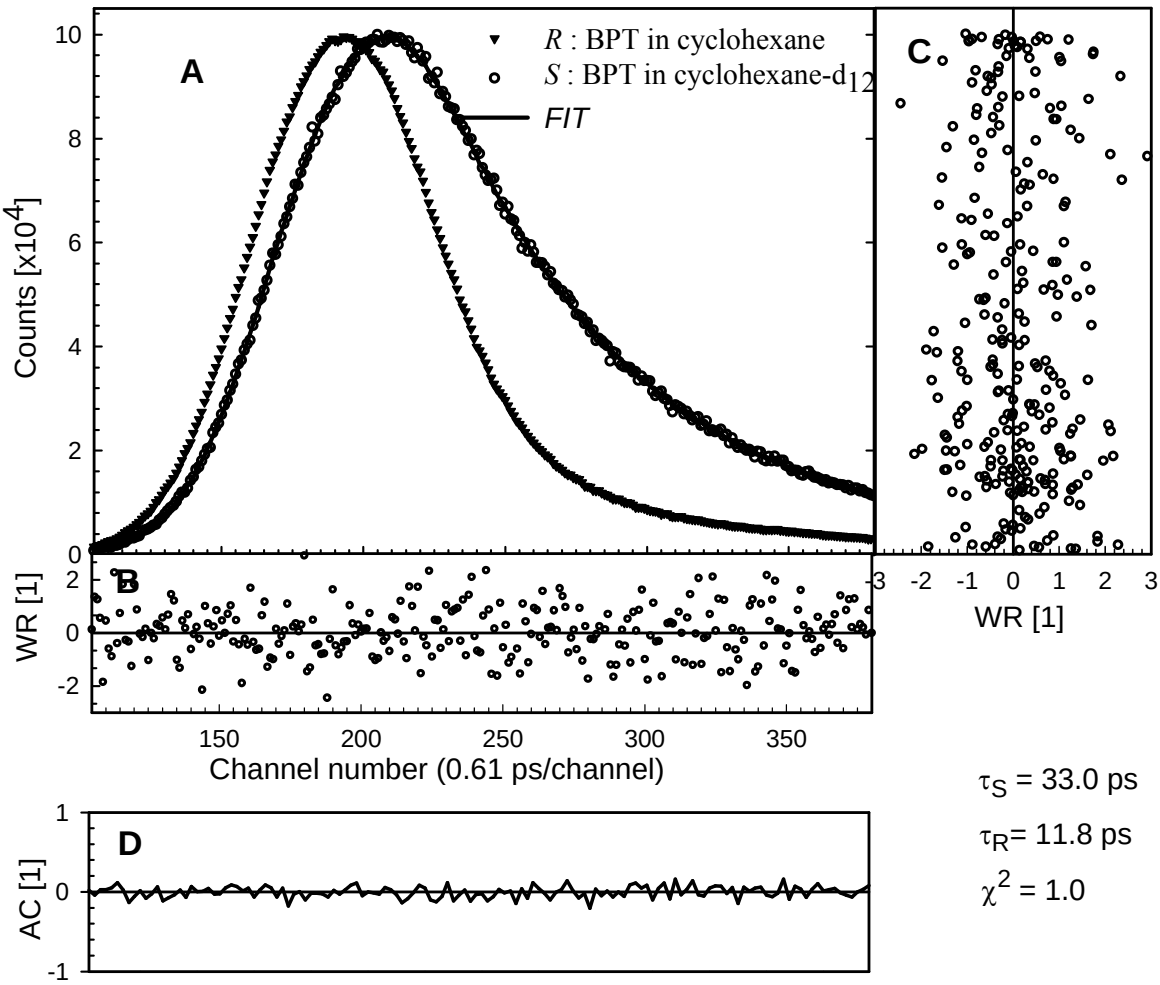

Figure 3.2. (A): Experimental decays of fluorescence (TCSPC) monitored at 465 nm obtained for BPT (1×10^{-3} M) at the magic angle, photoexcited at 403 nm, in: cyclohexane-d_{12} *(S-sample)* with fitted function *FIT* and cyclohexane *(R-reference)*. (B) and (C): Plot of the weighted residuals versus the time and the value of the *FIT* respectively. (D): Autocorrelation function of the weighted residuals.

However, Maciejewski et al previously determined a value of 19.5 ± 2.0 ps for BPT in n-hexane [5]. The FFUC spectroscopy technique was also used to confirm the results obtained by the TCSPC method. The lower sensitivity of the FFUC spectroscopy technique needed the use of a shorter excitation wavelength (380 nm) for which the absorption coefficient of BPT is higher. Thus, an excess of vibrational energy of about 1500 cm^{-1} was carried to the S_2 state. At a wavelength close to the maximum of the $S_2 \rightarrow S_0$ emission band (465 nm), a single-exponential decay is observed.

Table 3.1. Fluorescence lifetimes of BPT in the S_2 state obtained for 4 sets of samples S1→S4 (cyclohexane-d_{12}) and references R1→R4 (cyclohexane) data. The data have been processed as described in Chapter 2. The excitation and observation wavelengths were 403 and 465 nm respectively.

Sample	Reference	τ_S [ps] cyclohexane-d_{12}	τ_R [ps] cyclohexane-h_{12}	χ^2
S1	R1	32.4	11.0	1.0
	R2	32.6	11.2	1.0
	R3	32.8	11.3	1.0
	R4	32.3	10.7	1.0
S2	R1	33.0	11.7	0.9
	R2	32.8	11.5	0.9
	R3	33.0	11.5	1.0
	R4	32.8	11.3	0.9
S3	R1	33.1	12.0	1.0
	R2	33.1	12.0	1.0
	R3	33.4	12.3	1.1
	R4	32.9	11.7	0.9
S4	R1	33.1	12.0	1.1
	R2*	33.0	11.8	1.0
	R3	33.2	11.8	1.0
	R4	32.6	11.1	1.1

*see Fig.3.2

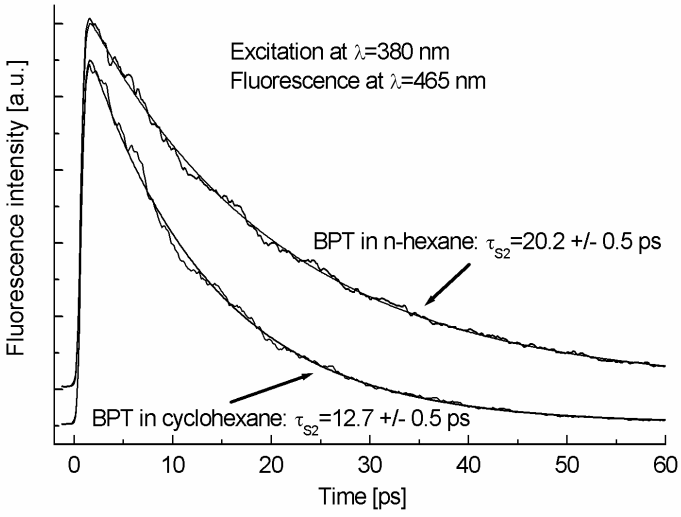

Figure 3.3. Single-exponential S_2 state fluorescence decays of BPT (3×10^{-4} M) in n-hexane and cyclohexane measured by femtosecond fluorescence up-conversion spectroscopy. The excitation and fluorescence wavelengths were 380 and 465 nm respectively.

Even measurements performed within a shorter time window (from -0.1 to - 3 ps) show an instantaneous rise of the signal (within 150 fs time resolution of the experimental set-up). Fluorescence kinetics measured in the blue or red wings of the emission band show a biexponential character of the S_2 state fluorescence decay. That will be discussed in detail in Chapter 4. Table 3.2 shows consistency between the τ_{S2} lifetimes of BPT in the S_2 state measured using the two different fluorescence techniques.

Table 3.2. Fluorescence lifetimes τ_{S2} of BPT in the S_2 state measured by TCSPC at 465 or 530 nm in n-hexane, cyclohexane-h_{12} and cyclohexane-d_{12}. The results obtained by FFUC spectroscopy are also shown.

BPT in:	$\lambda_{fluorescence}$ [nm]	TCSPC τ_{S2} [ps]	FFUC τ_{S2} [ps]
n-Hexane	465	19.5 ± 2.0*	20.2 ± 0.5
n-Hexane	530	19.5 ± 2.0*	20.2 ± 0.5**
Cyclohexane	465	11.6 ± 1.0	12.7 ± 0.5
Cyclohexane	530	11.0 ± 1.5	
Cyclohexane-d_{12}	465	32.9 ± 1.0	
Cyclohexane-d_{12}	530	31.8 ± 1.0	

*from reference [5] **a second time-constant (~2.8 ps) was found.

3.2.3. Nanosecond transient absorption and phosphorescence measurements.

Before going into detail, over the femtosecond transient absorption measurements, it is worth presenting the absorption and emission data obtained for BPT in n-hexane in the nanosecond/microsecond time scale. All measurements were made using deoxygenated solutions of BPT (≈ 6.5×10^{-5} M). The pump energy was 0.8 mJ per laser pulse. Transient absorption spectra and the corresponding kinetics recorded at 470 nm as well as the phosphorescence kinetics obtained at 630 nm are presented in Fig.3.4a, b and c respectively.

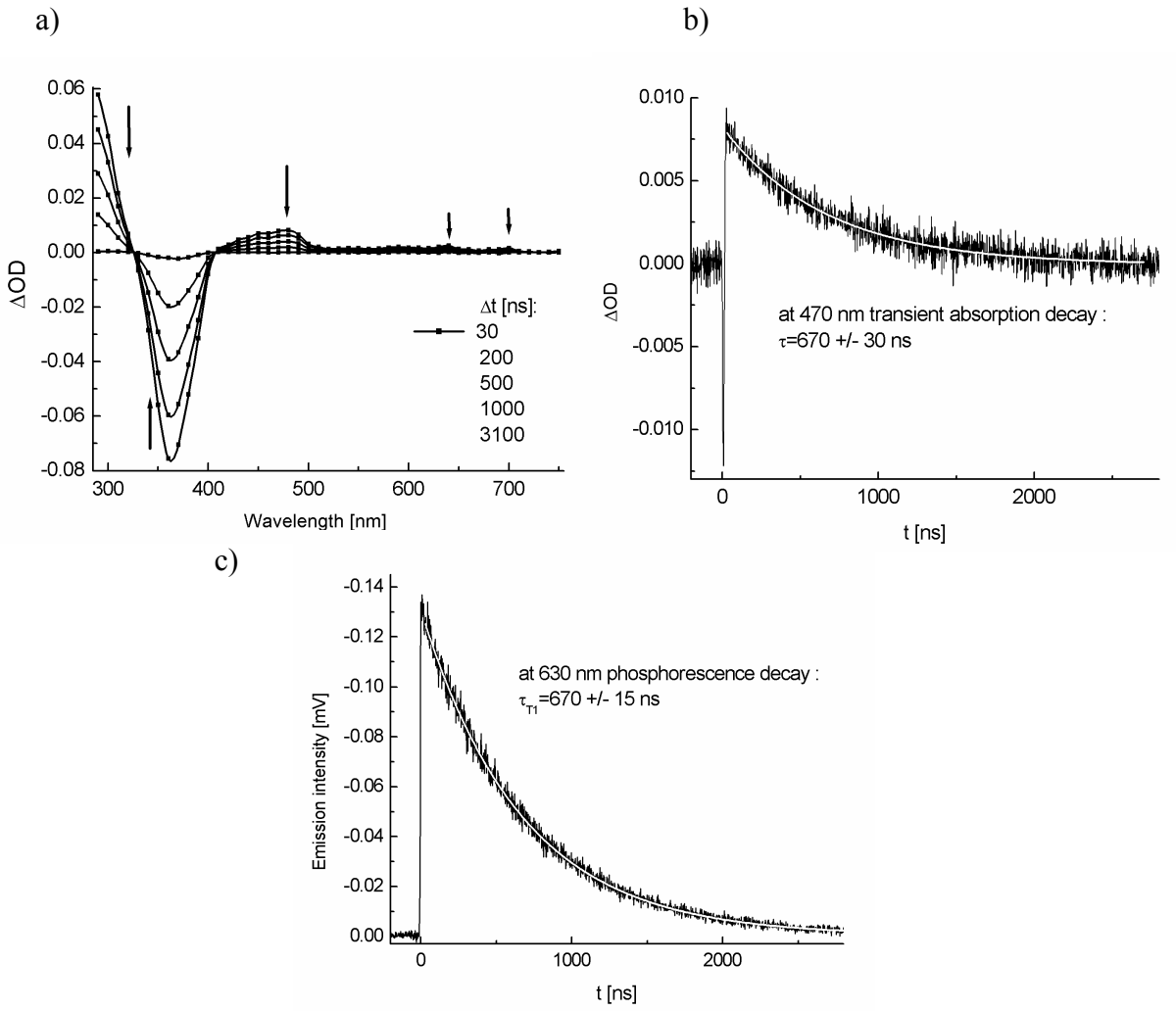

Figure 3.4. Time-resolved absorption and emission measurements of BPT (6.5×10^{-5} M) in n-hexane at 355 nm with an energy of 0.8 mJ per pulse. a) Transient absorption spectra within the 30 - 3100 ns time window (the phosphorescence emission contribution is subtracted). b) Transient absorption decay recorded at 470 nm. c) Phosphorescence emission decay recorded at 630 nm. The solid white lines correspond to the best single exponential fits to the experimental data.

The absorption kinetics recorded within the 290 - 750 nm spectral range (see Fig.3.4b) can all be fitted with a single exponential function with the same characteristic time (670 ns). The same time (670 ± 15 ns) is obtained from the phosphorescence decay $T_1 \rightarrow S_0$ recorded at 630 nm. We can thus ascribe the positive bands observed on the transient absorption spectra to the triplet state spectra. The negative band peaking at ≈370 nm corresponds to the Ground State Depletion (GSD) signal induced by the pump pulse. GSD dynamics is related to the recovery of BPT in the ground state due to $T_1 \rightarrow S_0$ transition. Very similar transient

absorption spectra, as well as, monoexponential signal decays, were obtained for BPT in inert perfluorohydrocarbon solvents (perfluoro-n-hexane, perfluoro-1,3-dimethylcyclohexane and perfluoro-tetradecahydrophenanthrene). There is thus no indication of the formation of an additional species such as a radical for BPT in hydrocarbons on this time scale.

It is worthwhile analysing the results in detail. Fig.3.4b represents the absorption decay recorded at 470 nm. In the -4 to 22 ns time window a negative signal that can be attributed to the S_2 state fluorescence is observed. The transient absorption spectra within a time window ranging from 30 to 3100 ns are presented in Fig.3.4a. In the 290 - 325 nm spectral region an intense absorption signal is observed, however its amplitude is reduced due to the superimposed negative signal of GSD. In the 325 - 410 nm spectral range only a negative band is observed which can be mainly attributed to the GSD signal due to the fact that its shape is very similar to that of the ground state absorption spectrum of BPT in n-hexane (see Fig.3.1). The extinction coefficient value ε(365nm) obtained from steady-state absorption measurements is 16060 $M^{-1}cm^{-1}$. In the 410 - 750 nm spectral range, only the absorption of the triplet state T_1 is observed and an approximated value of the extinction coefficient ε(470nm) of 1800 ± 300 $M^{-1}cm^{-1}$ can be estimated for the first time, from the ratio ε(365nm)/ε(470nm) ≈ 9. Note in Fig.3.4a and 3.6 that the presence of weak maxima at 580, 630, and 690 nm have never been observed, so far, due to poor signal-to-noise ratio of previously used experimental systems (see reference [13]). The 580 nm and 630 nm spectral positions of the T_1 absorption bands are consistent with the excitation spectrum of BPT in jet-cooled conditions using two photon resonance-enhanced processes $S_0 \xrightarrow{h\upsilon} T_1 \xrightarrow{h\upsilon} T_n \sim> S_2$ excited by an excimer-pumped pulsed dye laser [14].

A self-quenching rate constant of 2.0×10^{10} $M^{-1}s^{-1}$ and a triplet state lifetime of 7.1 μs have been determined for BPT in 3-methylpentane at infinite dilution using phosphorescence measurements [15]. From these data and according to the fact that 3-methylpentane and n-hexane present similar viscosity (0.31 cP and 0.3 cP, respectively), the Stern-Volmer equation (see Eq.1.1) allows us to predict a triplet state lifetime of 690 ± 30 ns for a 6.5×10^{-5} M concentration of BPT in n-hexane, which is experimentally confirmed (670 ± 15 ns).

3.2.4. Femtosecond transient absorption measurements.

Femtosecond transient absorption measurements were performed within a time window of 1 ps to 1.5 ns following the 380 or 403 nm excitation of BPT. Such studies were performed in both hydrocarbon solvents (n-hexane, dodecane, hexadecane, cyclohexane, cyclohexane-d_{12}) and also in perfluoro-n-hexane in order to establish the role of inter and intramolecular processes in the BPT S_2 state deactivation. The spectral evolution was nearly the same in all these solvents but the kinetics were different. As an example, Fig.3.5a shows the data obtained in the 430 - 750 nm spectral range upon 403 nm excitation of BPT in n-hexane between 1 and 100 ps. No further spectral evolution is observed on the 100 - 1500 ps time domain. At first sight, three spectral components can be distinguished in this evolution: on one hand, the 1 ps spectrum shows a negative band peaking at 460 nm and a positive one maximising around 650 nm, both decaying within 100 ps. On the other hand, the 100 ps spectrum shows a band peaking at 450 - 480 nm with a broad tail extending up to 750 nm that shows weak maxima at 580, 630, and 690 nm. The negative band has approximately the same spectral shape and position as the $S_2 \rightarrow S_0$ fluorescence spectrum in Fig.3.1. Thus, it can be ascribed to the stimulated $S_2 \rightarrow S_0$ emission.

a) b)

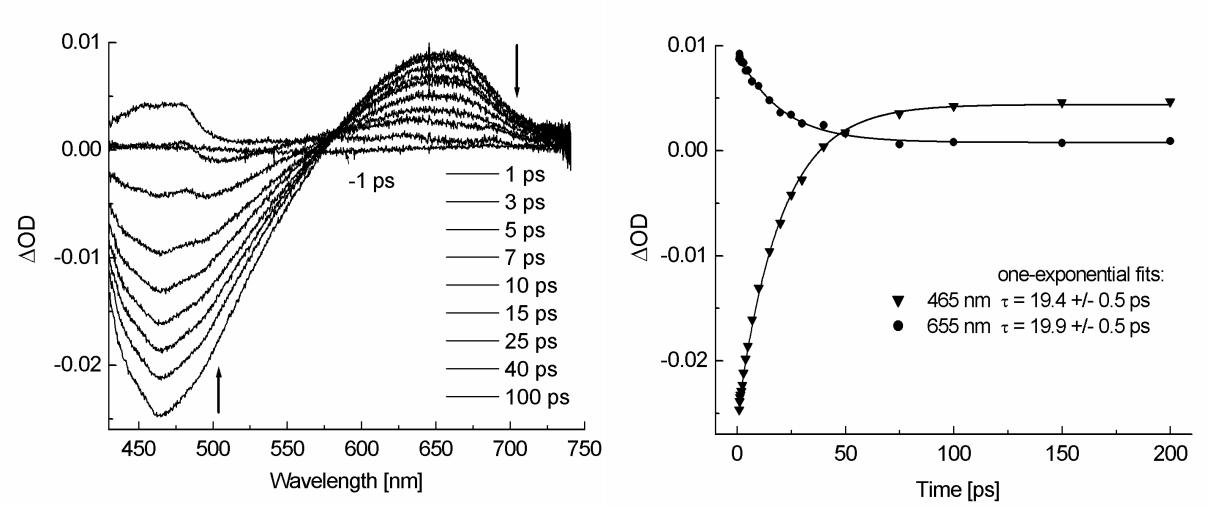

Figure 3.5. a) Transient absorption spectra recorded from 1 ps to 100 ps at the magic angle after photoexcitation of BPT (1×10^{-3} M) in n-hexane at 403 nm. The -1 ps spectrum (the probe pulse is set 1 ps before the pump pulse) is also given to show the background signal. b) Time-dependence of the signal at 465 nm (▼) and 655 nm (•) in the 1 - 200 ps time range. The solid lines are the best single exponential fits to the data.

An isosbestic point is observed at 585 nm between this negative band and the 650 nm positive band showing that both bands decay with the same kinetics and thus are likely to be the same species. Accordingly, we attribute the band peaking at 650 nm to the S_2 state absorption, $S_2 \rightarrow S_n$. After 100 ps, the final absorption spectrum can be attributed to the BPT triplet state transition, $T_1(n,\pi^*) \rightarrow T_n$, by analogy with the T_1 state spectrum recorded in the nanosecond time scale (see Fig.3.6).

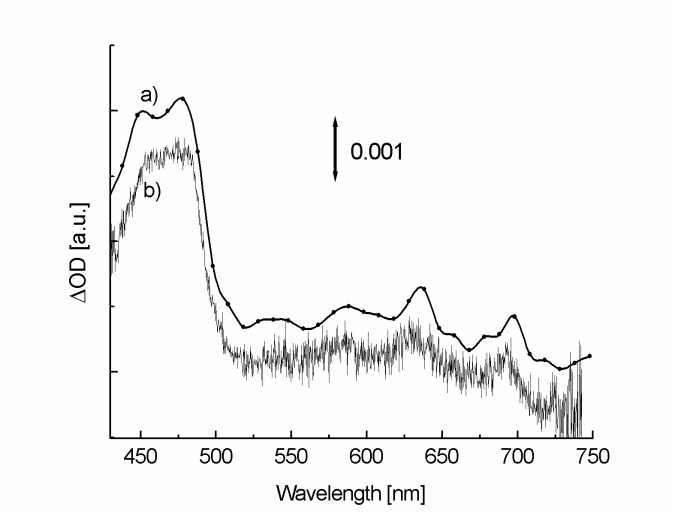

Figure 3.6. Transient absorption spectra obtained for BPT in n-hexane at pump-probe delays of a) 30 ns (the phosphorescence emission contribution is subtracted) and b) 100 ps (from Fig.3.5a). Both spectra are vertically shifted for a better presentation.

It is worth noting that the relative amounts of the initial S_2 state and final T_1 state species, as measured from the ratio $I_{max}(S_2)/I_{max}(T_1)$ of the S_2 absorption band intensity at 1 ps and T_1 state absorption band intensity at 100 ps, are nearly similar in all the investigated hydrocarbons, as well as in perfluoro-n-hexane. We can see in Fig.3.5a that the above mentioned ratio is approximately equal to $I_{max}(S_2)/I_{max}(T_1) = 2$. Applying the hypothesis that almost all the BPT molecules in the S_2 state deactivate to the T_1 state (this point will be discussed below), we can deduce that the extinction coefficients of the S_2 absorption band at 650 nm and T_1 absorption band at 480 nm follow the relation $\varepsilon_{S2}^{max} \sim 2\varepsilon_{T1}^{max}$. Thus, an approximate value of $\varepsilon_{S2}^{max} = 3600 \pm 300$ $M^{-1}cm^{-1}$ is derived from the $\varepsilon_{T1}^{max} = 1800 \pm 300$ $M^{-1}cm^{-1}$, a value determined from nanosecond transient absorption measurements. Finally, the fact that the isosbestic point at 585 nm (see Fig.3.5a) is not perturbed by the presence of the T_1 absorption band suggests that the S_2 decay and T_1 appearance have comparable kinetics. In summary, in hydrocarbon solvents and in

perfluoro-n-hexane, the spectral evolution can be accounted for by the presence of two species only, the excited S_2 and T_1 states. No indication of the formation of an additional species such as the excited S_1 state or a radical species is found. To get information on the kinetics, we quantified the time evolution of the transient absorption spectra every 10 nm by fitting the data with monoexponential functions using the non-linear least square Levenberg-Marquadt algorithm. Fig.3.5b represents an example of the kinetic traces at 465 nm (▼) and 655 nm (●) derived from the set of absorption spectra recorded for BPT in n-hexane in the 1 - 200 ps time range. The solid lines are the best single exponential fits to the data. Table 3.3 shows the time constants τ obtained from data fitting using single exponential functions for wavelengths ranging from 430 to 740 nm.

For each solvent (hydrocarbons and perfluoro-n-hexane), a single exponential function allows us to fit the kinetic traces at all wavelengths with the same characteristic time τ. The fact that the rise time in the 425 - 500 nm spectral region (where the S_2 stimulated emission and T_1 absorption overlap) is equal to the decay time of the S_2 absorption at 650 nm confirms that the triplet state appearance and S_2 state decay kinetics are synchronised. Care was taken to the choice of experimental conditions in order to avoid additional effects. Contributions from vibrational relaxation and from molecular rotational diffusion were excluded by adjusting the pump wavelength to the 0-0 transition and by setting the pump and probe beam polarisations at 54.7° (magic angle configuration). Moreover, the influence of solvation effects can also be neglected due to weak solvent-solute interactions (BPT S_2 state dipole moment is as small as 1 D) [16]. The time constant values obtained by femtosecond transient absorption (Table 3.4) and by fluorescence (Table 3.2) measurements are consistent within experimental error. Thus, the time constants presented in Table 3.4 can be considered as the BPT S_2 state lifetimes in the various studied hydrocarbon solvents. The BPT S_2 state lifetime in perfluoro-n-hexane (170 ± 10 ps), measured upon excitation at 380 nm, is also given in Table 3.4. The recording of a transient absorption spectrum using an excitation wavelength of 403 nm was unfeasible due to the low solubility of BPT in perfluoro-n-hexane and also due to the low absorption extinction coefficient of BPT in its ground state at this wavelength. The slightly shorter lifetime 170 ± 10 ps obtained by transient absorption measurements versus 183.5 ± 2 ps measured by TCSPC [5] can be explained by a difference in purity of the solvents. The shortening of the BPT S_2 state lifetime from 170 ps to less than 20 ps on going from the perfluoro-n-hexane to the hydrocarbon solvents confirms the existence of an efficient intermolecular quenching process in the latter case.

Table 3.3. Time-constants τ and amplitudes of monoexponential functions fitted to the kinetic traces derived from data presented in Fig.3.5a in the 1 - 200 ps time range for selected wavelengths in the 430 - 740 nm spectral range.

Selected wavelength [nm]	Amplitude	τ [ps]
430	-0.0158	19.6
440	-0.0223	19.9
450	-0.0257	20.0
460	-0.0280	19.8
470	-0.0282	19.9
480	-0.0268	20.1
490	-0.0236	19.4
500	-0.0199	18.8
510	-0.0165	19.0
520	-0.0134	19.1
530	-0.0108	19.6
540	-0.0082	19.1
550	-0.0060	19.6
560	-0.0038	18.5
570	-0.0019	19.4

Selected wavelength [nm]	Amplitude	τ [ps]
590	0.0018	19.5
600	0.0036	20.7
610	0.0051	20.6
620	0.0061	20.2
630	0.0069	20.0
640	0.0077	20.0
650	0.0082	19.9
660	0.0083	20.7
670	0.0080	20.4
680	0.0066	19.6
690	0.0045	17.9
700	0.0033	19.6
710	0.0028	20.2
720	0.0021	21.5
730	0.0018	22.3
740	0.0020	21.6

For instance, the ratio of the τ_{S2} values in perfluoro-n-hexane and in n-hexane shows that the C_6H_{14} molecules quench at least 90 % of BPT molecules in the S_2 state. Note that the BPT S_2 state lifetime in cyclohexane-d_{12} is about three times longer that in cyclohexane-h_{12}. This kinetic isotope effect, observed upon deuteration of the solvent, confirms that the hydrogen atoms of the solvent are involved in the quenching process of the S_2 state by hydrocarbon solvents. The amplitude of this isotope effect is similar to that usually observed for hydrogen atom transfer reactions. For instance, between cyclohexane and the azoalkanes S_1 state or xanthone T_1 state [17, 18]. Accordingly, we assigned the BPT S_2 state quenching mechanism to a hydrogen atom transfer from the solvent to the excited state.

Table 3.4. S_2 state lifetime for BPT in different solvents (403 nm excitation).

Solvent	τ_{S2} [ps]
n-Hexane	20.0 ± 1.0
Dodecane	17.0 ± 1.0
Hexadecane	16.3 ± 1.0
Cyclohexane	13.1 ± 1.0
Cyclohexane-d_{12}	35.8 ± 2.0
Perfluoro-n-hexane	170 ± 10

The BPT energy gap value $\Delta E(S_2\text{-}S_1)$ is practically identical in all hydrocarbons used (about 8500 cm^{-1}), so according to the energy gap law (see Eq.1.2) the radiationless rate constant k_{nr} must be the same. However, Table 3.4 shows that the τ_{S2} lifetime is progressively shortened from 20.0 to 13.1 ps on going from n-hexane to dodecane, then hexadecane, and finally cyclohexane, which reflects a gradual increase of the quenching rate constant. From a structural point of view, this increase can be correlated to the increasing number of solvent secondary carbon atoms relative to the primary ones through this series of hydrocarbons [3, 6]. This effect is due to the fact that the C-H bond on a secondary carbon atom has a slightly lower energy than on a primary one [19 - 21]. The low energy of the BPT S_2 state ($E_{S2} \approx 72.8$ kcal/mol) enables us to differentiate the dynamics of hydrogen abstraction from these two sites. In this respect, for each hydrocarbon, the overall quenching rate constant k_H has a statistical character and can be expressed as a function of two specific rates $k_H(I)$ and $k_H(II)$ characterising the quenching rates by the hydrogen atom on the primary and secondary carbon sites respectively [6]:

$$k_H = \frac{A}{N} \cdot k_H(I) + \frac{B}{N} \cdot k_H(II), \qquad (3.1)$$

where N is the total number of C-H bonds in the hydrocarbon molecule, and A and B are the numbers of C-H bonds on the primary and secondary carbon sites, respectively.

According to the low quantum yield of photochemical decomposition (<0.4 %) [1], an accurate value of k_H can be estimated from the expression (see its general formula Eq.1.4):

$$\tau_{S2} = \frac{1}{k_r + k_{nr} + k_H}, \qquad (3.2)$$

where k_r and k_{nr} are the radiative and radiationless rate constants, respectively. The value k_r+k_{nr} can be determined directly from the S_2 state lifetime in inert perfluorohydrocarbons

where the excited state undergoes only intramolecular deactivation. From previous studies, it appears that perfluoro-tetradecahydrophenanthrene (PFTDHP) is the perfluorohydrocarbon solvent where the intramolecular properties of BPT S_2 state are the closest to those found in hydrocarbons (similar k_r and $\Delta E(S_2\text{-}S_1)$ energy gap values for BPT) [5, 6]. The fluorescence decay of the S_2 state of BPT in PFTDHP gives the τ_{S2} lifetime of 177 ± 2 ps**,** which corresponds to $k_r+k_{nr} = 5.6\times10^9\ s^{-1}$ (see Table 1.1). The BPT S_2 state quenching rate constants k_H deduced from this value by using Eq.3.2 in n-hexane, dodecane, hexadecane, and cyclohexane, are presented in Table 3.5. The specific rate constants $k_H(I)$ and $k_H(II)$ calculated from Eq.3.1 characterising the quenching of BPT S_2 state by hydrogen atoms localised on primary and secondary carbon sites respectively, are also given in Table 3.5.

Table 3.5. BPT S_2 state lifetime τ_{S2} measured by femtosecond transient absorption spectroscopy, total quenching rate constant k_H, and specific quenching rate constants $k_H(I)$ and $k_H(II)$ determined from the number of C-H bonds on the primary (*A*) and secondary (*B*) carbon atoms in the four investigated hydrocarbon solvents.

Solvent	τ_{S2}[ps] ± 1.0	$k_H\times10^{10}$ [s^{-1}]	Number of C-H bonds		$k_H(I)\times10^{10}$ [s^{-1}]	$k_H(II)\times10^{10}$ [s^{-1}]
			A	B		
n-Hexane	20.0	4.4	6	8	1.8	6.4
Dodecane	17.0	5.3	6	20	1.8	6.4
Hexadecane	16.3	5.6	6	28	1.8	6.4
Cyclohexane	13.1	7.1	0	12	-	7.1

It is evident that, for a given C-H bond, not only the energy of this bond but also the accessibility of the H atom to the thio group of BPT in the S_2 state (steric hindrance effect) should be considered in the dynamics of quenching by H-atom abstraction. This aspect is not taken into account in Eq.3.1. However, the hydrocarbon solvents were chosen in this way, so that easy access to all C-H bonds is equally possible. Table 3.5 shows that $k_H(I)$ and $k_H(II)$ values are constant for the three linear hydrocarbon solvents used. Thus very similar C-H energy bonds in CH_3 groups or in all CH_2 groups (4 in n-hexane, 8 in dodecane, 14 in hexadecane) can be assumed whatever their position in the hydrocarbon chain. This is a very important conclusion regarding the controversies, which exist around this subject [19, 22] and the difficulties in acquiring accurate measurements for the energy of the different C-H bonds

[20, 21]. The results obtained for BPT and similarly those obtained for XT [6] in linear hydrocarbon solvents, show that the significant decrease in the energy of the secondary C-H bonds in subsequent methylene groups in the hydrocarbon chain postulated by Semenov [22] is not correct.

Table 3.5 shows a higher rate constant $k_H(II)$ calculated for cyclohexane (7.1×10^{10} s^{-1}) compared to that in linear hydrocarbons (6.4×10^{10} s^{-1}). The reason for that may be a slightly lower secondary C-H bond energy in the cyclic hydrocarbon molecule [20, 21]. The BPT S_2 state quenching rate constants $k_H(I)$ and $k_H(II)$ are about 20 % higher than those previously reported for xanthione S_2 state ($k_H(I) = 1.4\times10^{10}$ s^{-1}, $k_H(II) = 5.0\times10^{10}$ s^{-1}) [6]. This can be explained by the higher reactivity of the S_2 state of BPT (E_{S2}~72.8 kcal/mol) compared to that of xanthione (E_{S2}~67 kcal/mol). However, as expected, a similar ratio of $k_H(I)/k_H(II) = 0.28$ is found for the S_2 state of BPT and xanthione. Finally, the rate constant k_D for the quenching by deuterated cyclohexane, determined from Eq.3.2 by supposing that the k_r+k_{nr} value is unchanged compared to that in hydrogenated cyclohexane and amounts to 2.2×10^{10} s^{-1}. It corresponds to a ratio $k_H(II)/k_D(II)$ of 3.2, which is consistent with the 3.3 value obtained for XT S_2 state in the same solvents measured by TCSPC [23].

Since the BPT S_2 state quenching involves hydrogen atoms on primary and secondary carbon sites, different activation energies must characterise these two different quenching reactions. A higher activation barrier can explain the lower quenching rate constant $k_H(I)$ compared to $k_H(II)$ calculated for the quenching by hydrogen atom on primary and secondary carbon site, respectively. The activation barrier can be calculated using the Arrhenius Eq.3.3 [24], which is usually used to determine the activation energy E_a from the dependence of the reaction rate constant k on temperature T:

$$k = A\,exp(-E_a / RT), \tag{3.3}$$

where A is a constant, E_a is the activation energy, R is the universal gas constant (8.314 $Jmol^{-1}K^{-1}$). The ratio of the quenching rate constants for two comparable systems (BPT S_2 state in hydrocarbons and in water, see Table 1.1) assuming the same constant A value can be written by the following formula:

$$\frac{k_1}{k_2} = \frac{exp(-E_{a1} / RT)}{exp(-E_{a2} / RT)}. \tag{3.4}$$

For BPT in hydrocarbon solvents, one can successively consider k_1 to be equal to the quenching rate constant $k_H(I)$ or $k_H(II)$.

Table 3.6. Calculated activation energy barriers for BPT S_2 state quenching by linear hydrocarbons at T=293 K.

C-H bond	Quenching rate constant k_1 [$\times 10^{10}$ s^{-1}]	Assumed rate constant k_2 [$\times 10^{12}$ s^{-1}]	Activation energy E_{a1} [kJ/mol]
Primary	1.8	1	10
Secondary	6.4	1	7

For the calculations of the activation energy, k_2 is assumed to be 1×10^{12} s^{-1}, the value of which is close to the highest intermolecular quenching rate constant found for BPT in water (see Table 1.1). This high k_2 rate constant corresponds to an almost barrierless reaction ($E_{a2}\approx0$ in Eq.3.4). Table 3.6 shows the activation energy (E_{a1}) calculated for both the considered S_2 state quenching mechanisms occurring with rate constant $k_H(I)$ or $k_H(II)$. The activation energy for the quenching of BPT S_2 state by hydrogen atom on primary and secondary carbon sites are 10 ± 4 kJ/mol and 7 ± 4 kJ/mol, respectively.

3.2.5. Discussion.

The results obtained for BPT in perfluoro-n-hexane can be easily interpreted in the light of earlier established photophysical properties of BPT. Observations of an apparent direct deactivation of the S_2 state towards the T_1 state are consistent with the absence of S_1 absorption. It agrees with the previously proposed intramolecular deactivation pathway $S_2\rightarrow S_1\rightarrow T_1$ [1, 2, 5, 25] if the lifetime of the S_1 state is assumed to be much shorter than the S_2 and T_1 states lifetimes. Such a hypothesis is consistent with the S_1 state lifetime of ~0.5 ps that has been measured experimentally in real time for thioxanthione in three solvents of different properties (acetonitrile, acetone, 1-octanol) [12]. As the $S_1\rightarrow T_1$ intersystem crossing process (ISC) is much faster than any other deactivation process of the S_1 state (fluorescence or internal conversion to the ground state), the quantum efficiency of population of the T_1 state from the S_1 is nearly unity [25]. This high efficiency of the ISC can be explained not only by the presence of thiocarbonyl heavy sulphur atom, but also by the El-Sayed rule [26, 27]. This rule describes the relationship that exists between the ISC rate constant and the electronic configuration of the excited states. Transitions between states of different electronic configurations (for instance $^1(n,\pi^*)\rightarrow{}^3(\pi,\pi^*)$) are allowed and take place efficiently, while transitions between states of the same electronic configuration (for instance $^1(n,\pi^*)\rightarrow{}^3(n,\pi^*)$)

are prohibited. The nature of the lowest triplet state T_1 of BPT in hydrocarbon solvents is (n,π^*). Consequently a direct ISC $S_1(n,\pi^*)\rightarrow T_1(n,\pi^*)$ can not take place efficiently. The presence of $T_2(\pi,\pi^*)$ state very close to the T_1 state allows an efficient $S_1(n,\pi^*)\rightarrow T_2(\pi,\pi^*)\rightarrow T_1(n,\pi^*)$ deactivation.

Three author's observations show that the S_2 state of BPT is quenched by a process involving the reaction coordinate of intermolecular hydrogen-atom abstraction from the hydrocarbon solvent:

- The shortening by about one order of magnitude of the S_2 lifetime in all the hydrocarbon solvents compared to that measured in perfluoro-n-hexane.
- The notable isotopic effect observed on the S_2 state lifetime upon deuteration of the solvent (k_H/k_D=3.2 in cyclohexane).
- The dependence of the S_2 state lifetime on the mean energy of the solvent C-H bonds.

Such a reaction of H-atom transfer to the S_2 state has been proposed for a number of aliphatic and aromatic thioketones [1, 7, 8, 28]. However, surprisingly, this quenching process does not lead to any detectable primary reaction products. Even the application of femtosecond transient absorption spectroscopy within this thesis does not provide evidence of the presence of the radical species $BPTH^{\bullet}$ expected as a result of the hydrogen atom abstraction reaction. Moreover, the transient absorption measurements performed in n-hexane and perfluoro-n-hexane indicate that the yield of formation of the T_1 state of BPT is comparable in hydrocarbons and PF solvents, in agreement with what was deduced from steady-state phosphorescence measurements [29]. We conclude that the S_2 state intermolecular quenching reaction in hydrocarbon solvents leads to the T_1 state with the same efficiency as the intramolecular deactivation pathway in PF solvents. Finally, the T_1 state growth kinetics are not delayed relative to the S_2 state decay kinetics. Two plausible interpretations for these observations are proposed.

First, it can be envisaged that the radical products, $BPTH^{\bullet}$ and hydrocarbon ($-H^{\bullet}$) (designated as $R^{\bullet}$ in the following), are actually formed by H-atom abstraction at rates $k_H(I)$ and $k_H(II)$ from the primary and secondary carbon atoms respectively, of the hydrocarbon donor, but have extremely low instantaneous concentrations due to the very short lifetime of $BPTH^{\bullet}$. This lifetime is estimated to be less than 3 ps, because a longer $BPTH^{\bullet}$ lifetime would significantly disturb the single exponential character of the transient absorption kinetics in the spectral range where the decay of the stimulated emission and the rise of the triplet state absorption are observed. The literature provides a few examples of short-lived radicals (even

less than 1 ps), although they are created exclusively by photodissociation of the parent molecule [30 - 33]. Extremely low instantaneous concentrations of the BPTH$^{\bullet}$ radical would make it impossible to detect by transient absorption spectroscopy. This short lifetime could be explained by an ultrafast spin-allowed process of geminate cage recombination of BPTH$^{\bullet}$ and R$^{\bullet}$ (back H-atom transfer) to yield the BPT S_1 state and the parent RH ground state molecule (rate $k_{-H} >> k_H$). The triplet state is then produced by intersystem crossing from S_1 (rate constant k_{ISC}) as in the intramolecular deactivation pathway. The corresponding reaction is summarised in Scheme 3.1.

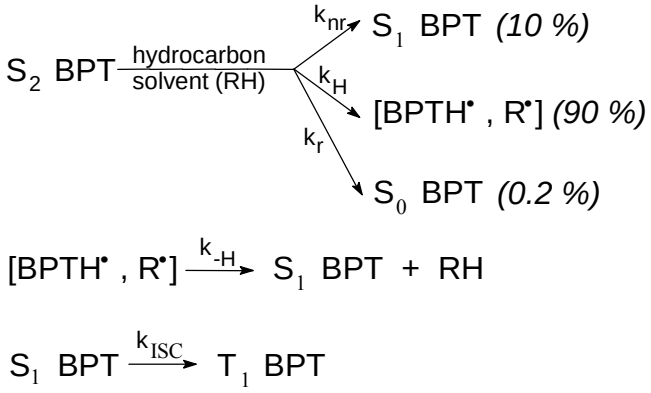

Scheme 3.1.

From previous structural studies of thiocarbonyl radicals [8, 28, 34, 35], we can expect two types of BPTH$^{\bullet}$ radicals, i.e. the sulphur centred (Ar-HC-S$^{\bullet}$) form or/and the carbon centred (Ar-C$^{\bullet}$-SH) one. Its short lifetime supports the suggestion made by de Mayo, on the basis of an analysis of the stable photoproducts, that the radical formed in the case of hydrogen abstraction by the $S_2(\pi,\pi^*)$ state of adamantanethione in cyclohexane has a 2 ps lifetime [7, 8]. In this study, a very fast radical recombination process in the solvent cage with only 10 % of radical escape was also assumed to account for the short lifetime of the adamantanethione radical.

An alternative interpretation of our results would be that the reaction is entirely inefficient, despite the efficient S_2 state quenching. The radical products, BPTH$^{\bullet}$ and R$^{\bullet}$, are not really formed. Such a situation corresponds to the so-called "aborted hydrogen atom abstraction", a concept proposed and widely studied by Nau et al. for the quenching of the excited $S_1(n,\pi^*)$ state of azoalkanes and ketones by hydrogen donor solvents [17, 36 - 39]. It arises in the case of weakly exothermic, or even endothermic, hydrogen abstraction processes, if a conical intersection between the excited-state and the ground state potential energy surfaces lies on the way to the products in the proximity of the transition state. The system starts to progress along the reaction coordinate of hydrogen abstraction (as attested by the

observed isotope effect) but the reaction is interrupted on the excited-state surface at the conical intersection, which provides an efficient radiationless decay channel towards the ground state. The view that this deactivation route might apply to the photochemical reactivity of BPT in hydrocarbons is plausible by presuming that the conical intersection links the excited S_2 and S_1 state surfaces, as shown in Fig.3.7. The actual place of the conical intersection point on the potential energy surface would need theoretical evaluation. The quenching process would thus correspond to that shown in Scheme 3.2.

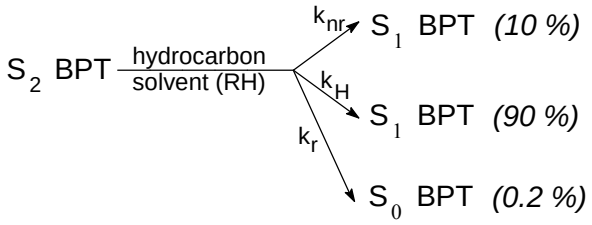

Scheme 3.2.

The two schemes are consistent with the observation that the T_1 state grows and the S_2 state decay have the same kinetics and that the T_1 state yield is comparable to that measured in inert perfluorohydrocarbon solvents. They can also account for the observed kinetic isotope effect.

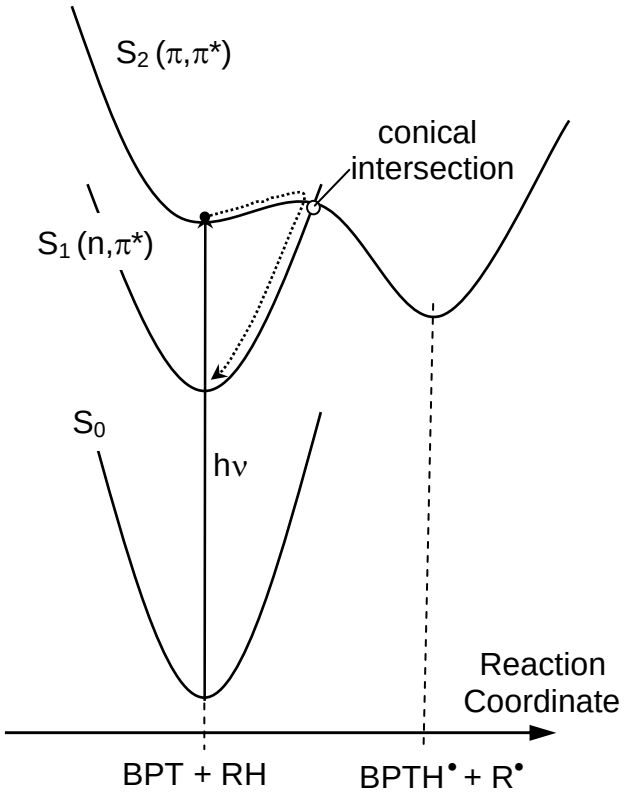

Figure 3.7. Schematic potential energy surface diagram corresponding to: aborted hydrogen abstraction from hydrocarbon (RH) in the S_2 state of BPT.

The involvement of the hydrocarbon C-H bonds in the quenching process has been evidenced on the basis of three observations: (1) a shortening by about one order of magnitude of the S_2 state lifetime in hydrocarbons relative to that in perfluorohydrocarbons, (2) a notable kinetic isotope effect on the quenching process upon deuteration of the hydrocarbon molecule (k_H/k_D=3.2), and (3) a dependence of the S_2 state quenching rate constant on the mean energy of the hydrocarbon C-H bonds. We conclude that the reaction coordinate of intermolecular hydrogen atom abstraction is involved in the quenching process. The fact that the radical products expected in this reaction are not observed can be explained either by assuming that ultrafast back hydrogen transfer occurs in solvent cage, or by considering that the reaction is aborted well before the hydrocarbon C-H bond breaking and the BPT-H$^{\bullet}$ bond formation are completed. In the latter case, the progress along the reaction path to a conical intersection is assumed to lead to electronic deactivation of S_2 through transition to the S_1 state energy surface.

3.3. Acetonitrile solvent.

3.3.1. Steady-state measurements.

Fig.3.8 shows the results of steady-state absorption ($S_0 \rightarrow S_n$, $n \geq 2$) and S_2 fluorescence studies of BPT in acetonitrile. The spectral properties are similar to those obtained in hydrocarbons (see Fig.3.1). The strong absorption band ($S_0 \rightarrow S_2$ transition) has a maximum at 371 nm (ε = 17900 $M^{-1}cm^{-1}$). For concentrations of BPT up to 10^{-3} M, the shape and intensity of the absorption and emission spectra do not indicate any aggregation of BPT molecules. Thus, time-resolved measurements performed using concentrations between 10^{-5} - 10^{-3} M are not be affected by dimers formation.

The choice of pump wavelengths at 355, 380 and 403 nm ensures a selective excitation to the S_2 state of BPT, because the energy difference between the vibrationally relaxed S_3 and S_2 states is about 7000 cm^{-1}.

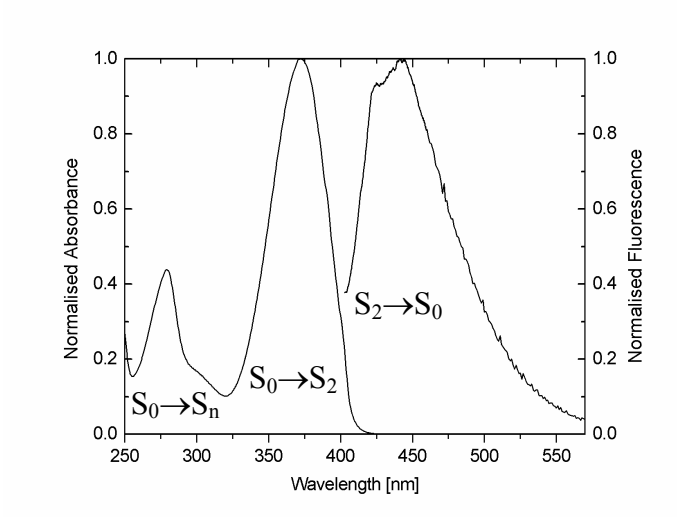

Figure 3.8. Steady-state absorption, $S_0 \rightarrow S_2$, $S_0 \rightarrow S_n$ ($n \geq 3$), and emission $S_2 \rightarrow S_0$ spectra of BPT in acetonitrile (λ_{exc} = 403 nm).

3.3.2. Time-resolved fluorescence measurements.

In order to characterise the lifetime τ_{S2} of the fluorescent S_2 state of BPT, we used the picosecond time-correlated single counting (TCSPC) method, as well as, the femtosecond fluorescence up-conversion (FFUC) technique. The molecular rotational diffusion effects were eliminated, since experiments were performed using the magic angle configuration. One of the advantages of the TCSPC technique is its high sensitivity, so we were able to use a

pump wavelength set at 403 nm, which provides almost no significant vibrational excitation in the S_2 state. The less sensitive FFUC method required a shorter excitation wavelength (380 nm) in order to pump the BPT molecules more efficiently. Fig.3.9 represents the measurements performed for BPT in acetonitrile and in acetonitrile-d_3. The TCSPC results obtained for two different monitored wavelengths of the S_2 state emission (470 nm and 530 nm) are presented in Table 3.7. The S_2 state lifetime of BPT in acetonitrile-d_3 is about 1.6 times longer than that in acetonitrile-h_3.

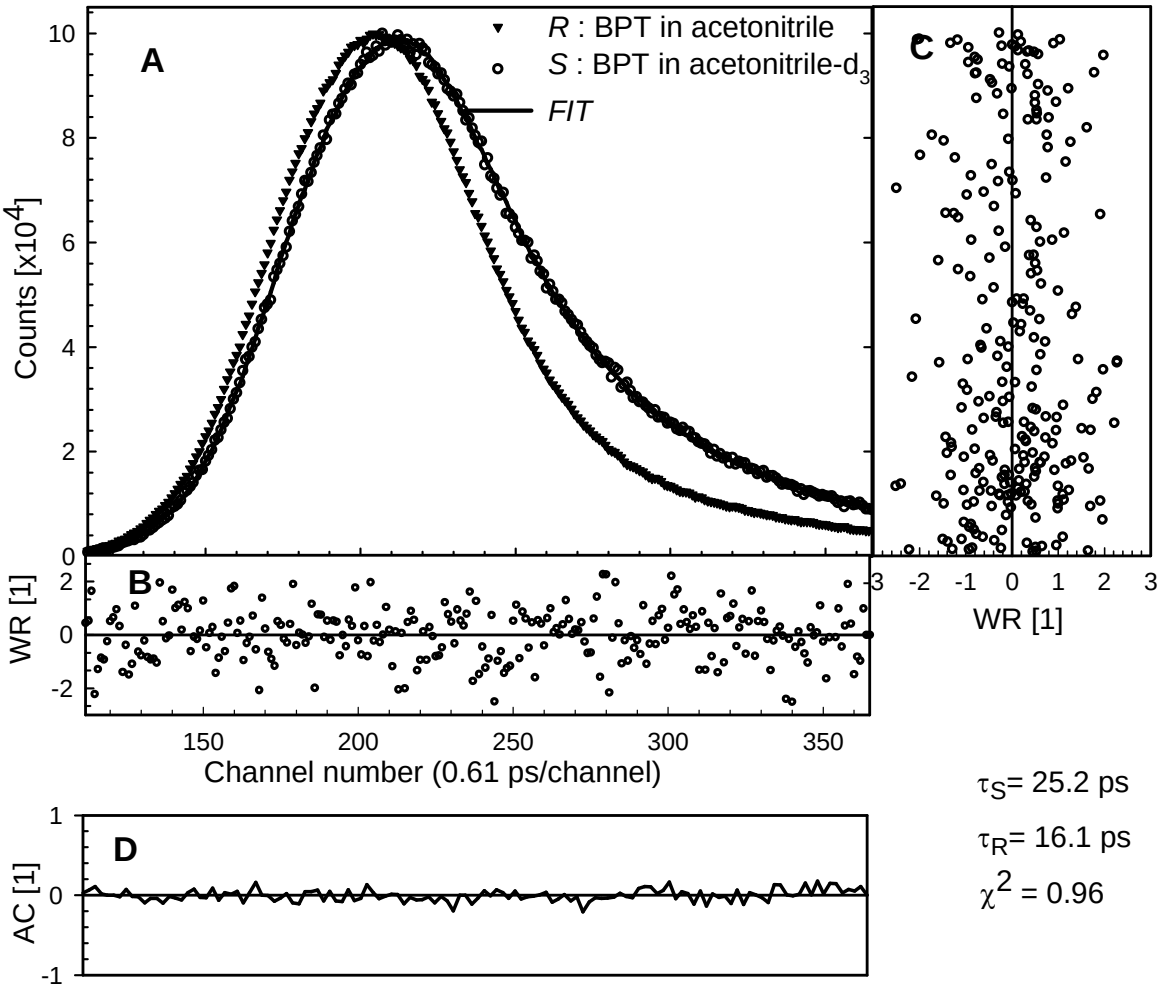

Figure 3.9. (A): Two experimental decays of fluorescence (TCSPC) monitored at 470 nm obtained for BPT (3×10^{-4} M) at the magic angle, photoexcited at 403 nm, in: acetonitrile-d_3 (*S - sample)* with fitted function *FIT* and acetonitrile *(R - reference)*. (B) and (C): Plot of the weighted residuals against the time and the value of the *FIT* respectively. (D): Autocorrelation function of the weighted residuals.

The observed isotope effect on the kinetics confirms that a reaction coordinate, thus implying that a hydrogen atom is involved in the BPT S_2 state quenching process by acetonitrile. The TCSC results are confirmed by the fact that a similar lifetime τ_{S2} is obtained for BPT in acetonitrile-h_3 at 470 nm using the FFUC method (single-exponential decay fitting function, see Fig.3.10). An instantaneous rise of the fluorescence (rise time shorter than 150 fs) is observed when measurements are performed using a shorter time window (up to 3 ps).

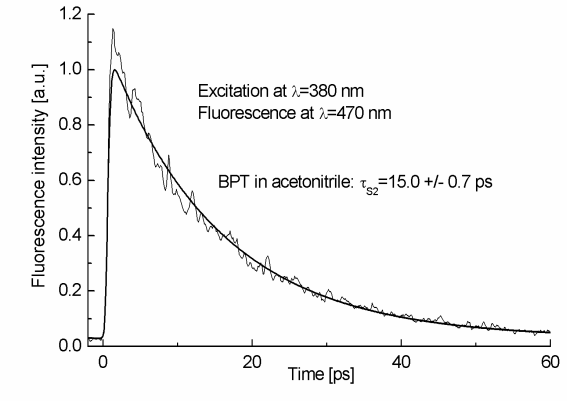

Figure 3.10. Single-exponential fluorescence decay for the S_2 state of BPT (3×10^{-4} M) in acetonitrile measured by femtosecond fluorescence up-conversion spectroscopy.

Table 3.7. Lifetime of the S_2 state of BPT obtained by TCSPC and FFUC from fluorescence decay of BPT S_2 state in acetonitrile and acetonitrile-d_3. S_2 state fluorescence was determined at two selected wavelengths: 470 and 530 nm.

Solvent	$\lambda_{fluorescence}$ [nm]	TCSPC τ_{S2} [± 1.3 ps]	FFUC τ_{S2} [± 0.7 ps]
Acetonitrile	470	14.9	15.0
Acetonitrile	530	16.3	
Acetonitrile-d_3	470	24.1	
Acetonitrile-d_3	530	25.8	

3.3.3. Nanosecond transient absorption and phosphorescence measurements.

Before going into the details of the femtosecond transient absorption results, it is worth presenting the absorption and emission data obtained using the nanosecond/microsecond time scale. All the measurements were performed using deoxygenated solution of BPT (≈ 5.7×10^{-5} M) in acetonitrile. The pump energy per laser pulse was 0.8 mJ. The transient absorption spectra and the corresponding kinetics recorded at 460 nm as well as the phosphorescence kinetics obtained at 630 nm are presented in Fig.3.11a, b and c respectively.

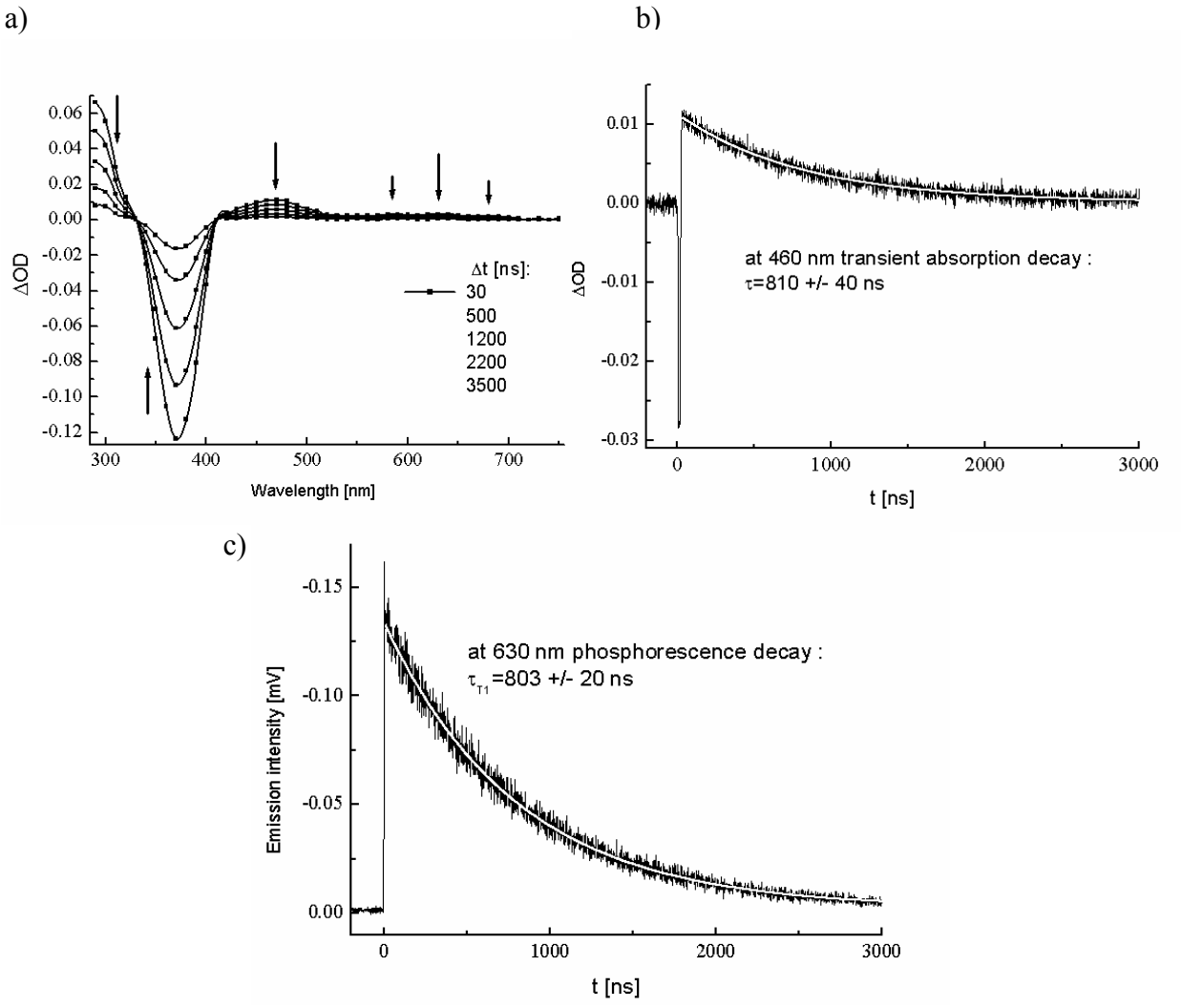

Figure 3.11. Time-resolved absorption and emission measurements of BPT (5.7×10^{-5} M) in acetonitrile at 355 nm with energy 0.8 mJ per pulse. a) Transient absorption spectra within the 30 - 3500 ns time window (the phosphorescence emission contribution is subtracted). b) Transient absorption decay recorded at 460 nm. c) Phosphorescence emission decay recorded at 630 nm. The solid white lines are the best single exponential fits to the experimental data.

The absorption kinetics observed within the 290 - 750 nm spectral range can be fitted with a single exponential function with the same characteristic time (810 ns). The same time (803 ± 20 ns) is obtained from the $T_1 \rightarrow S_0$ phosphorescence decay recorded at 630 nm. We can thus attribute the positive bands observed on transient absorption spectra to the triplet state spectra. The negative band peaking at ≈370 nm corresponds to the Ground State Depletion (GSD) signal induced by the pump pulse. GSD dynamics are related to the recovery of BPT in the ground state due to the $T_1 \rightarrow S_0$ transition. The transient absorption spectra are very similar to those obtained for BPT in hydrocarbons and perfluorohydrocarbons. There is thus no indication of the formation of an additional species such as exciplexes or radicals on this time-scale.

It is worth analysing the results in some detail. Fig.3.11b shows the transient absorption decay of the BPT triplet T_1 state analysed at 460 nm. The reconstructed transient absorption spectra within the 30 - 3500 ns time window are presented in Fig.3.11a. In the 290 - 330 nm spectral range, an intense absorption is observed. However, its amplitude is reduced by the presence of a negative signal (GSD). In the 330 - 410 nm spectral range only one negative band is visible and this can be mainly assigned to GSD because its shape is similar to that of the ground state absorption spectrum of BPT in acetonitrile (see Fig.3.8). The extinction coefficient ε(365nm) obtained from steady-state absorption measurements is equal to 17900 $M^{-1}cm^{-1}$. In the 410 - 750 nm spectral region, only the absorption of the triplet T_1 state is observed with an absorption band peaking at 470 nm. Weak maxima at 580, 630, and 680 nm are also observed (see Fig.3.11a and 3.13a), which are similar to those for the T_1 state of BPT in hydrocarbon solvents. An approximated value of the extinction coefficient ε(470nm) = 1600 ± 300 $M^{-1}cm^{-1}$ can be estimated from the ratio ε(365nm)/ε(470nm) ≈ 11.

3.3.4. Femtosecond transient absorption measurements.

Fig.3.12a shows the transient absorption spectra recorded at the magic angle within the 1 - 100 ps time window after excitation at 403 nm of a 10^{-4} M solution of BPT in acetonitrile. In these experimental conditions, contribution from the vibrational relaxation and from the molecular rotational diffusion are excluded.

The transient absorption spectra presented in Fig.3.12a are very similar to those obtained for BPT in hydrocarbon solvents (see Fig.3.5a). Their assignments can be directly derived from those made for hydrocarbon solvents. The presence of only two species is observed, the singlet S_2 state and the triplet T_1 state.

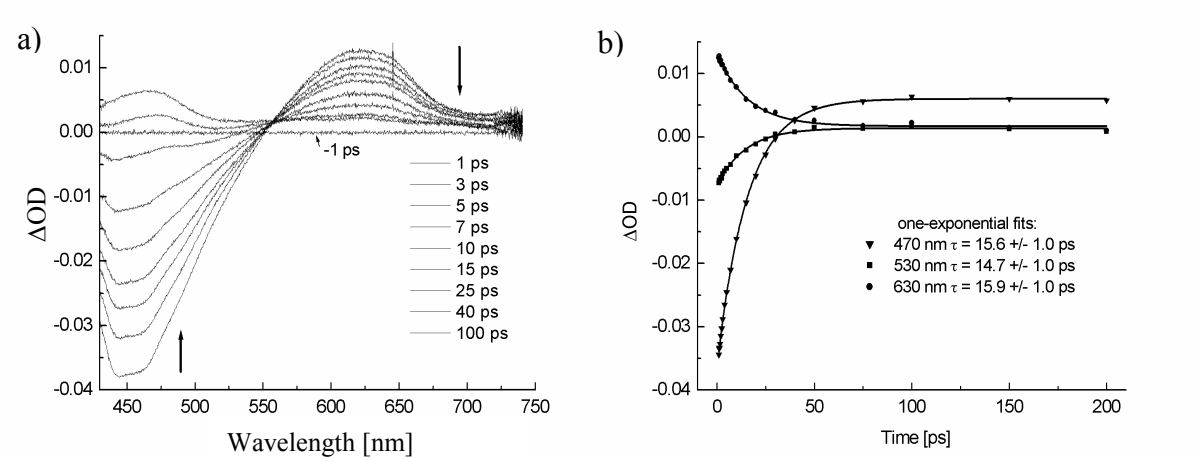

Figure 3.12. a) Transient absorption spectra recorded at the magic angle from -1 ps to 100 ps after photoexcitation of BPT (1×10^{-4} M) in acetonitrile at 403 nm (pump pulse energy is 12 μJ). b) Kinetic traces for selected wavelengths: (▼) 470, (■) 530 and (●) 630 nm. Solid lines are best fits to the data (from 1 ps to 200 ps).

The attribution of the final absorption spectrum in Fig.3.12a (at time delay 100 ps) to the BPT triplet state $T_1(\pi,\pi^*)\rightarrow T_n$ transition is confirmed without ambiguity by nanosecond transient absorption measurements (see Fig.3.13). The main difference between the transient absorption spectra of BPT recorded in acetonitrile and that in hydrocarbon solvents is the shape of the triplet T_1 state absorption band at 100 ps, which is less structured in acetonitrile than in the hydrocarbons. The electronic configuration of the lowest triplet state $T_1(\pi,\pi^*)$ in polar solvents (acetonitrile) compared to that in non-polar solvents $T_1(n,\pi^*)$ [40] may possibly explain this modification of the band shape.

It is worthwhile noticing that in Fig.3.12a the relative amounts of the initial S_2 state and final T_1 state species, as measured from the ratio $I_{max}(S_2)/I_{max}(T_1)$ of the S_2 absorption band intensity at 1 ps and T_1 state absorption band intensity at 100 ps is equal to 2, and thus is like that found when using hydrocarbon solvents. Assuming that almost all the BPT molecules in the S_2 state deactivate to the T_1 state, the extinction coefficients of the S_2 absorption band at 620 nm and T_1 absorption band peaking at 470 nm follow the relation $\varepsilon_{S2}^{max} \sim 2\varepsilon_{T1}^{max}$. An approximate value of $\varepsilon_{S2}^{max} = 3200 \pm 600$ $M^{-1}cm^{-1}$ can be derived from the above determined $\varepsilon_{T1}^{max} = 1600 \pm 300$ $M^{-1}cm^{-1}$.

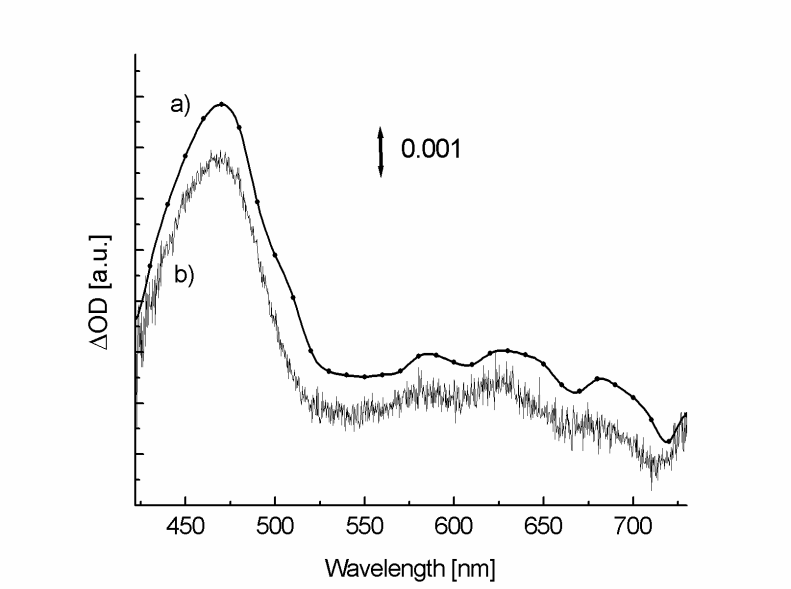

Figure 3.13. Transient absorption spectra obtained for BPT in acetonitrile at pump-probe delays of a) 30 ns (the phosphorescence emission contribution is subtracted) and b) 100 ps. Both spectra are shifted for a better presentation.

The calculated extinction coefficient ε_{S2}^{max} (3200 $M^{-1}cm^{-1}$) is close to that obtained in hydrocarbon solvents (3600 $M^{-1}cm^{-1}$), thus, the previous assumption of an efficient (almost 100 %) deactivation of the S_2 state to the T_1 state in acetonitrile seems to be correct. Finally, the fact that the isosbestic point at 560 nm (see Fig.3.12a) is not perturbed by the presence of the T_1 absorption band suggests that the S_2 decay and T_1 appearance have comparable kinetics. Kinetics obtained every 10 nm from the transient absorption spectra presented in Fig.3.12a were fitted to a single exponential function. A single time-constant of 15.6 ± 1.0 ps was determined for the whole spectral range (430 - 750 nm). The significant isotope effect already observed by fluorescence was also observed for transient absorption measurements. The time-constant found in acetonitrile-d_3 (25.8 ± 1.5 ps) is almost two times longer than that in acetonitrile-h_3. Table 3.8 shows that the time-constants determined by femtosecond transient absorption and up-conversion methods are similar within experimental error. The transient absorption measurements provide not only confirmation of the S_2 state lifetime τ_{S2}, but also show that similarly to what was observed for BPT in hydrocarbons, the rise of the triplet T_1 band parallels the decay of the singlet S_2 band as attested by the presence of a clear isosbestic point. The presence of other transient species (exciplexes) is not observed.

Table 3.8. Comparison between the time-constants obtained by TCSPC and by transient absorption for BPT in acetonitrile and acetonitrile-d_3 analysed at two selected wavelengths (470 and 530 nm).

Solvent	$\lambda_{observation}$ [nm]	TCSPC τ_{S2} [± 1.3 ps]	Transient absorption τ [± 1.0 ps]
Acetonitrile	470	14.9	15.6*
Acetonitrile	530	16.3	14.7*
Acetonitrile-d_3	470	24.1	25.3**
Acetonitrile-d_3	530	25.8	24.3**

Average values in the 430 - 750 nm spectral range: *15.6 ± 1.0 ps and **25.8 ± 1.5 ps.

3.3.5. Discussion.

The shortening of the S_2 state lifetime τ_{S2} by about an order of magnitude on going from perfluorohydrocarbons to acetonitrile (see Table 1.1) demonstrates the existence of an efficient quenching process of the S_2 state of BPT by acetonitrile. It is surprising, because according to the literature acetonitrile is usually considered as a chemically inert solvent towards molecules in the excited states. At first we considered that the quenching process could be attributed to a singlet-singlet energy transfer from BPT in the S_2 state to acetonitrile. However, such a process would be highly endothermic and thus can be ruled out. Neither can the quenching of the S_2 state of thioketones be explained by a vibronic coupling between the S_2 and S_1 states of thioketones involving the high-energy solvent vibrational modes as attested by the results reported by Topp et al [3]. Another mechanism has been proposed in the literature in order to explain the quenching of aromatic thioketones in the S_2 state by acetonitrile [2, 3]. It has been suggested that the interaction of thioketones in the S_2 state with the π-electrons of the cyano group leads to an S_2 state exciplex. This proposition has been recently supported by a femtosecond transient absorption investigation of the quenching of the S_2 state of xanthione (XT) by acetonitrile. In this study the S_2 state exciplex spectral signature has been observed for the first time [4]. As in acetonitrile, the π-electrons of benzene have been proposed to play an important role in the efficient exciplex formation quenching process of the S_2 state of aromatic thioketones [2]. In the case of XT in benzene,

almost no isotope effect has been reported (τ_{S2}=11 ps and 12 ps in benzene-h_6 and benzene-d_6, respectively [3]). This is consistent with the fact that benzene is a poor hydrogen atom donor (C-H bond energy of 465.3 ± 3.4 kJ/mol [20]), thus implying that hydrogen atom abstraction is unlikely to occur in this solvent. Consequently, a pure exciplex formation quenching process has been proposed for XT in benzene [2, 3]. However, such an exciplex formation mechanism alone can not explain the quenching process in the case of BPT in acetonitrile since we observed a notable increase of the BPT S_2 state lifetime (by about 60 %) on going from hydrogenated to deuterated acetonitrile. This solvent isotope effect suggests, as in the case of hydrocarbon solvents, that a reaction coordinate, which implies the motion of a hydrogen atom of the acetonitrile molecule is involved in the quenching process. Acetonitrile is generally not considered as a hydrogen atom donor solvent despite the relatively weak H-C bond energy (392.9 ± 8.4 kJ/mol) compared to ≈ 400 - 440 kJ/mol for the H-C bond of alkanes [20]. Thus, the C-H bond energy is not the main factor that governs the hydrogen transfer from acetonitrile to molecules in the excited states, as demonstrated by their unusual low reactivity towards acetonitrile [41]. However, Nau and co-workers have proposed an aborted hydrogen atom transfer quenching mechanism from acetonitrile to the S_1 state of azoalkanes to explain the observed 2.6 value of the isotope effect [17, 36].

To take into account the fact that most of thioketones are quenched by the S_2 state exciplex formation with acetonitrile and that a notable isotope effect exists in the case of BPT, we tenatively propose that the quenching of the BPT S_2 state by acetonitrile by a double, exciplex formation and aborted hydrogen atom abstraction processes. The proposed hydrogen abstraction scheme is similar to that in hydrocarbon solvents (see Fig.3.7). The formation of an S_2 state exciplex can be rationalised by the following interactions between BPT in the S_2 state and acetonitrile molecules:

- π-π interaction between the four π electrons from the nitrile group N≡C and the two electrons (π*) and (π) from the thio group >C=S. The π electrons of the benzo moiety may also be involved in the exciplex formation.
- Charge-transfer between BPT in the S_2 state (donor) and acetonitrile (acceptor).

Moreover, the exciplex in the S_2 state can be stabilised by interactions with its surrounding acetonitrile molecules due to:

- Dipole-dipole interactions (dipole moment of acetonitrile and BPT in the S_2 state are 4 D and ~1.0 D respectively),
- Dispersion interactions (attractive interaction between induced dipoles).

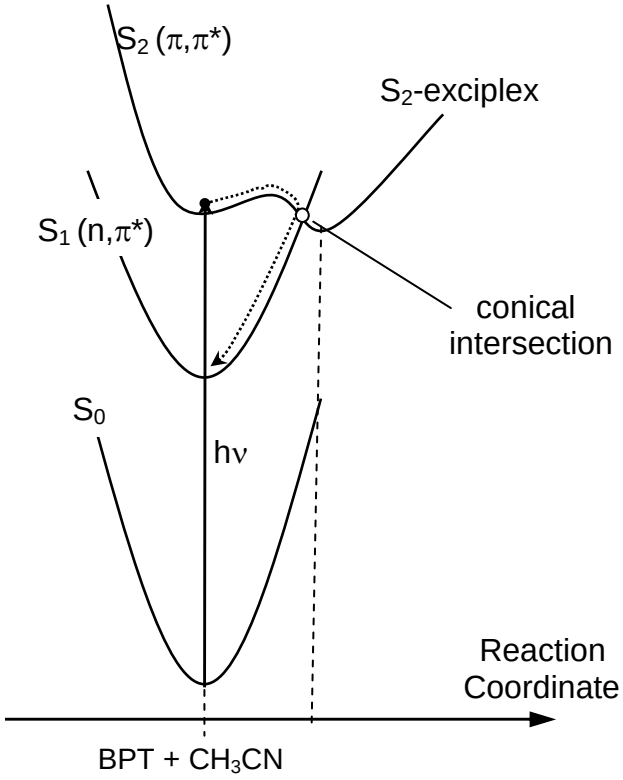

Figure. 3.14. Schematic potential reaction coordinate for the deactivation of the S_2 state of BPT by acetonitrile.

We suppose that the S_2 state exciplex deactivation occurs through a conical intersection point between the S_1 state of BPT and the S_2 exciplex potential curves, since unlike XT, no evidence of an exciplex formation was found in the case of BPT in acetonitrile (see Fig.3.14).

The low net photochemical consumption of thioketones ($\Phi_D<10^{-3}$) supports this idea, that the "back-reaction" deactivates the system to the S_1 state of BPT. The fact that the growth of the triplet state T_1 absorption band parallels the decay of the S_2 state of BPT indicates that the intermediate species between the BPT S_2 and T_1 states have very short lifetimes. Thus helps to explain the failure of their experimental observation.

The lifetime of the S_2 state of BPT can be expressed by following formula:

$$\tau_{S2} = \frac{1}{k_{Exciplex} + k_H + k_{nr} + k_r}, \qquad (3.5)$$

where $k_{Exciplex}$ and k_H are the exciplex formation and hydrogen abstraction quenching rate constants respectively, and k_{nr} and k_r are the nonradiative and radiative rate constants (intramolecular processes) respectively. A constant energy gap of $\Delta E(S_2\text{-}S_1)$ = 7150 cm^{-1} in acetonitrile and in acetonitrile-d_3 is obtained by using steady-state measurements. According

to Table 1.1, the $k_{nr}+k_r$ value is about 1.5×10^{10} s^{-1}. We can determine the sum of the quenching rate constants $k_{Exciplex}+k_H$ as 5.2×10^{10} s^{-1} in acetonitrile and 2.6×10^{10} s^{-1} in acetonitrile-d_3 from the measured τ_{S2} lifetimes (τ_{S2}(aceto-h_3) = 14.9 ps and τ_{S2}(aceto-d_3) = 24.1 ps), the ($k_{nr}+k_r$) value and the Eq.3.5. As a result 78 % of the BPT S_2 state molecules are quenched by acetonitrile. Scheme 3.3 represents the pathways of the BPT S_2 state deactivation in acetonitrile.

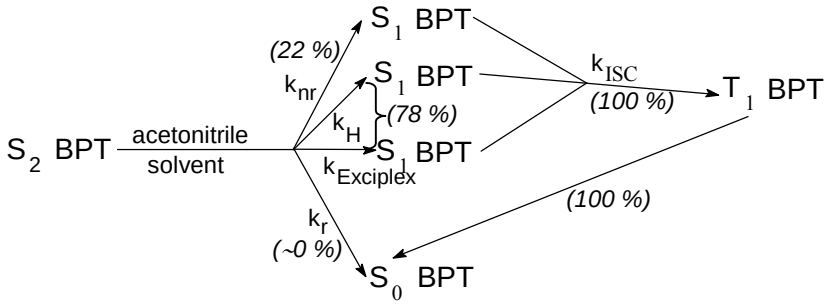

Scheme 3.3.

Two quenching mechanisms of the BPT S_2 state by acetonitrile have been tentatively proposed in order to explain why as many as 78 % of BPT in the S_2 state are quenched by interaction with acetonitrile molecules: an aborted formation of a S_2 state exciplex and an aborted hydrogen abstraction. Taking into account, that the nature of both mechanisms is different, we can assume that these two reaction coordinates are independent.

3.4. Aqueous solution.

3.4.1. Steady-state measurements.

Fig.3.15 presents the results of steady-state absorption ($S_0 \rightarrow S_n$, $n \geq 2$) and S_2 state fluorescence studies of BPT in water. The spectral properties are similar to those previously obtained in acetonitrile and hydrocarbons (see Fig.3.1 and Fig.3.8). The strong absorption band ($S_0 \rightarrow S_2$ transition) has a maximum at 377 nm (ε=19000 $M^{-1}cm^{-1}$). For BPT concentrations up to 5×10^{-4} M (limit of solubility at room temperature), the shape and intensity of the absorption and emission spectra do not indicate any aggregation of the BPT molecules. Thus, time-resolved measurements performed at concentrations ranging from 1×10^{-5} to 5×10^{-4} M are not affected by dimer formation.

The choice of pump wavelengths at 350, 355, 380 and 403 nm ensures a selective excitation of BPT to the S_2 state, since the energy difference between the vibrationally relaxed S_3 and S_2 state is about 7000 cm^{-1}. Changing the solvent from H_2O to D_2O has no influence on either the absorption or the emission spectra of BPT.

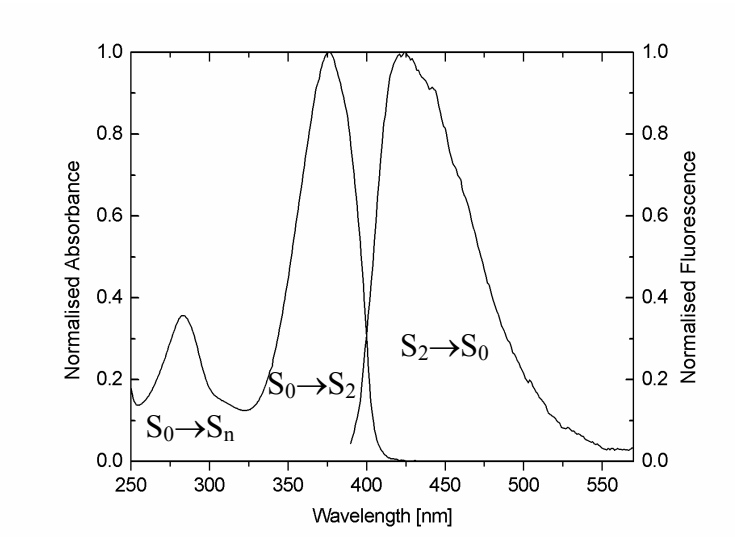

Figure 3.15. Steady-state absorption, $S_0 \rightarrow S_2$, $S_0 \rightarrow S_n$ ($n \geq 3$), and emission $S_2 \rightarrow S_0$ spectra of BPT in water (λ_{exc} = 370 nm).

3.4.2. Femtosecond fluorescence up-conversion measurements.

No reliable kinetics could be obtained using the time-correlated single photon counting method due to the very short lifetime τ_{S2} of BPT S_2 state in water. Thus, the femtosecond fluorescence up-conversion technique was applied to determine the τ_{S2} value in

water. Due to the low solubility of BPT in water, the spectra recorded using a pump wavelength of 403 nm (low energy absorption edge) were very weak. In order to obtain a good signal-to-noise ratio, the pump wavelength was tuned to 380 nm or 350 nm. The data are free from molecular rotational diffusion effects, since the angle between the pump and the gate beam polarisation was set at 54.7° (magic angle). Fig.3.16 presents the fluorescence measurements performed for solutions of BPT (5×10^{-4} M) in H_2O and in D_2O upon excitation at 380 and 350 nm.

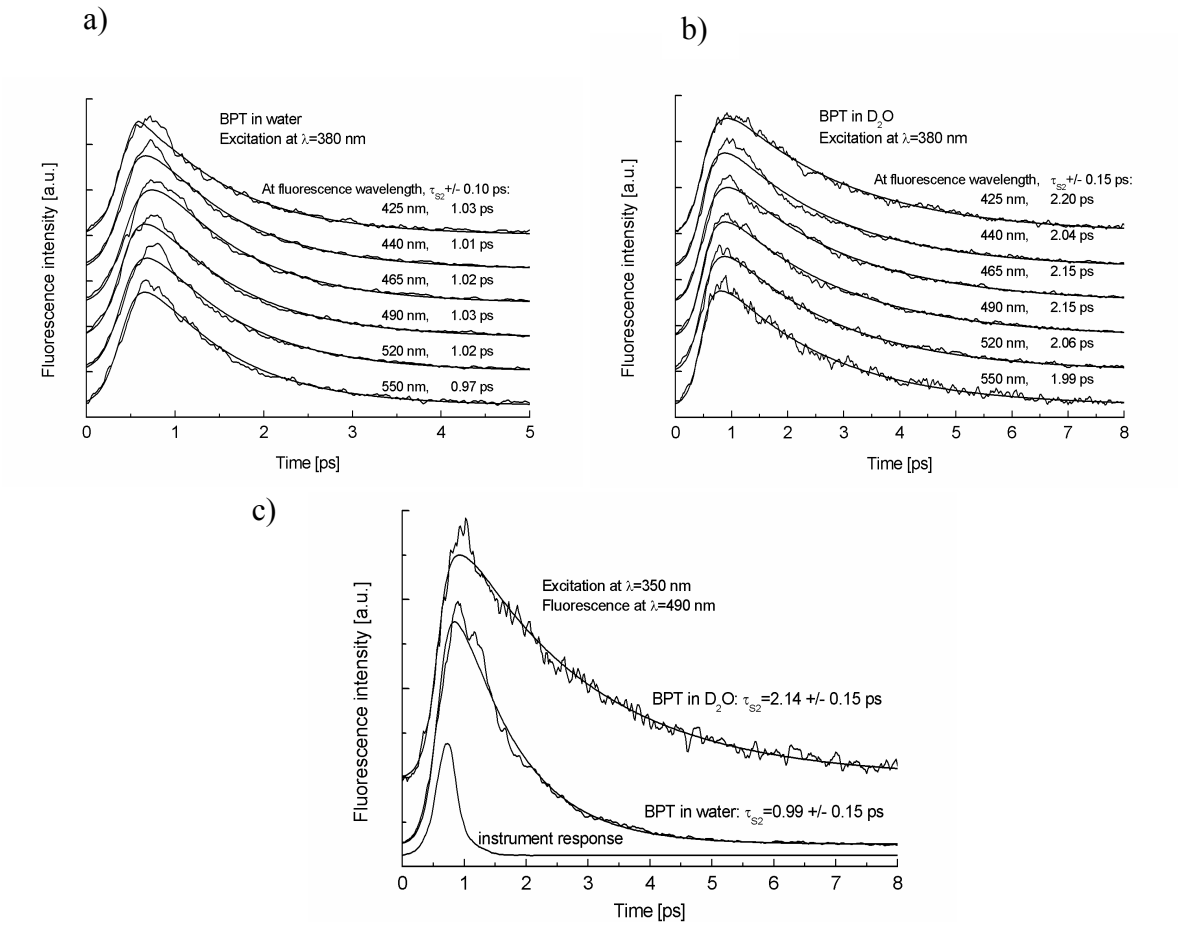

Figure 3.16. Normalised experimental decays of fluorescence at different wavelengths ranging from 425 to 550 nm obtained upon 380 nm photoexcitation of BPT (5×10^{-4} M) in (a) H_2O and (b) D_2O. The obtained lifetimes τ_{S2} are also given. Fig.3.16c presents results obtained on 350 nm photoexcitation of BPT in H_2O and D_2O. The instrument response function is also presented. The smoothed solid lines are the best fits to the experimental data.

The fitting analysis was carried out assuming a single population of molecules in the excited emitting state by using the following single exponential function:

$$F(t) = A_1 \exp(-t/\tau_{S2}) + C. \quad (3.6)$$

A convolution function $IRF(t) \otimes F(t)$ was used to take into account the instrument response function *IRF(t)* (see Chapter 2). The use of a biexponential fitting function (with an additional component, $A_2(-t/\tau_{rise})$ in Eq.3.6, to take into account a possible noninstantaneous rise time of the signal) does not change the obtained lifetime τ_{S2} of the BPT S_2 state. The obtained rise time τ_{rise} is shorter than 150 fs and can not be resolved with the time resolution of the experimental set-up (150 fs). Whatever the excitation wavelength (350 or 380 nm) and the fluorescence wavelength (from 425 to 550 nm), the S_2 state lifetimes of BPT are 1.0 ± 0.1 ps and 2.1 ± 0.15 ps in H_2O and D_2O, respectively. The BPT S_2 state lifetime in D_2O is approximately twice as long as it is in H_2O. In femtosecond fluorescence up-conversion measurements, vibrational relaxation processes such as intramolecular vibrational redistribution and vibrational cooling, should result in a modification of the rise time of the kinetic trace and a spectral narrowing of the S_2 state emission bandwidth respectively [42]. In the case of BPT in the S_2 state in water the vibrational relaxation is not observed, because the growth component (τ_{rise}) is too short to be resolved and no spectral narrowing of the S_2 state emission bandwidth is observed neither.

All the experimental fluorescence decays contain an additional ultrafast component centred around 750 fs (see the ultra short-lived peak located at the top of the curves in Fig.3.16). Experiments performed on neat solvent ruled out the possible contribution of artifacts such as white light continuum generation in the sample, or unphase-matched up-converted pump pulse. Since no artifact contributes to the observed signal, another explanation for the presence of the additional ultrafast component must be proposed. After excitation of BPT to the S_2 state, a very fast solvation process due to rotational motions of the instantaneously released polar water molecules in the first solvent shell surrounding the solute can be expected [43 - 51]. Such a solvation process is likely to occur, due to a decrease in the dipole moment by 1.9 D to about 1 D as a result of charge transfer from the sulphur atom to the carbon atom of the thiocarbonyl group and to the carbon atoms of the ring associated with the $S_0 \rightarrow S_2$ transition [16]. The solvation process is usually observed by the presence of additional decay signal on the blue side of the emission spectrum, and rise signal on the red side [50]. However, Fig.3.16 shows only an ultrafast additional decay signal, so a very fast solvation process can be ruled out of consideration. A more convincing explanation is an

ultrafast quenching process within a hydrogen-bonded complex directly excited from the ground state to the S_2 state. For BPT in the ground state the total electron density ~-6.4 e (see Table 1.2) on the sulphur atom, ensures good conditions for hydrogen bond formation between the electron lone pair located on the sulphur atom and the water molecules. The hydrogen bond formation was determined by steady-state absorption measurements, since the BPT $S_0 \rightarrow S_1(n,\pi^*)$ absorption band is blue-shifted by 2000 cm^{-1} in water compared to that in acetonitrile. In contrary to hydrogen bonding affinity, the non-specific (dielectric) solute-solvent interactions are similar in both water and acetonitrile solvents and are almost equal, *f(ε,n)* values are 0.64 and 0.61 respectively, according to the Lippert-Mataga polarity function [52]:

$$f(\varepsilon,n) = 2\left(\frac{\varepsilon - 1}{2\varepsilon + 1} - \frac{n^2 - 1}{2n^2 + 1}\right), \qquad (3.7)$$

where ε is the static dielectric constant and n is the optical refractive index of the solvent. The almost identical non-specific solute-solvent interaction values ensure that the observed shift of 2000 cm^{-1} is mostly due to specific solute-solvent interactions (hydrogen bond formation). Since BPT in the ground state can be free or hydrogen-bonded to the solvent, equilibrium between the two forms should be considered. If both forms with a similar absorption spectra are photoexcited by the pump wavelength (adjusted to the BPT $S_0 \rightarrow S_2$ absorption band), two species, the free BPT in the S_2 state and the excited hydrogen-bonded complex S_2-(BPT···H-OH) can be expected. Accordingly, the ultrafast signal is assigned to the intracomplex quenching process, while the signal observed on longer time-scale is ascribed to the decay of the non-hydrogen bonded S_2 state population. Its short time-constant (1.0 ± 0.1 ps in H_2O) shows an extremely high reactivity. Thus, the main goal of the following study was the characterisation of the ultrafast quenching mechanism of the free BPT S_2 state by water.

3.4.3. Nanosecond transient absorption and phosphorescence measurements.

Before going into detail of femtosecond transient absorption measurements, it is worth presenting the absorption and emission data obtained for BPT in water on the nanosecond/microsecond time scale. All the measurements were made using 6.6×10^{-5} M deoxygenated solutions of BPT. The pump energy was 0.8 mJ per laser pulse. Transient absorption spectra and the corresponding kinetics recorded at 470 nm as well as the

phosphorescence kinetics obtained at 630 nm are presented in Fig.3.17a, b and c respectively. The absorption kinetics obtained within the 290 - 750 nm spectral range can be fitted to a single exponential function with the same characteristic time (280 ns). The same time (280 ± 15 ns) is obtained for the phosphorescence decay $T_1 \rightarrow S_0$ recorded at 630 nm. We can thus attribute the positive bands observed on the transient absorption spectra to the triplet state absorption spectra. The negative band peaking at ≈370 nm corresponds to the Ground State Depletion (GSD) signal induced by the pump pulse. GSD dynamics are related to the recovery of BPT in the ground state due to $T_1 \rightarrow S_0$ transition. These results are very similar to those obtained for BPT in acetonitrile implying that only the non-hydrogen bonded triplet T_1 state of BPT and GSD signals are observed.

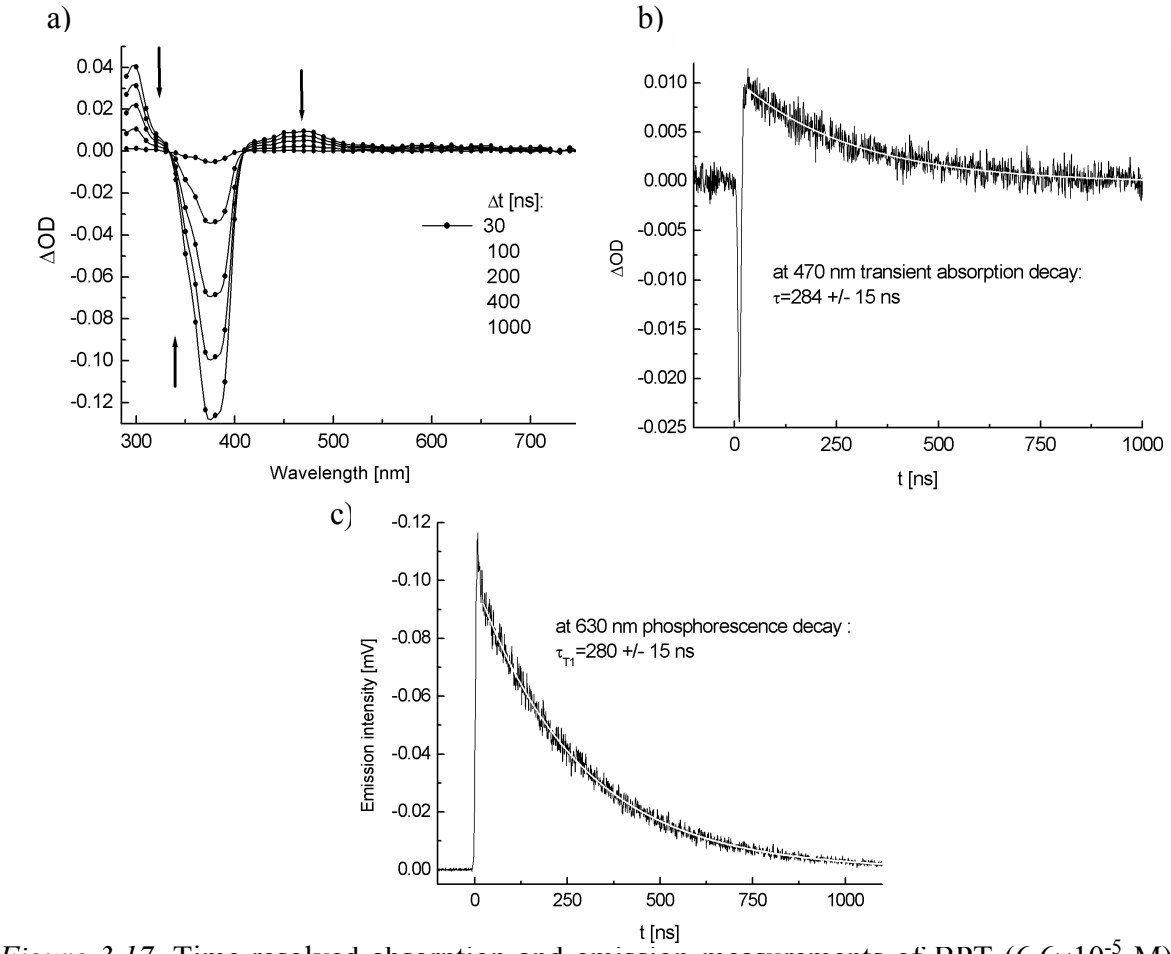

Figure 3.17. Time-resolved absorption and emission measurements of BPT (6.6×10^{-5} M) in water at 355 nm with laser energy 0.8 mJ per excitation pulse. a) Transient absorption spectra within 30 - 1000 ns time window (the phosphorescence emission contribution was subtracted). b) Transient absorption decay recorded at 470 nm. c) Phosphorescence emission decay recorded at 630 nm. The solid white lines are the best single exponential fits to the experimental data.

No indication of the formation of an additional species (complexes or radicals) was found on this time scale. It is worth analysing the data in some detail. Fig.3.17b represents the transient absorption decay of the BPT triplet T_1 state analysed at 470 nm. Note that in the 4 - 22 ns time window a short negative signal is seen and this can be attributed to the S_2 state fluorescence decay. Transient absorption spectra within the 30 - 1000 ns time window are presented in Fig.3.17a. In the 290 - 330 nm spectral range, an intense absorption of the T_1 triplet state is observed. However, its amplitude is reduced by the presence of a negative signal (GSD). In the 330 - 410 nm spectral region only the negative band is visible and this can be mainly assigned to GSD signals since its shape is similar to that of the ground state absorption spectrum of BPT in water (see Fig.3.15). As a consequence, the contribution of the triplet state absorption is very weak at λ = 377 nm. Thus, an absorption extinction coefficient of $\varepsilon(377\text{ nm}) = 19000\ M^{-1}cm^{-1}$ can be assumed by analogy with that from steady-state absorption measurements. In the 410 - 750 nm spectral range, only the absorption of the triplet T_1 state is observed with a maximum of the absorption band situated at 470 nm. The well-resolved weak maxima at 580, 630, and 680 nm, observed in the case of BPT in hydrocarbons and acetonitrile, are much weaker in H_2O (see Fig.3.19). An approximated value of the extinction coefficient of BPT in the triplet $T_1(\pi,\pi^*)$ state in water $\varepsilon(470\text{ nm}) = 1500 \pm 300\ M^{-1}cm^{-1}$ can be estimated from the ratio $\varepsilon(377nm)/\varepsilon(470nm) \approx 13$. The value of the extinction coefficient $\varepsilon(470nm)$ of the BPT triplet T_1 state in water is thus similar to those found in acetonitrile and hydrocarbons.

3.4.4. Femtosecond transient absorption measurements.

The transient absorption spectra of BPT in H_2O or D_2O were recorded within the 1 - 200 ps time window after photoexcitation at 380 nm. The recording of transient spectra using 403 nm excitation wavelength was unfeasible due to the low solubility of BPT in water and the low absorption coefficient of BPT at this wavelength. The spectra obtained in both solvents are very similar. Only the kinetics are different. The spectra recorded for BPT in water for a set of time delays ranging from 1 to 15 ps are presented in Fig.3.18a. No further evolution of the signal was observed in the 15 - 200 ps time range. These spectra are free from rotational diffusion since the magic angle configuration was used. Moreover, the fluorescence up-conversion measurements have shown that the contribution from vibrational relaxation processes in the S_2 state of BPT in water can be neglected. The assignment of the spectra obtained in H_2O can be directly derived from those made for BPT in acetonitrile or the

hydrocarbons. Spectra are thus assigned to the singlet S_2 and the triplet T_1 excited states. Moreover, the attribution of the final absorption spectrum in Fig.3.18a (at time delay 15 ps) to the absorption of the BPT triplet $T_1(\pi,\pi^*)$ state is confirmed without ambiguity by the comparison with the nanosecond transient absorption measurements (see Fig.3.19). No contribution from other species (hydrogen-bonded BPT S_2 state, radicals) is found. The decay of the S_2 state and the appearance of the T_1 state have comparable kinetics since the isosbestic point observed at 545 nm is not perturbed (see Fig.3.18a).

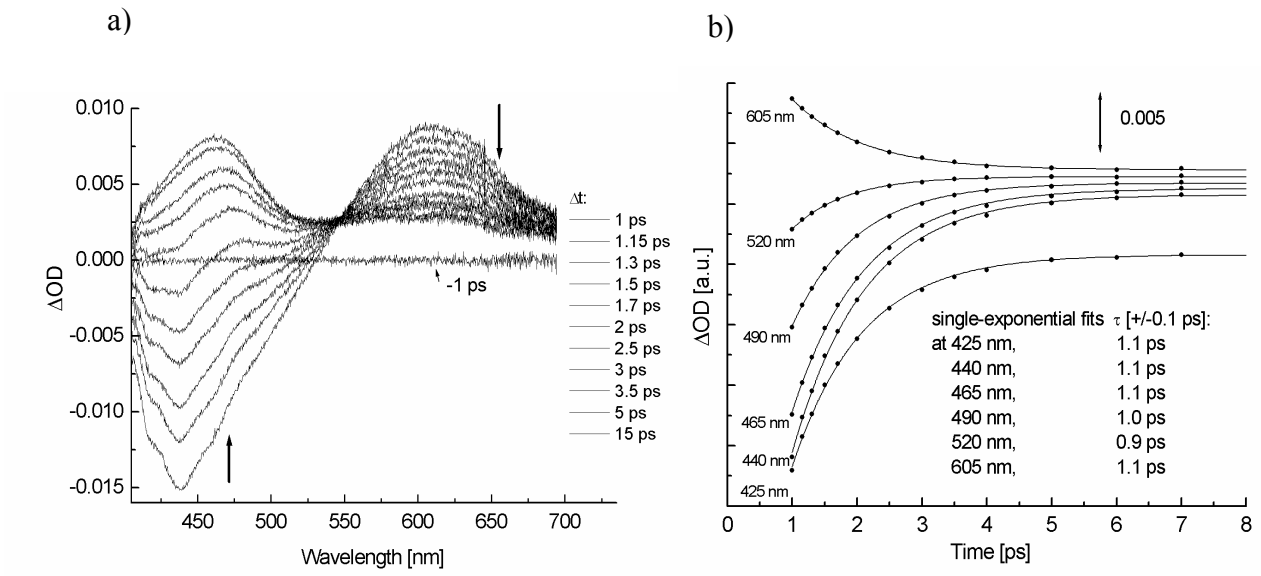

Figure 3.18. a) Transient absorption spectra recorded with the magic angle configuration from -1 ps to 15 ps after photoexcitation of BPT (1.1×10^{-4} M) in water at 380 nm (pump pulse energy was 15 μJ). b) Kinetic traces for selected wavelengths: 425, 440, 465, 490, 520 and 605 nm. The kinetics were vertically shifted for a better presentation. Solid lines are the best fits to the data (from 1 ps to 15 ps).

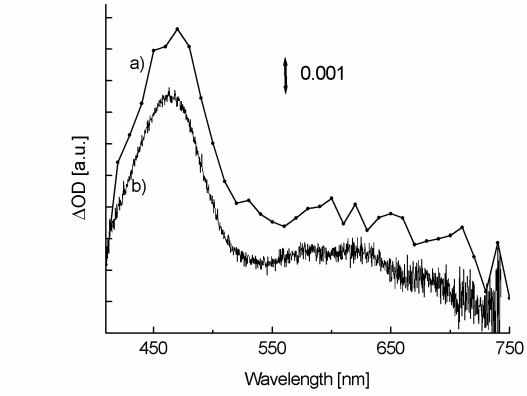

Figure 3.19. Transient absorption spectra obtained for BPT in water with pump-probe delays of a) 30 ns (the phosphorescence emission contribution was subtracted) and b) 15 ps (from Fig.3.18a). Both spectra are shifted for a better presentation.

Since the spectral changes occur within a very short time scale, it is important to mention that the chosen set of time delays ensures that the observed signal is free from artifacts (stimulated Raman scattering, two-photon absorption, cross-phase modulation), which take place at shorter time delays [53]. This was confirmed by experiments performed for neat water where no signal was observed for delays longer than 0.8 ps.

It is worth noting that the relative amounts of the initial S_2 and final T_1 states, as measured with respect to the ratio $I_{max}(S_2)/I_{max}(T_1)$ of the maximum of the $S_2 \rightarrow S_n$ absorption band at short time to the maximum of the $T_1 \rightarrow T_n$ absorption band at 15 ps, is 1.65 in both H_2O and D_2O. In acetonitrile this ratio was about 1.7 when the same 380 nm excitation wavelength was used. This means that, if we assume that the extinction coefficients (ε_{T1}^{max} and ε_{S2}^{max}) are similar in water and acetonitrile, almost all BPT molecules in the S_2 state deactivate to the T_1 state.

Kinetics obtained every 10 nm from the transient absorption spectra presented in Fig.3.18a were fitted to a single exponential function. A deconvolution fitting procedure is usually used to take into account the finite temporal apparatus resolution from the measured transient absorption decays. Since the instrument response function (width of 120 fs) is short compared to the expected time-constant (1.0 ps), the fitted function kinetics presented in Fig.3.18b were determined without any deconvolution procedure. The validity of this treatment was confirmed by doing the fitting procedure with and without the deconvolution treatment, which led to similar results. In the whole 420 to 680 nm spectral range (see Fig.3.18a and b) a single time-constant of 1.0 ± 0.1 ps was found. The same analysis, performed for BPT in D_2O, gives a time-constant of 2.2 ± 0.2 ps. Note, that these time-constants determined by transient absorption spectroscopy are the same as those obtained by fluorescence up-conversion (see Table 3.9).

Table 3.9. Comparison between the time constants obtained by femtosecond fluorescence up-conversion and transient absorption for BPT in water and D_2O. S_2 state fluorescence and transient absorption signals were analysed at wavelengths ranging from 425 to 550 nm and from 420 to 680 nm respectively.

Solvent	Up-conversion τ_{S2} [ps]	Transient absorption τ [ps]
Water	1.0 ± 0.1	1.0 ±0.1
D_2O	2.1 ± 0.15	2.2 ± 0.2

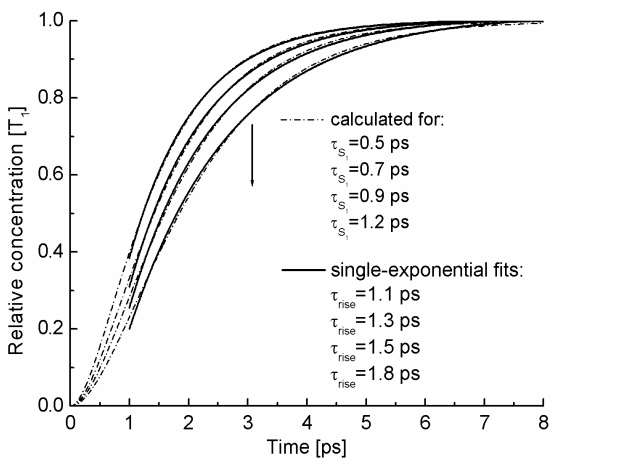

Figure 3.20. Simulations of the relative concentration of the triplet T_1 state population for different S_1 state lifetimes according to reaction mechanism $[S_2] \xrightarrow{1/\tau_{S2}} [S_1] \xrightarrow{1/\tau_{S1}} [T_1]$ and the formula $[T_1]=1-\exp(-t/\tau_{S2})-(\exp(-t/\tau_{S2})-\exp(-t/\tau_{S1}))\cdot \tau_{S1}/(\tau_{S2}-\tau_{S1})$. It was assumed that the BPT S_2 state has the lifetime of 1 ps. The best fitted single-exponential functions (solid lines) were fitted in the 1 - 8 ps time range.

As already mentioned, the decay of the S_2 state and the appearance of the T_1 state have comparable kinetics. These evolutions are not perturbed by the S_1 state absorption spectrum. Thus, the S_1 state lifetime is expected to be very short and consequently its instantaneous concentration very low. We tried to estimate the longest possible S_1 state lifetime, which does not modify the 1.0 ± 0.1 ps triplet growth-time assuming a $S_2 \rightarrow S_1 \rightarrow T_1$ deactivation pathway. Fig.3.20 shows the results of the simulations performed for the S_2 state lifetime of 1.0 ps and for different S_1 state lifetimes. We can conclude that the triplet state growth-time is only properly reproduced for S_1 state lifetimes shorter than 0.5 ps. This simulation confirms the very short $S_1(n,\pi^*)$ state lifetime previously assumed in the hydrocarbons and acetonitrile. In addition, if we assume a more complex deactivation pathway involving additional intermediate species between S_2 and T_1 states, their lifetime should be extremely short as well.

It was mentioned that the BPT S_2 state absorption spectrum in water is very similar to that obtained in acetonitrile. This confirms our assumption that only the nonhydrogen bonded BPT molecules in the S_2 state are present in the solution after the initial very fast hydrogen bonded S_2 state static quenching process. This situation is different from that reported by Yamaguchi and Hamaguchi for all-trans retinal in 1-butanol/cyclohexane mixed solvents [54]. They have used femtosecond transient absorption spectroscopy to demonstrate that all of the

retinal molecules in the $S_2(\pi,\pi^*)$ state are hydrogen bonded. This conclusion has been supported by the fact that the S_2 state absorption spectra of all-trans retinal in neat cyclohexane were very different than that in hydrogen-bonding solvent (1-butanol/cyclohexane).

3.4.5. Discussion.

The transient absorption and up-conversion measurements show coherently two aspects of the quenching process of the BPT S_2 state by water:

- The calculated quenching rate constant is extremely high since the S_2 state lifetime is reduced to 1 ps in H_2O
- The S_2 state lifetime is about two times longer in D_2O than in H_2O.

This isotope effect suggests that the reaction coordinate of the quenching process involves a proton of the solvent. The first reaction that we can think of in water is proton transfer reaction (H^+) due to a classical or a tunneling mechanism between the BPT S_2 state and a water molecule. However, such a mechanism can be neglected because the thiocarbonyl group of BPT is less basic in the excited S_2 state than in the ground state (~0.4 e lowering of the electron density for the sulphur atom, see Table 1.2). A second possible mechanism is hydrogen atom transfer (aborted or not) from the solvent to the excited solute. Nau and co-workers have considered water in the framework of hydrogen atom donor solvents to explain on one hand the quenching process (an aborted hydrogen atom transfer) of the S_1 state of azoalkanes by water [17] and on other hand the large (4 times) isotope effect on the quenching rate constant observed on going from H_2O (13×10^5 s^{-1}) to D_2O (2.9×10^5 s^{-1}). However, this explanation seems to be doubtful since the OH bond energy is high (498 kJ/mol) compared to the ≈400 - 440 kJ/mol energy of the CH bond of alkanes [20]. If an aborted hydrogen atom abstraction occurs from water to the BPT S_2 state, the observed quenching rate constant should be much lower than that in hydrocarbon solvents and consequently the lifetime τ_{S2} much longer if we assume the same rates for radiative and nonradiative processes in hydrocarbon and water solvents. Moreover, if we suppose that the hydrogen atom transfer takes place and yields the formation of a radical followed by a geminate radical recombination, the growth of the triplet T_1 state population should be delayed compared to the decay of BPT in the S_2 state. Furthermore, no signal corresponding to the formation of radicals was observed on the experimental spectra. Consequently, we consider that this mechanism can be ruled out. A quenching mechanism by solute-solvent

interaction (dipole-dipole, π-π) can be also excluded, because the solvent molecules are characterised by a medium dipole moment (1.8 D) and do not possess π electrons. The last mechanism we can think about in order to try and explain the quenching of the BPT S_2 state is the formation of a hydrogen bonded S_2 state complex between an excited solute molecule and a solvent molecule. In this case, the "free" ground state BPT molecules are excited to the "free" S_2 state for which a new acid-base equilibrium is established. This S_2 state complex formation is probably aborted before the complete hydrogen bond formation since no signal corresponding to this complex has been observed on the femtosecond experimental data. A simple schematic representation of this mechanism is presented in Fig.3.21 (①). The observed isotope solvent effect implies that a proton H^+ (deuterium D^+) from the H-O (D-O) water bond is involved in the quenching process. The slower quenching dynamics observed in deuterated water compared to H_2O can be possibly attributed to the weaker hydrogen bond network of H_2O compared to D_2O as the solvent [55]. Moreover, the mass difference between H^+ and D^+ can also play an important role in the quenching dynamics.

Note, that the photoexcitation of the hydrogen-bonded complex in the ground state can lead directly to the S_2 state complex potential energy curve (see ② in Fig.3.21). As already mentioned, the subsequent very fast barrierless quenching process is possibly confirmed by the ultrafast initial decay component found on the femtosecond S_2 state fluorescence kinetics (Fig.3.16).

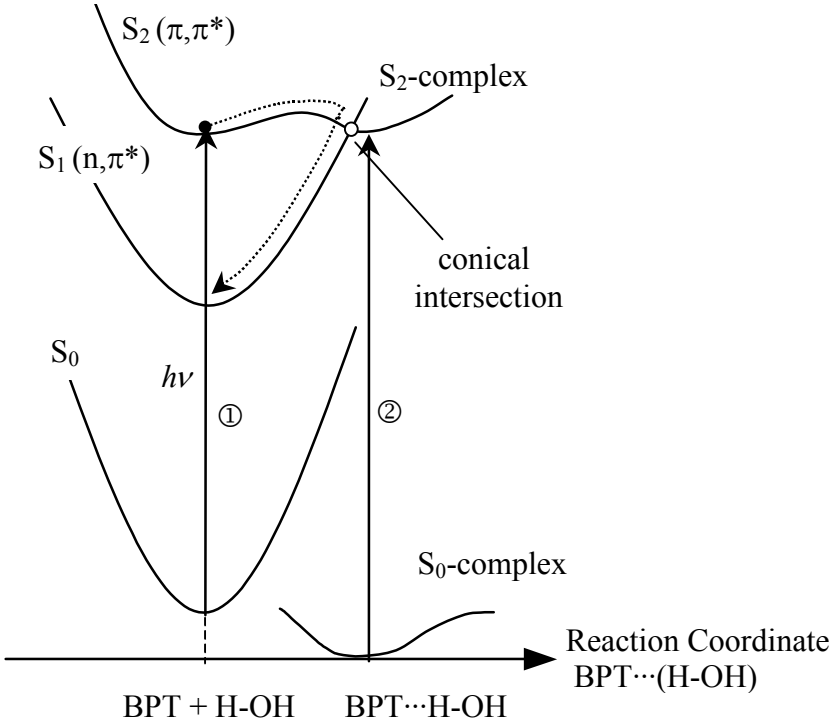

Figure 3.21. Schematic potential reaction coordinate for: aborted S_2-complex formation in water (or deuterated water) by reactive S_2-BPT molecule (①), deactivation of directly excited hydrogen-bonded complex (②).

Eq.3.8 gives the lifetimes τ_{S2} for the free BPT S_2 state in H_2O and D_2O.

$$\tau_{S2} = \frac{1}{k_{complex} + k_{nr} + k_r}, \qquad (3.8)$$

where $k_{complex}$ is the hydrogen-bonded complex formation quenching rate constant. The value $k_{nr}+k_r = 12.2\times10^{10}$ s^{-1} from Table 1.1 is assumed to be constant, because the same energy gap of $\Delta E(S_2\text{-}S_1) = 4200$ cm^{-1} was obtained from the steady-state measurements in both H_2O and D_2O solvents. The determined lifetimes using up-conversion fluorescence spectroscopy ($\tau_{S2}(H_2O) = 1.0 \pm 0.1$ ps and $\tau_{S2}(D_2O) = 2.2 \pm 0.2$ ps), the Eq.3.8 and the known ($k_{nr}+k_r$) value allows us to determine the $k_{complex}$ rate constants as 87.8×10^{10} s^{-1} and 33.2×10^{10} s^{-1} in H_2O and D_2O respectively. Scheme 3.4 describes the proposed BPT S_2 state deactivation process.

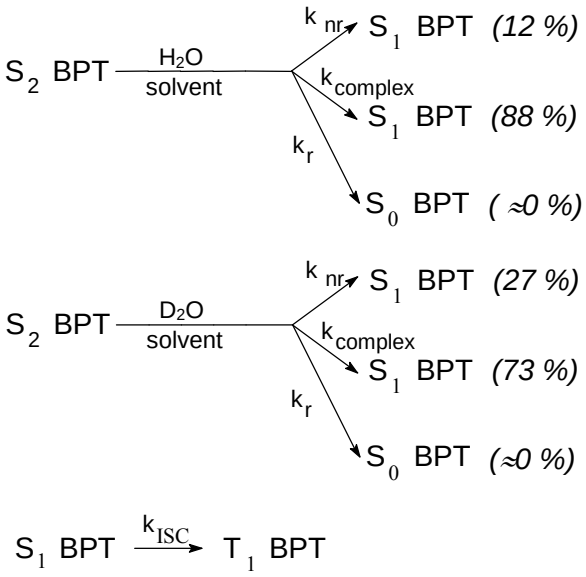

Scheme 3.4.

The quenching rate constant $k_{complex}$ is about 20-fold higher than that in hydrocarbons. Two reasons can be proposed to explain this very high quenching rate constant in water:

- The small change of charge distribution during the approaching of the H^+ proton of the H-O bond towards the thiocarbonyl group of S_2 BPT is sufficient to induce the transition through the conical intersection point (almost barrierless reaction).
- The low energy gap $\Delta E(S_2–S_1) = 4220$ cm^{-1}, compared to that found in hydrocarbons (~8300 cm^{-1}) and acetonitrile (7150 cm^{-1}), can favour the transition through the conical intersection point due to closer S_2 and S_1 potential curves.

To summarise a very efficient quenching mechanism of the BPT S_2 state by water was observed by femtosecond transient absorption and emission spectroscopies. An aborted S_2 state hydrogen-bonded complex formation has been tentatively proposed as the quenching

mechanism. The very short lifetime of BPT S_1 state postulated in hydrocarbons and acetonitrile was confirmed by the observation of an instantaneous growth of the BPT triplet T_1 state population ($S_1 \xrightarrow{ISC} T_1$ transition). This is consistent with the short lifetime of thioxanthione in the S_1 state (~0.5 ps) in acetonitrile, acetone and 1-octanol reported by Tittelbach-Helmrich and Steer [12].

3.5. References.

1. A. Maciejewski, R. P. Steer, *Chem. Rev.*, 93 (1993) 67.
2. A. Maciejewski, D. R. Demmer, D. R. James, A. Safarzadeh-Amari, R. E. Verrall, R. P. Steer, *J. Am. Chem. Soc.*, 107 (1985) 2831.
3. C. Ho, A. L. Motyka, M. R. Topp, *Chem. Phys. Lett.*, 158 (1989) 51.
4. M. Lorenc, A. Maciejewski, M. Ziolek, R. Naskrecki, J. Karolczak, J. Kubicki, B. Ciesielska, *Chem. Phys. Lett.*, 346 (2001) 224.
5. J. Kubicki, A. Maciejewski, M. Milewski, T. Wrozowa, R. P. Steer, *Phys. Chem. Chem. Phys.*, 4 (2002) 173.
6. K. Dobek, A. Maciejewski, J. Karolczak, W. Augustyniak, *J. Phys. Chem. A.*, 106 (2002) 2789.
7. K. Y. Law, P. de Mayo, *J. Am. Chem. Soc.*, 99 (1977) 5813.
8. K. Y. Law, P. de Mayo, *J. Am. Chem. Soc.*, 101 (1979) 3251.
9. D. S. L. Blackwell, K. Lee, P. de Mayo, G. L. R. Petrasunias, G. Reverdy, *Nouv. J. Chim.* 3 (1979) 123.
10. A. Maciejewski, M. Sikorski, W. Augustyniak, M. Fidecka, *J. Photochem. Photobiol.,* 94 (1996) 119.
11. G. Burdzinski, A. Maciejewski, G. Buntinx, O. Poizat, C. Lefumeux, *Chem. Phys. Lett.*, 368 (2003) 745.
12. D. Tittelbach-Helmrich, R. P. Steer, *Chem. Phys. Lett.*, 262 (1996) 369.
13. M. Sikorski, W. Augustyniak, I. V. Khmelinskii, V. V. Korolev, N. M. Bazhin, *Chem. Phys. Lett*, 209 (1993) 403.
14. A. A. Ruth, F. J. O'Keefe, M. W. D. Mansfield, R. P. Brint, *Chem. Phys. Lett.*, 264 (1997) 605.
15. A. Maciejewski, M. Szymanski, R. P. Steer, *J. Phys. Chem.*, 92 (1988) 6939.
16. H. K. Sinha, O. K. Abou-Zied, R. P. Steer, *Chem. Phys. Lett.,* 201 (1993) 433.

17. W. M. Nau, G. Greiner, H. Rau, J. Wall, M. Olivucci, J.C. Scaiano, *J. Phys. Chem. A*, 103 (1999) 1579.
18. C. Coenjarts, J. C. Scaiano, *J. Am. Chem. Soc.*, 122 (2000) 3635.
19. N. Cohen, S. W. Benson, *Chem. Rev.*, 93 (1993) 2419.
20. J. A. Kerr, *Handbook of Chemistry and Physics*, 79th ed.; D. R. Lide editor, CRC Press: Boca Raton, FL, 1998; Chapter 9: *Strength of Chemical Bonds*, Tables 9 - 64.
21. J. Berkowitz, G. B. Ellison, D. Gutman, *J. Phys. Chem.*, 98 (1994) 2744.
22. N. N. Semenov, *Some problems in Chemical Kinetics and Reactivity*, translated by M. Boudart, Princeton University Press, Princeton, 1958, Volume 1, 49-56 (original Russian edition 1954).
23. G. Burdzinski, D. Komar, J. Kubicki, A. Maciejewski, T. Wrozowa, to be published.
24. P. W. Atkins, *The Elements of Physical Chemistry*, second edition, Oxford University Press 1996.
25. B. Nickel, H. Eisenberger, M. T. Wick, R. P. Steer, *J. Chem. Soc., Faraday Trans.*, 92 (1996) 1101.
26. M. A. El-Sayed, *J. Chem. Phys.*, 36 (1962) 573.
27. M. A. El-Sayed, *J. Chem. Phys.*, 38 (1963) 2834.
28. D. S. L. Blackwell, K. Lee, P. de Mayo, G. L. R. Petrasunias, G. Reverdy, *Nouv. J. Chim.* 3 (1979) 123.
29. A. Maciejewski, M. Szymanski, R. P. Steer, *J. Phys. Chem.*, 92 (1988) 2485.
30. B. J. Schwartz, J. C. King, J. Z. Zhang, C. B. Harris, *Chem. Phys. Lett.*, 203 (1993) 503.
31. T. Lian, S. E. Bromberg, M. C. Asplund, H. Yang, C. B. Harris, *J. Phys. Chem.*, 100 (1996) 11994.
32. M. Chachisvillis, I. Garcia-Ochoa, A. Douhal, A. H. Zewail, *Chem. Phys. Lett.*, 293 (1998) 153.
33. S. C. Hayes, M. J. Philpott, P. J. Reid, *J. Chem. Phys.*, 109 (1998) 2596.
34. Z. B. Alfassi, Ed.; *S-Centered Radicals*; John Wiley & Sons: Chichester, 1999.
35. C. Chatgilialoglu, K.-D. Asmus, Eds.; *Sulfur-Centered Reactive Intermediates in Chemistry and Biology*, NATO-ASI vol. 197, Plenum Press, New York, London, 1990.
36. W. M. Nau, W. Adam, J.C. Scaiano, *Chem. Phys. Lett.*, 253 (1996) 92.
37. W. M. Nau, *Ber. Bunsenges. Phys. Chem.*, 102 (1998) 476.
38. W. M. Nau, G. Greiner, J. Wall, H. Rau, M. Olivucci, M. A. Robb, *Angew. Chem. Int. Ed.*, 37 (1998) 98.
39. W. M. Nau, *EPA Newsl.*, 70 (2000) 6.

40. A. Maciejewski, M. Szymanski, R. P. Steer, *Chem. Phys. Lett.*, 143 (1988) 559.
41. G. Buntinx, R. Naskrecki, O. Poizat, *J. Phys. Chem.*, 100 (1996) 19380.
42. S. Akimoto, I. Yamazaki, T. Sakawa, M. Mimuro, *J. Phys. Chem. A*, 106 (2002) 2237.
43. W. Jarzeba, G. C. Walker, A. E. Johnson, M. A. Kahlow, P. F. Barbara, *J. Phys. Chem.*, 92 (1988) 7039.
44. R. Jimenez, G. R. Fleming, P. V. Kumar, M. Maroncelli, *Nature*, 309 (1994) 471.
45. N. Nandi, S. Roy, B. Bagchi, *J. Chem. Phys.*, 102 (1995) 1390.
46. P. J. Reid, C. Silva, P. F. Barbara, L. Karki, J. T. Hupp, *J. Phys. Chem.*, 99 (1995) 2609.
47. R. M. Stratt, M. Maroncelli, *J. Phys. Chem.*, 100 (1996) 12981.
48. B. Zolotov, A. Gan, B. D. Fainberg, D. Huppert, *Chem. Phys. Lett.*, 265 (1997) 418.
49. Y. Nagasawa, Y. Ando, D. Kataoka, H. Matsuda, H. Miyasaka, T. Okada, *J. Phys. Chem. A*, 106 (2002) 2024.
50. S. K. Pal, J. Peon, A. H. Zewail, *PNAS*, 99 (2002) 1763.
51. S. K. Pal, J. Peon, B. Bagchi, A. H. Zewail, *J. Phys. Chem. B*, 106 (2002) 12376.
52. J. R. Lakowicz, *Principles fluorescence spectroscopy-second edition*, Kluwer Academic / Plenum Publishers, New York, 1999.
53. M. Lorenc, M. Ziolek, R. Naskrecki, J. Karolczak, J. Kubicki, A. Maciejewski, *Appl. Phys. B*, 74 (2002) 19.
54. S. Yamaguchi, H. Hamaguchi, *J. Phys. Chem. A*, 104 (2000) 4272.
55. K. C. Medhi, G. S. Kastha, *Ind. J. Phys.*, 37 (1963) 275.

CHAPTER 4.

Vibrational relaxation and orientational anisotropy decay of benzopyranthione in the S_2 state.

4.1. Introduction.

Femtosecond up-conversion and transient absorption studies of the depopulation of the S_2 state of thioketones have led us to show for the first time according to our knowledge that other phenomena such as vibrational relaxation and orientational anisotropy decay can influence the measured signal. Thus, we decided to study these processes in detail. On one hand, their characterisation ensures a proper interpretation of the S_2 depopulation signal, on other hand, there are very few reports about the study of these processes for molecules in the S_2 state [1 - 7]. For such studies we chose to use hydrocarbon solvents, because in such solvents the S_2 state lifetime of a model thioketone benzopyranthione (BPT) is relatively long compared to those of acetonitrile and water. Moreover, it gives opportunity to use different solvents of the same polarity and of various bulk viscosities.

4.2. Vibrational relaxation in the S_2 state.

If a molecule is photoexcited with an energy higher than the energy of the 0-0 transition, the excess energy, acquired by the Franck-Condon active modes, is rapidly redistributed among the solute's internal degrees of freedom (intramolecular vibrational redistribution) and transferred to the first solvent shell and then to the bulk solvent (vibrational cooling). These processes can be investigated by ultrafast spectroscopic methods, in particular femtosecond fluorescence up-conversion and transient absorption techniques. For large size solute molecules, intramolecular vibrational redistribution typically occurs within the subpicosecond time-scale, however vibrational cooling generally proceeds on a picosecond time scale [8 - 14]. Recently, a model describing the vibrational cooling process has been presented by Kovalenko and co-workers [14]. They have shown that in the case of a strong solute-solvent coupling (for example via hydrogen bonding), the function describing the vibrational cooling process is a biexponential function with a fast component, reflecting the solute-first solvent shell heat transfer and a slower component corresponding to the cooling of the first solvent shell by the bulk solvent. When the solute-solvent coupling is weak, only a monoexponential function is expected, which is determined by the heat transfer from the solute to the bulk solvent. This has been experimentally observed for the S_1 state of stilbene in cyclohexane and in acetonitrile [14]. The same monoexponential vibrational cooling process can be expected for vibrationally excited thioketones in the S_2 state in

hydrocarbons. Very little is known about the vibrational relaxation of molecules in the S_2 state in solution. Such a process has been reported for β-carotene, neurosporene, all-*trans*-1,8-diphenyl-1,3,5,7-octatetraene and malachite green [1 - 5]. Thioketones are good models to investigate the vibrational relaxation processes in the S_2 state due to their relatively long lifetime τ_{S2} compared to that of the previously mentioned molecules. Moreover, in the case of BPT in hydrocarbons, the energy difference between the vibrationally relaxed S_3 and S_2 states is about 7000 cm^{-1}, thus making it possible to selectively photoexcite the S_2 state.

Vibrational relaxation of the BPT S_2 state was studied using femtosecond transient absorption and fluorescence up-conversion methods. The change of the pump wavelength from 403 nm (related to the 0-0 transition) to 380 nm provides an excess of about 1500 cm^{-1} of vibrational energy to the BPT S_2 state in hydrocarbon solvents. The analysis of the kinetics obtained by transient absorption spectroscopy for BPT in n-hexane excited at 380 nm shows a biexponential decay on the low energy side of the $S_2 \rightarrow S_n$ absorption band: the longer decay time t_1 represents the S_2 state depopulation (by analogy with that obtained with the 403 nm excitation wavelength), the shorter decay time t_2 can be related to the vibrational relaxation process. In order to eliminate the contribution of the population decay, a normalisation procedure of the transient absorption spectra at 650 nm was applied (see Fig.4.1a). Vibrational cooling in the singlet excited state is usually evidenced by a narrowing of the band of the transient absorption spectra versus time [13].

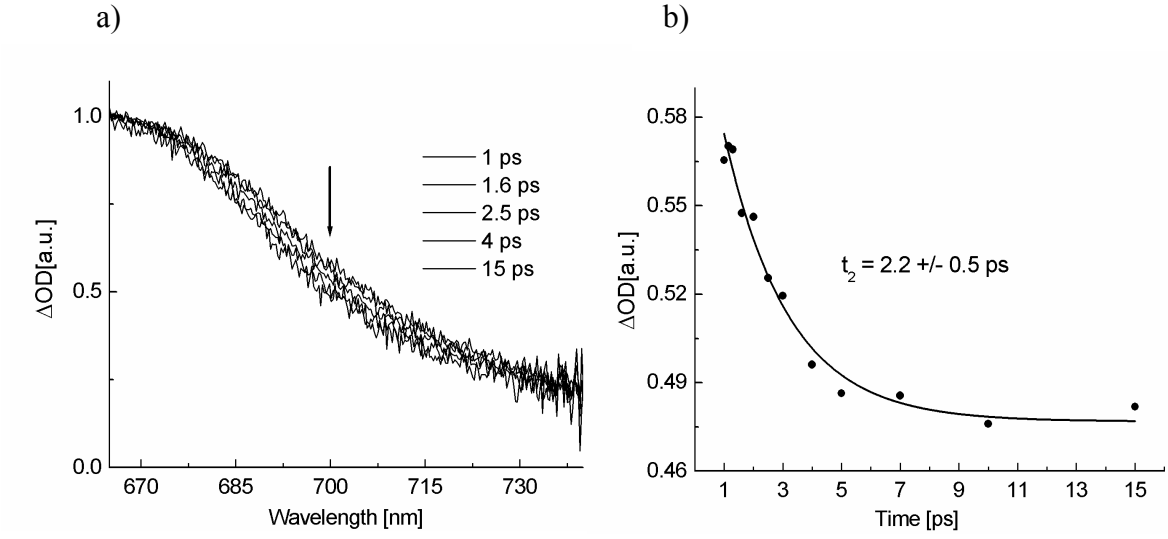

Figure 4.1. a) Normalised (650 nm) transient absorption spectra measured at the magic angle at time delays ranging from 1 to 15 ps after photoexcitation of BPT (1×10^{-3} M) in n-hexane at 380 nm. b) Kinetic trace at 700 nm and best fit single exponential function.

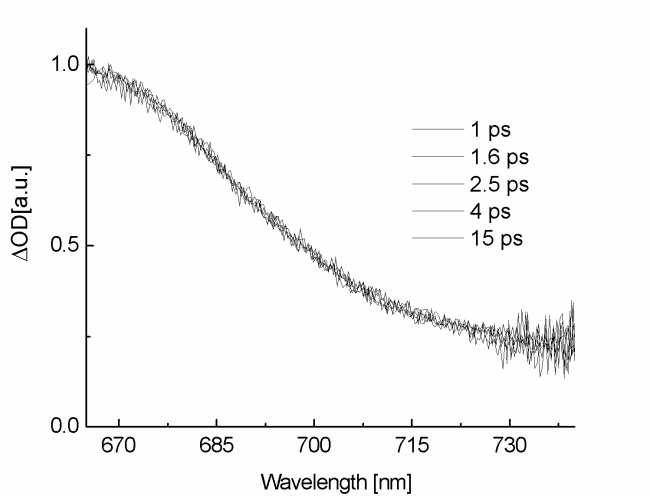

Figure 4.2. Normalised (650 nm) transient absorption spectra measured at the magic angle for time delays ranging from 1 to 15 ps after photoexcitation of BPT (1×10^{-3} M) in n-hexane at 403 nm.

The dynamics of the narrowing of the BPT S_2 state band is characterised in Fig.4.1b by a monoexponential decay function with a time-constant of 2.2 ± 0.5 ps [15]. This time-constant is assumed to be only heat transfer from the hot solute to the bulk solvent. In the case where the pump wavelength is adjusted to the 0-0 transition (403 nm), the narrowing of the transient absorption spectra is not observed (Fig.4.2), as expected.

The femtosecond fluorescence up-conversion method can provide complementary information on the BPT S_2 state vibrational cooling in n-hexane. At the fluorescence maximum (465 nm), the experimental data were well fitted, taking into account a deconvolution procedure, to a single exponential function $F(t) = A_1 \exp(-t/t_1) + C$ (see Fig.4.3a) for all the pump wavelengths in the 315 - 380 nm range. A 315 nm pump wavelength provides the S_2 state of BPT with an excess of vibrational energy of approximately 6900 cm^{-1}. Intramolecular vibrational redistribution process is usually observed, on femtosecond fluorescence measurements, by the modification of the fluorescence rise-time [2]. However, in our case such a component can not be resolved for BPT S_2 state in n-hexane due to the time resolution of the experimental set-up used (150 fs). The measured lifetime t_1 of the BPT in the S_2 state at different excitation wavelengths (380, 350, 330 and 315 nm) is the same (20.2 ps) within the experimental error (see Fig.4.3a). The situation is drastically different when the fluorescence is observed on the red or blue side of the emission band. In this case, a biexponential function $F(t) = A_1\exp(-t/t_1) + A_2\exp(-t/t_2) + C$ was used to fit the experimental data (see Fig.4.3b).

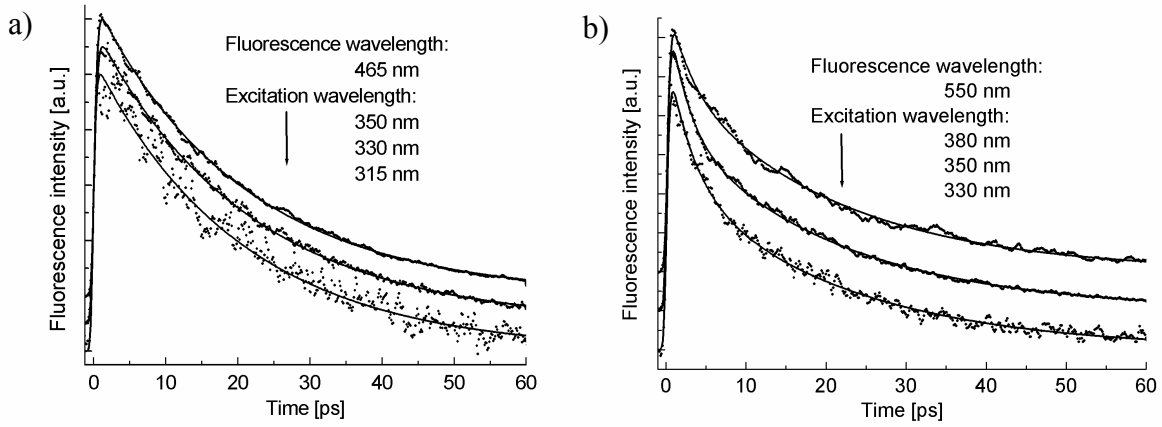

Figure 4.3. Fluorescence decays recorded for ~10^{-4} M BPT in n-hexane at (a) 465 nm for different excitation wavelengths (350, 330 and 315 nm) fitted by monoexponential function, (b) 550 nm for excitation wavelengths 380, 350 and 330 nm fitted by biexponential function.

The lifetime t_1 of BPT in the S_2 state was set as fixed during the deconvolution and fitting procedure. A time-constant t_2 of 2.8 ± 0.5 ps was determined from the data recorded for three excitation wavelengths (330, 350 and 380 nm). The amplitude ratio A_2/A_1 was found to increase from 0.3 to 0.4 on going from 380 to 330 nm excitation wavelengths. The t_2 value is consistent with that determined by femtosecond transient absorption spectroscopy for the vibrational relaxation processes for BPT in its S_2 state.

It was mentioned that the time-constant t_2 is assumed to be the only characteristic of the heat transfer from the hot solute to the bulk solvent. However, another process can also be considered. The radiationless decay of BPT in its S_2 state can also be enhanced when there is a large excess of vibrational energy. Under such conditions transitions can take place at an energy above that of the activation barrier, and thus the S_2 state quenching process by the hydrocarbon solvents should be enhanced. Such a process should be characterised by a time-constant <1 ps, which is shorter than that the of observed t_2 value.

In conclusion, we have shown that the kinetic behaviour of BPT S_2 state in n-hexane as determined by transient absorption or fluorescence up-conversion methods depends on the pump energy. When the pump energy is adjusted to the 0-0 transition, the dynamics of the S_2 state of BPT is well described by a single exponential function (t_1 = 20.2 ps) which corresponds to the depopulation of the S_2 state. When an excess of vibrational energy is provided to the S_2 state of BPT by using a higher pump energy, a second exponential function has to be added to the previous one to take into account the S_2 state vibrational relaxation

process ($t_2 = 2.5 \pm 0.5$ ps), the amplitude of which increases with the pump energy. As a consequence, a population relaxation study requires an excitation wavelength adjusted to that of the 0-0 transition. This ensures the elimination of intramolecular vibrational redistribution and vibrational cooling processes, as well as, possible vibrational wave-packet motion in the S_2 state.

Another interesting aspect of excited S_2 state dynamics is the molecular rotational diffusion, which has never been studied so far for thioketones.

4.3. Orientational anisotropy.

To the author's knowledge, the decay of orientational anisotropy of solute in the S_2 state has never been observed in real time because the lifetime τ_{S2} is usually very short compared to that of the expected rotational correlation time of molecules [1, 6, 7]. Aromatic thioketones are usually characterised by a relatively small molecular volume and a long-lived S_2 state. They are thus convenient compounds to measure the decay of S_2 state rotational diffusion, which provides a mechanistic aspect of the dynamics of the interaction between the excited solute and it's surrounding. For these studies the author used two complementary femtosecond methods: the transient absorption and the fluorescence up-conversion methods.

Lessing and Von Jena have shown that transient absorption measurements performed at the magic angle (54.7^0) between linearly polarised pump and probe beams allow us to determine the population kinetics free from molecular reorientational diffusion [16]. For the same reason, fluorescence decay measurements are usually made with a 54.7^0 angle between pump and observation polarisations [17]. Obviously, in the case when the molecular reorientational diffusion is required to be measured, angles other than the magic angle are used. Let us discuss the phenomenon in some detail.

Before the pump pulse excites the solute molecules, they are randomly oriented in the solution. The probability of the absorption of a photon pump by a solute molecule depends on the relative orientation of the absorption transition dipole moment $\vec{\mu}$ and of the electric vector $\vec{\varepsilon}$ of the linearly polarised pump pulse. The molecules with the absorption transition dipole moment oriented parallel to the electric vector $\vec{\varepsilon}$ have the highest probability to be excited. Thus, sample photoexcitation by a linearly polarised pump pulse results in a set of preferentially oriented molecules along the direction of electric vector $\vec{\varepsilon}$. The subsequent

rotational diffusion of the excited chromophores results in a decrease of this preferential orientation order and thus of the transition dipole moments. The relaxation of the photoinduced orientational anisotropy can be monitored by:

- Fluorescence spectroscopy of the excited states,
- Transient absorption spectroscopy where the orientational anisotropy signal can be present in: the stimulated emission, the excited state absorption or the ground state depletion signals (eventually, their superposition).

In both methods the experiments are usually performed for two different configurations of (pump/gate or pump/probe, respectively) beam polarisations: parallel (*par*) and perpendicular (*perp*). The induced transient polarisation anisotropy is extracted from the experimental data according to the following formulas [18 - 20]:

$$r_\lambda(t) = \frac{I_\lambda^{par}(t) - k \cdot I_\lambda^{perp}(t)}{I_\lambda^{par}(t) + 2 \cdot k \cdot I_\lambda^{perp}(t)}, \qquad (4.1)$$

fluorescence up-conversion

$$r_\lambda(t) = \frac{\Delta OD_\lambda^{par}(t) - \Delta OD_\lambda^{perp}(t)}{\Delta OD_\lambda^{par}(t) + 2 \cdot \Delta OD_\lambda^{perp}(t)}, \qquad (4.2)$$

transient absorption

where: $I_\lambda^{par}(t)$ and $I_\lambda^{perp}(t)$ are the time-dependent fluorescence intensities at a given observation wavelength λ for the *par* and *perp* polarisations, respectively, k is a normalisation factor that corrects the difference of experimental sensitivity observed between the two polarisations, $\Delta OD_\lambda^{par}(t)$ and $\Delta OD_\lambda^{perp}(t)$ are the transient absorption kinetics measured at given probe wavelength λ for the *par* and *perp* polarisations, respectively.

In the case when the up-converted fluorescence (or transient absorption) signal is dominated by one species, the transient anisotropy function *r(t)* is equal to [19 - 21]:

$$r(t) = 0.4 \left\langle P_2[\hat{\mu}_1(0) \circ \hat{\mu}_2(t)] \right\rangle, \qquad (4.3)$$

where $\hat{\mu}_i = \vec{\mu}_i / |\vec{\mu}_i|$ for $i=1,2$, $\vec{\mu}_1$ is the transition dipole moment associated with the preparation of the excited state (absorption), $\vec{\mu}_2$ is the transition dipole moment associated with the probing event (e.g. fluorescence or absorption), $P_2(x) = 0.5(3x^2 - 1)$ is the second-order Legendre polynomial, the angle brackets denote a weighted average over the rotational state distribution of molecules in the sample. When only one species is probed, the calculated

anisotropy $r(t)$, including the initial value $r(t_0)$, generally varies between the $-0.2 \leq r(t) \leq 0.4$ limits.

4.3.1. Femtosecond fluorescence up-conversion and transient absorption measurements.

BPT S_2 state femtosecond fluorescence up-conversion measurements were performed in different linear hydrocarbons (n-hexane, n-heptane, n-octane, n-decane, n-dodecane) and in cyclohexane in order to determine the influence of bulk solvent viscosity η on the orientational anisotropy dynamics. All anisotropy decays were fitted to a single exponential decay function:

$$r(t)=r(t_0)exp(-t/\tau_{or})+C, \qquad (4.4)$$

where τ_{or} is the orientational time-constant and C is the offset of $r(t)$ (see Fig.4.4). The obtained results show an anisotropy initial value $r(t_0)$ located in the $0.29 < r(t_0) < 0.34$ range and an offset C lower than 0.05. The value of the initial anisotropy $r(t_0)$ is close to the theoretical value of 0.4 which is expected when the fluorescence transition moment is parallel to that of the absorption (see Eq.4.3). Fig.4.5 presents the dependence of the rotational time-constant τ_{or} on the solvent viscosity approximated by a linear function with a slope of 2.6 ± 1 ps/cP and an intercept of 2.6 ps. Further discussion of the intercept is ignored because its interpretation is not clear [18].

Fluorescence up-conversion results were completed by femtosecond transient absorption measurements. Two kinetic traces of stimulated emission recorded at 465 nm for BPT in n-hexane for two pump/probe polarisations (parallel and perpendicular) are presented in Fig.4.6a. Since the intensity of the triplet T_1 state absorption signal is low within the 0 - 15 ps time window, only the decay of the stimulated emission from the S_2 state is considered. Fig.4.6b presents the single exponential anisotropy decay of BPT in the S_2 state, which is consistent with that obtained by the fluorescence up-conversion method (see inset in Fig.4.4a). The anisotropy was also investigated at other wavelengths than 465 nm. In the 440 - 550 nm spectral range the initial anisotropy $r(t_0)$ value is close to 0.4 (Fig.4.6c), thus absorption and stimulated emission dipoles are almost collinear according to Eq.4.3. However, in the 615 - 700 nm spectral range, the initial anisotropy $r(t_0)$ value is close to 0.05.

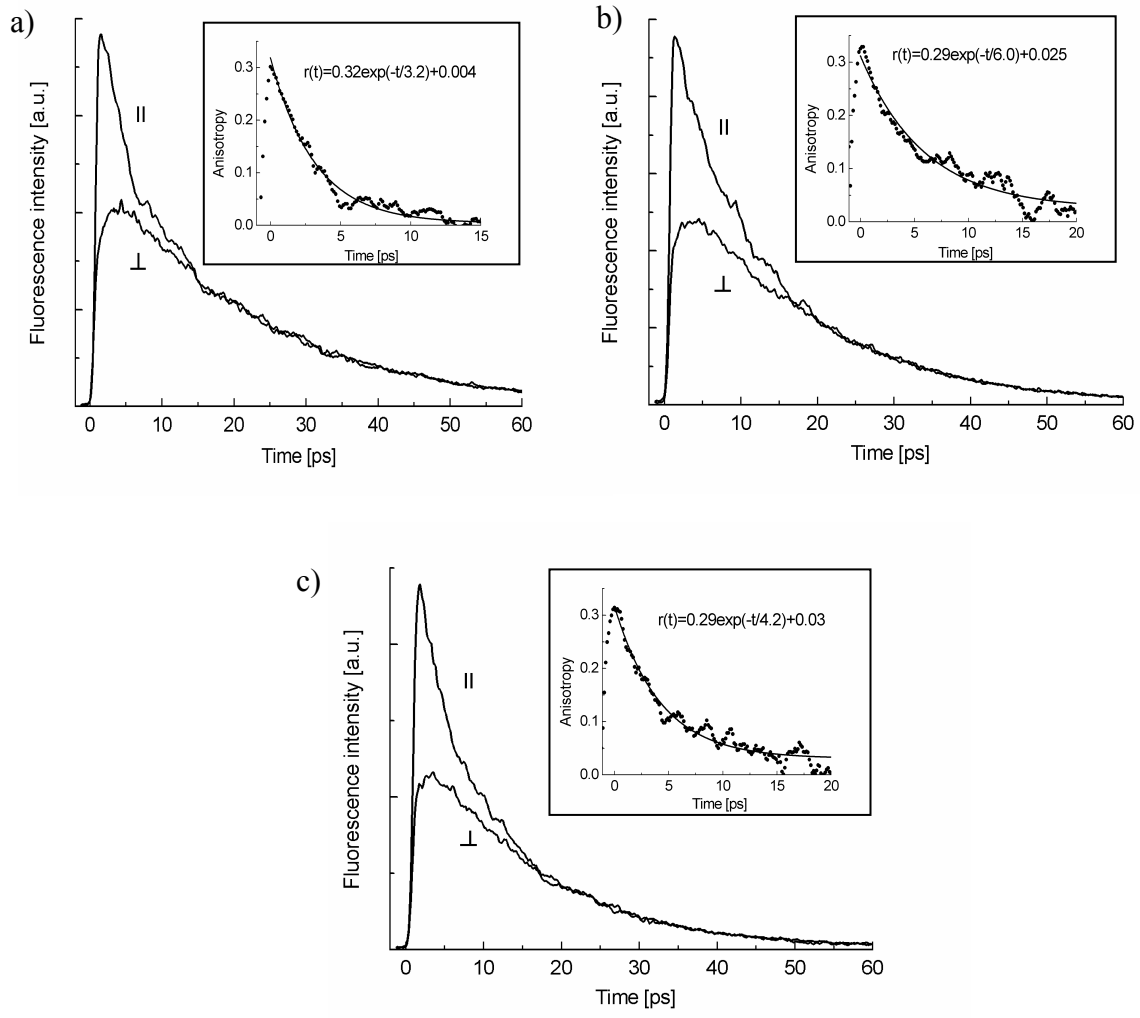

Figure 4.4. Polarised femtosecond up-converted fluorescence decays of BPT in n-hexane (a), BPT in dodecane (b), $BPTC_4$ in n-hexane (c), measured at fluorescence wavelength 465 nm for a solute concentration of 3×10^{-4} M (signals are tail-matched) after photoexcitation at 380 nm. The corresponding anisotropy decays determined by Eq.4.2 with fitted single exponential function are presented in the insets.

This can be explained by a difference of about 50° (according to Eq.4.3) between the directions of the absorption dipole moments of the $S_0 \rightarrow S_2$ and $S_2 \rightarrow S_n$ transitions, thus showing a difference in the electronic structures of the S_0, S_2 and S_n states. At wavelengths where the measured signal was very weak (close to the isosbestic point and the red edge of S_2 absorption band), the calculated anisotropy was noisy, meaningless, and consequently not plotted in Fig.4.6c.

It has previously been mentioned that the measured anisotropy decays (see Fig.4.4 and Fig.4.6b) were well fitted by a single exponential functions for all hydrocarbons used. Since BPT is a rigid molecule with fixed transition dipole moments, the rotational diffusion of the

BPT S_2 state is the only reason for the observed anisotropy decays. It is known that rotational diffusion depends on the solvent viscosity, on the size and shape of the diffusing species, as well as, on the solute-solvent interactions [18]. However, both BPT in the S_2 state and the hydrocarbons used are known to be almost non-polar. It is worth comparing the obtained slope ($\tau_{or}/\eta = 2.6 \pm 1$ ps/cP in Fig.4.5) with that for the theoretical estimation despite the fact that such a comparison can only be qualitative [18]. For a simple estimation of the rotational correlation time τ_{or}, a modified Debye-Stokes-Einstein model can be used [18, 22]:

$$\tau_{or} = \frac{\eta VF}{kTS}, \tag{4.5}$$

where η is the viscosity, k is the Boltzmann constant, T is the temperature in Kelvin, V is the hydrodynamic volume of the solute, S is a shape factor which accounts for a nonspherical solute molecular shape as calculated from Perrin's equations, and F is a friction coefficient. The friction coefficient F is equal to 1 ("stick" boundary conditions), when a fluid layer which is adjacent to the solute moves with the same velocity as the solute. In the "slip" boundary conditions, F<1 and depends on the solute molecular shape, only the rotating motions that displace the solvent molecules result in friction. A BPT molecular volume V of about 140 $Å^3$ (van der Waals model) was calculated using the *HyperChem 7* software package (molecular geometry was optimised at Polak-Ribiere/6-31G* level). A significant change of the volume V, due to the $S_0 \rightarrow S_2$ excitation, is not expected. The shape of BPT seems to be rather an oblate rotor than a prolate ellipsoid (see Fig.4.7).

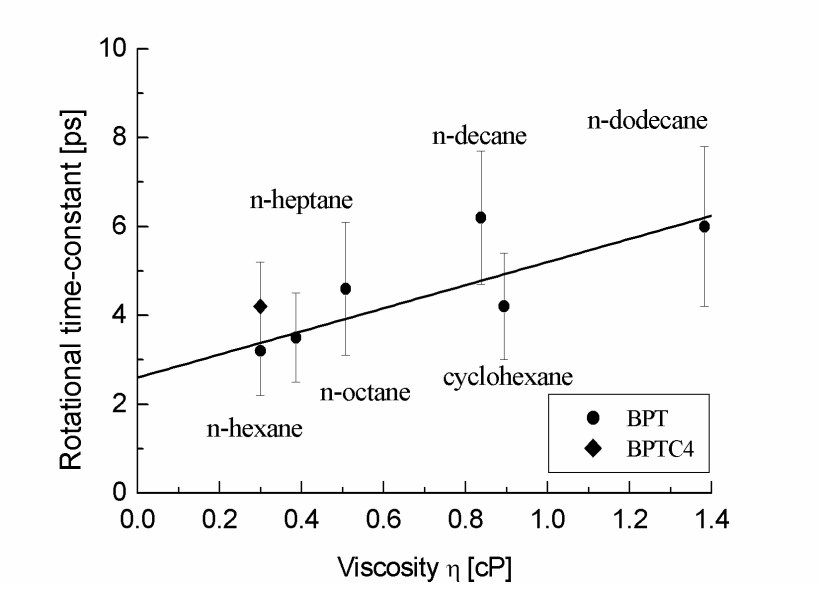

Figure 4.5. Dependence of the rotational time constant of BPT S_2 state versus solvent viscosity (●). For the sake of comparison $BPTC_4$ in n-hexane is also presented (♦).

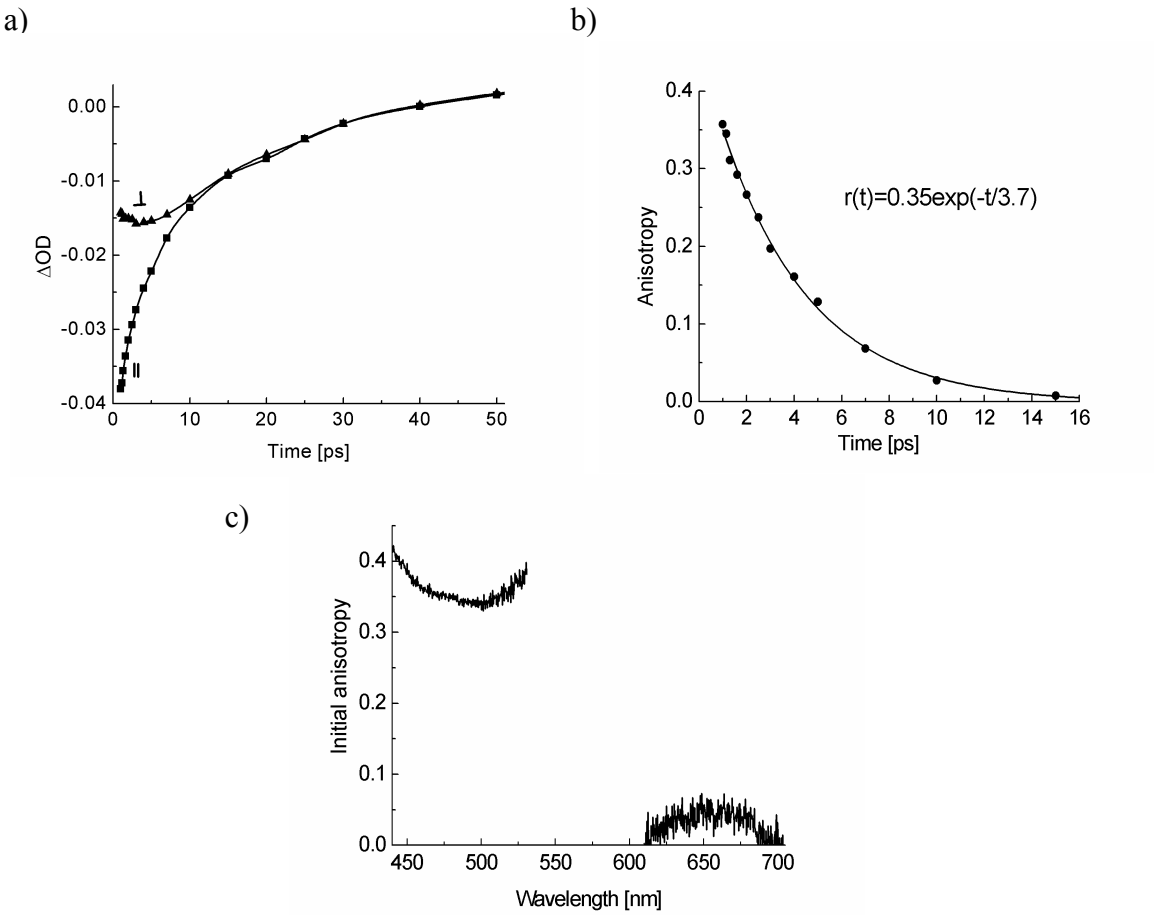

Figure 4.6. a) Stimulated emission kinetics recorded at 465 nm for BPT in n-hexane (1×10^{-3} M) after photoexcitation at 403 nm with perpendicular and parallel polarisations of pump and probe beams, shown as triangles and squares, respectively. b) Corresponding anisotropy decay *r(t)* (see Eq.4.2) fitted to a monoexponential function (according to Eq.4.4) c) The calculated spectrum $r_{t0}(\lambda)$ of the initial anisotropy.

Thus, this disklike shape of BPT is approximated to a symmetric oblate ellipsoid, since semiaxis dimensions of 4.5, 4, 1.9 Å, along the x, y, z axis respectively were found (see Fig.4.7). For BPT molecules that rotate around the z axis (perpendicular to the plane of the molecule), the shape factor *S* is 0.66 and the slip friction coefficient *F* is 0.06 [17, 23 - 26]. Rotations around other axis of the molecule (x, y) result in a larger solvent displacement and are thus slower than rotations around the z axis. Thus, the observed rapid BPT S_2 state (Fig.4.4a shows only 3.2 ps in n-hexane) anisotropy decay can be ascribed to rotation around the z axis. This is consistent with the fact that the $S_0 \leftrightarrow S_2$ transition dipole moments lie into the molecular plane of BPT as for xanthione [27].

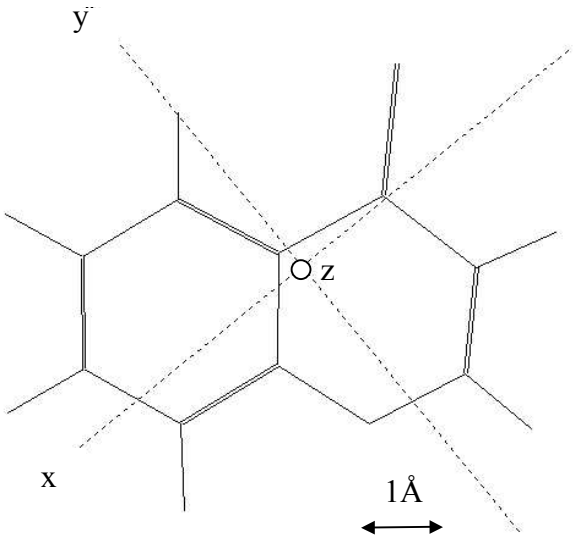

Figure 4.7. Optimised structure of benzopyranthione and definition of inertial axes *x*, *y* and *z*.

It was mentioned that the initial anisotropy $r(t_0)$ values of 0.4 are expected in the case when the fluorescence transition moment is parallel to the absorption transition moment, but the observed $r(t_0)$ value is slightly lower. This can be explained by a slightly out of the *xy* plane vibrationally induced component in the transition dipole moment affecting the initial anisotropy $r(t_0)$ value [28 - 30]. This is supported by the fact that, the initial value $r(t_0)$ obtained by transient gain spectroscopy (without an excess of vibrational energy) for the BPT S_2 state in n-hexane is slightly higher than that obtained by fluorescence up-conversion in the same solvent (1500 cm^{-1} excess energy). According to Eq.4.5, at T = 293 K under slip (F = 0.06) and stick (F = 1) boundary conditions, τ_{or}/η = 3.1 ps/cP and 52 ps/cP were found, respectively. The former is consistent with the experimental value of 2.6 ± 1 ps/cP, which evidences that BPT in the S_2 state rotates under slip condition in all studied hydrocarbons. Near slip boundary conditions have also been found in the literature for other molecules (coumarine 153, perylene, biphenyl, trans-4,4`-diphenylstilbene) in hydrocarbon solvents [17, 21, 30, 31]. According to Eq.4.5 it can be expected that the increase of the solute volume *V* results in an increase in the orientational time τ_{or}. The replacement of BPT by the n-butyl derivative $BPTC_4$ (calculated volume of 210 $Å^3$) changes the τ_{or} value from 3.2 to 4.2 ± 1.0 ps in n-hexane (see Fig.4.4).

It is interesting to note that the obtained orientational diffusion time of BPT in the S_2 state in n-hexane (3.2 ps) is consistent with those values reported for slightly bigger or smaller molecules in hydrocarbon solvents of similar viscosity (see Table 4.1).

In gas phase (frictionless conditions) the orientational time τ_{free} can be estimated by the following expression [32]:

$$\tau_{free} = \frac{2\pi}{9}\sqrt{\frac{I}{kT}}, \qquad (4.6)$$

where I is the moment of inertia, k is the Boltzmann constant, and T is the temperature in Kelvin. According to the geometrically optimised structure, BPT is a rotor with moments of inertia of 318, 539, 857 amu Å^2 around the x, y and z rotation axis respectively (see Fig.4.7). The resulting orientational times τ_{free} are 0.8, 1.0 and 1.3 ps respectively. The comparison of such values to the fastest rotational time experimentally observed (3.2 ± 1.0 ps in n-hexane), supports the idea that the nature of the BPT S_2 state molecular reorientation in solution is more diffusional than inertial.

It was mentioned that the experimentally observed anisotropy decays are well described by single exponential functions. However, the theory by Chuang and Eisenthal predicts that for oblate molecules with collinear transitions moments (as for BPT $S_0 \leftrightarrow S_2$) lying in the plane of molecule, a biexponential anisotropy decay is expected $r(t)=0.3\exp(-(2D_x+4D_z)t)+0.1\exp(-6D_x t)$, where D_x and D_z are the rotational diffusion coefficients around the x and z axis ($D_z > D_x = D_y$) [29, 33 - 35].

Table 4.1. Orientational time-constant of different solutes in hydrocarbons determined by picosecond transient absorption (PTA) or femtosecond fluorescence up-conversion (FFUP) spectrometer.

Solute	Volume [Å^3]	Solvent	Viscosity [cP]	Rotational time τ [ps]	Method	Reference
BPT	140	n-hexane	0.3	3.2± 1.0	FFUP	
$BPTC_4$	210	n-hexane	0.3	4.2± 1.0	FFUP	
Perylene	225	n-hexane	0.3	11± 2.0	PTA	22
7-azaindole dimer	~225	n-hexane	0.3	12	FFUP	36
Tetracene	224	n-heptane	0.34	13	FFUP	37
Coumarin 153	246	n-hexane	0.3	13	FFUP	18
Biphenyl	150	n-hexane	0.3	6.5	PTA	30
Aniline	100	isopentane	0.22	0.94± 0.05	FFUP	32

This discrepancy can possibly be accounted by the following phenomena. The approximation of the BPT S_2 state to a symmetric oblate rotor can be too rough. Moreover, as mentioned above, one of the transition moments can be slightly out of the *xy* molecular plane of the BPT [29]. Another explanation is that the solute experiences a small friction on rotation not only about *z* axis, but also about *x* and *y* axis. In this case, the anisotropy decay tends towards a single exponential function when the D_x and D_y values approach the D_z value.

In conclusion, in order to determine the influence of the bulk solvent viscosity on the orientational anisotropy dynamics of BPT in the S_2 state, fluorescence measurements were performed in different linear hydrocarbon solvents (n-hexane, n-heptane, n-octane, n-decane and n-dodecane) and in cyclohexane. BPT is a rigid molecule with fixed transition dipoles ($S_0 \leftrightarrow S_2$) lying in the plane of the molecule. In all solvents anisotropy decays were found to be monoexponential ($r(t)=r(t_0)exp(-t/\tau_{or})+C$). The initial value $r(t_0)$ obtained for the anisotropy is located in the 0.29 to 0.35 range. The dependence of the rotational time-constant τ_{or} on the solvent viscosity can be approximated by a linear function with a slope of 2.6 ± 1 ps/cP. The rotation dynamics can be explained in terms of the Stokes-Einstein-Debye hydrodynamics theory for a slip condition assuming a symmetric oblate shape of BPT in the S_2 state.

4.4. References.

1. A. N. Macpherson, T. Gillbro, *J. Phys. Chem. A*, 102 (1998) 5049.
2. S. Akimoto, I.Yamazaki, T. Sakawa, M. Mimuro, *J. Phys. Chem. A*, 106 (2002) 2237.
3. W. Atom Yee, R. H. O`Neil, J. W. Lewis, J. Z. Zhang, D. S. Kliger, *J. Phys. Chem. A*, 103 (1999) 2388.
4. S. Akimoto, I. Yamazaki, S. Takaichi, M. Mimuro, *Chem. Phys. Lett.*, 313 (1999) 63.
5. M. Yoshizawa, K.Suzuki, A. Kubo, S. Saikan, *Chem. Phys. Lett.*, 290 (1998) 43.
6. J. Azuma, N. Tamai, A. Shishido, T. Ikeda, *Chem. Phys. Lett.*, 288 (1998) 77.
7. G. G. Gurzadyan, T.-H. Tran-Thi, T. Gustavsson, *J. Chem. Phys.*, 108 (1998) 385.
8. F. Laermer, T. Elsaesser, W. Kaiser, *Chem. Phys. Lett.*, 156 (1989) 381.
9. A. Mokhtari, A. Cheriba, J. Chesnoy, *J. Opt. Soc. Am. B*, 7 (1990) 1551.
10. T. Gustavsson, G. Baldacchino, J-C. Mialocq, S. Pommeret, *Chem. Phys. Lett.*, 236 (1995) 587.
11. I. Martini, G. V. Hartland, *J. Phys. Chem.*, 100 (1996) 19764.
12. T. J. Kang, K. Ohta, K. Tominaga, K. Yoshihara, *Chem. Phys. Lett.*, 287 (1998) 29.
13. X. Tan, T. L. Gustafson, C. Lefumeux, G. Burdzinski, G. Buntinx, O. Poizat, *J. Phys. Chem. A*, 106 (2002) 3593.
14. A. A. Kovalenko, R. Schanz, H. Hennig, N. P. Ernsting, *J. Chem. Phys.*, 115 (2001) 3256.
15. G. Burdzinski, A. Maciejewski, G. Buntinx, O. Poizat, C. Lefumeux, *Chem. Phys. Lett.*, 368 (2003) 745.
16. H.F. Lessing, A. von Jena, *Chem. Phys. Lett.*, 42 (1976) 213.
17. G. Fleming, J. M. Morris, G. W. Robinson, *Chem. Phys.*, 17 (1976) 91.
18. M.-L. Horng, J. A. Gardecki, M. Maroncelli, *J. Phys. Chem. A*, 101 (1997) 1030.
19. L. A. Walker II, S. Pullen, B. Donovan, R. J. Sension, *Chem. Phys. Lett.*, 242 (1995) 177.
20. M. Volk, S. Gnanakaran, E. Golding, Y. Kholodenko, N. Pugliano, R. M. Hochstrasser, *J. Phys. Chem. A*, 101 (1997) 638.
21. G. R. Fleming, *Chemical Applications of Ultrafast Spectroscopy*, 1st ed.; Oxford University Press: New York, 1986.
22. Y. Jiang, G. J. Blanchard, *J. Phys. Chem.*, *98* (1994) 6436.
23. F. Perrin, *J. Phys. Rad.*, 5 (1934) 497.
24. F. Perrin, *J. Phys. Rad.*, 1 (1936) 1.
25. G. K. Youngren, A. Acrivos, *J. Chem. Phys.*, 63 (375) 3846.

26. R. J. Sension, R. M. Hochstrasser, *J. Chem. Phys*, 98 (1993) 2490.
27. H. K. Sinha, O. K. Abou-Zied, R. P. Steer, *Chem. Phys. Lett.,* 201 (1993) 433.
28. A. B. Meyers, M. A. Pereira, P. L. Holt, R. M. Hochstrasser, *J. Chem. Phys.*, *86* (1987) 5146.
29. J. Szczubiakowski, A. Balter, W. Nowak, A. Kowalczyk, K. Wisniewski, M. Wierzbowska, *Chem. Phys.*, 208 (1996) 283.
30. J. Benzler, K. Luther, *Chem. Phys. Lett.*, 279 (1997) 333.
31. X. Tan, T. L. Gustafson, *J. Phys. Chem. A*, 104 (2000) 4469.
32. M. Pereira, P. E. Share, M. J. Sarisky, R. M. Hochstrasser, *J. Chem. Phys.*, 94 (1991) 2513.
33. T. J. Chuang, K. B. Eisenthal, *J. Chem. Phys.*, 57 (1972) 5094.
34. J. R. Lakowicz, *Principles fluorescence spectroscopy-second edition*, Kluwer Academic / Plenum Publishers, New York, 1999.
35. G. J. Blanchard, *J. Phys. Chem. A*, 105 (2001) 6785.
36. S. Takeuchi, T. Tahara, *J. Phys. Chem. A*, 102 (1998) 7740.
37. N. Sarkar, S. Takeuchi, T. Tahara, *J. Phys. Chem. A*, 103 (1999) 4808.

CHAPTER 5.

Time-resolved resonance Raman and *ab initio* calculations studies of the structure of the T_1 state of thiocoumarin.

5.1. Introduction.

Very few vibrational data of aromatic thioketones and more particularly the excited state of aromatic thioketones are reported in the literature. The vibrational analysis of the ground state of xanthione (XT) (see structure in Fig.1.1) based on infrared and Raman spectra has been reported by Steer and co-authors [1]. In this paper, the experimental frequencies (solid sample) were compared to those obtained from *ab initio* and semiempirical calculations. However, in this study, the nature of the vibrational modes has not been described, since only vibrational modes involving the C=S group have been shortly discussed. Similarly, Steer and Sinha have presented a brief vibrational analysis of benzopyranthione (BPT) [2]. Somogyi and co-authors have analysed the infrared spectrum of pyranthione (PT) in the ground state by using *ab initio* calculations in order to determine an assignment for all the fundamental frequencies [3]. The vibrationally resolved emission excitation spectra of thioketones in the excited triplet T_1 or singlet S_2 states using a molecular supersonic jet have been recorded for XT, BPT and PT [2, 4 - 7]. However, the nature of the observed vibrational frequencies of the emission excitation spectra have been poorly described. Similarly, $S_0 \rightarrow T_1$ absorption spectrum of jet-cooled BPT and PT using cavity ring-down spectroscopy has been featured [8, 9]. Recently, Brint and co-authors have reported the phosphorescence excitation spectrum of jet-cooled XT in the strongly overlapping $S_0 \rightarrow T_1$ and $S_0 \rightarrow S_1$ absorption region [10]. 20 fundamental frequencies have been determined in the 14920 - 17600 cm^{-1} spectral range of the $S_0 \rightarrow T_1(n,\pi^*)$ absorption. The observed phosphorescence excitation spectrum has been considered to be dominated by a large activity of the C=S group. In this study, the authors have also calculated vibrational modes of the ground state of XT (Hartee-Fock level). The results have been found to be similar to those reported by Steer [1]. The BPT vibrational spectrum has also been discussed. Its phosphorescence excitation spectrum contains less vibrational modes than PT or XT, despite the lower symmetry (C_S) of BPT compared to that of PT or XT (C_{2v}). To explain this observation, the authors have proposed that due to the lower symmetry of BPT, the C=S motion is distributed across many modes, and thus the number of modes with sufficient C=S activity to be observed in the spectrum is reduced [10].

The lack of exhaustive vibrational analysis of thioketones in the excited triplet and singlet states in the literature motivated us to perform Raman measurements supported by *ab initio* calculations. BPT and XT were initially chosen as thioketone model compounds. Unfortunately, it was impossible to detect any transient resonance Raman signal for the excited S_2 or T_1 states, due to the low extinction coefficients values of triplet-triplet ($\varepsilon_{T1}^{max} \approx$

1800 $M^{-1}cm^{-1}$) and singlet-singlet ($\varepsilon_{S2}^{max} \approx 3000\ M^{-1}cm^{-1}$) absorption as well as because of the presence of strong fluorescence ($S_2 \rightarrow S_0$) and phosphorescence ($T_1 \rightarrow S_0$) emissions. Consequently, another aromatic thioketone was chosen for the Raman studies, the thiocoumarin (TC, isomer of BPT, see structure in Fig.1.1), which exhibits very weak fluorescence and phosphorescence emissions [11]. The S_2 state lifetime of TC measured by using the up-conversion fluorescence technique in n-hexane (0.45 ± 0.05 ps) and in acetonitrile (0.13 ± 0.05 ps) are too short to allow us to investigate this state by picosecond Raman spectroscopy (3 ps time resolution for the LASIR set-up). We thus focussed our resonance Raman investigation on the first excited triplet state T_1 of TC, which is characterised by a large extinction coefficient for triplet-triplet absorption ($\varepsilon_{T1}^{max} = 14000\ M^{-1}cm^{-1}$).

This chapter presents the first resonance Raman study of the lowest excited triplet state of TC in n-hexane. For the sake of comparison, the ground state Raman spectrum of TC is also presented and analysed. These experimental results are supported by the Density Functional Theory (DFT) calculations for the ground state and Hartree-Fock Configuration Interaction Singles (HF CIS) calculations for the triplet state.

5.2. Characterisation of the T_1 state of thiocoumarin by transient absorption and time-resolved resonance Raman spectroscopies.

The $S_0 \rightarrow S_2(\pi,\pi^*)$ transition of TC lies in the 313 - 435 nm spectral range. The excited singlet $S_2(\pi,\pi^*)$ state exhibits weak $S_2 \rightarrow S_0$ fluorescence with a quantum yield of 6×10^{-5} [11]. Weak phosphorescence from the $T_1(\pi,\pi^*)$ state in n-hexane has also been reported [11]. In order to record the resonance Raman spectrum of the TC triplet T_1 state in n-hexane, the probe wavelength must be set in resonance with a strong $T_1 \rightarrow T_n$ electronic transition. Firstly, we investigated first the absorption spectrum of TC in the triplet T_1 state. For this purpose, the triplet T_1 state was populated via fast $S_2 \rightarrow S_1$ internal conversion and $S_1 \rightarrow T_1$ intersystem crossing processes, with a quantum yield of 1 [12], following excitation to the S_2 state using 355 nm. Fig.5.1 presents the time evolution of the absorption spectra recorded in the 320 - 670 nm spectral range. The spectra are characterised by a negative band between 320 - 420 nm and a positive band in the 420 - 670 nm region. The signal in the 320 - 420 nm spectral range is related to the ground state depletion signal since its spectral position corresponds to that of the $S_0 \rightarrow S_2$ absorption band of TC. The decay kinetics of both the

negative and positive bands can be fitted with a single exponential function (about 510 ns, see the inset in Fig.5.1) indicating the presence of a single species in the solution. These bands are both sensitive to the presence of oxygen in the solution. We thus assigned the band in the 420 - 670 nm region to be the transient absorption ($T_1 \rightarrow T_n$) of TC in n-hexane. As a confirmation, its shape is similar to that reported for the TC triplet T_1 absorption spectrum in benzene [12]. Note that a slight difference exists between the spectral shape of the ground state depletion signal (see Fig.5.1) and that of the ground state absorption from Fig.1 in ref. [11]. This suggests that the ground state depletion band can be slightly perturbed by the superimposed triplet state absorption band. Assuming, a triplet quantum yield of 1, the comparison of the absorbance variation between the ground state depletion signal at 370 nm and the triplet state absorption signal at 470 nm provides a lower limit value of $\varepsilon_{T1}^{max} = 14000\ M^{-1}cm^{-1}$ for the triplet-triplet absorption coefficient. The comparison with the results obtained for the BPT triplet T_1 state with the same experimental conditions (laser pulse energy, sample absorption,...) highly supports this relatively high ε_{T1}^{max} value.

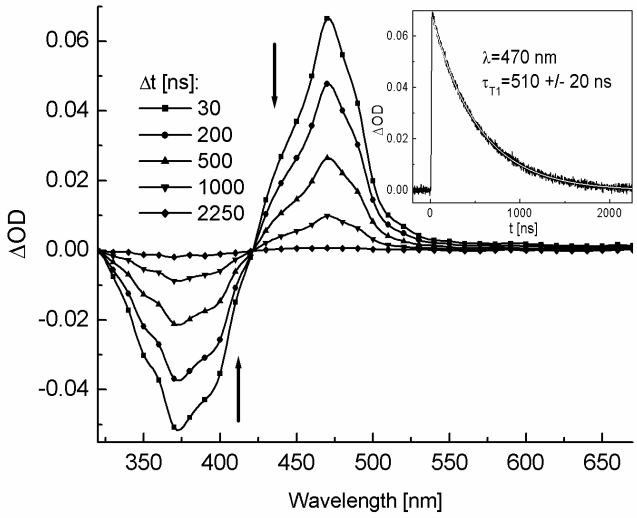

Figure 5.1. Transient absorption spectra of a deoxygenated solution of TC (0.9×10^{-4} M) in n-hexane excited at 355 nm with an energy of 0.8 mJ per pulse. Inset: transient absorption decay recorded at 470 nm, the solid white line presents the best single exponential fit to the experimental data.

The same pump excitation wavelength (355 nm) was used to record the nanosecond time-resolved resonance Raman spectra of the T_1 state of TC in n-hexane. The probe beam was tuned to 465 nm (outside the strong $S_0 \rightarrow S_2$ absorption band), near the absorption maximum of the $T_1 \rightarrow T_n$ absorption band to ensure strong resonance effects for the T_1 triplet

state Raman spectrum. The resonance Raman spectrum recorded in n-hexane in the 1650 - 200 cm^{-1} spectral range at a time delay of 20 ns is presented in Fig.5.2b. The spectrum shows many vibrational bands, the most intense are situated at 1541, 1509 and 1026 cm^{-1}. The time-dependent Raman spectra intensity changes were also measured. Consistently with what was observed by transient absorption spectroscopy, the Raman lines of the spectrum presented in Fig.5.2b originate from a single intermediate species since they all decay with the same kinetics. Moreover, this kinetics was found to be sensitive to the presence of oxygen in the solution. We can thus attribute the Raman spectrum in Fig.5.2b to the TC triplet T_1 state resonance Raman spectrum. Very similar resonance Raman spectra were obtained for solutions of TC in methanol and acetonitrile.

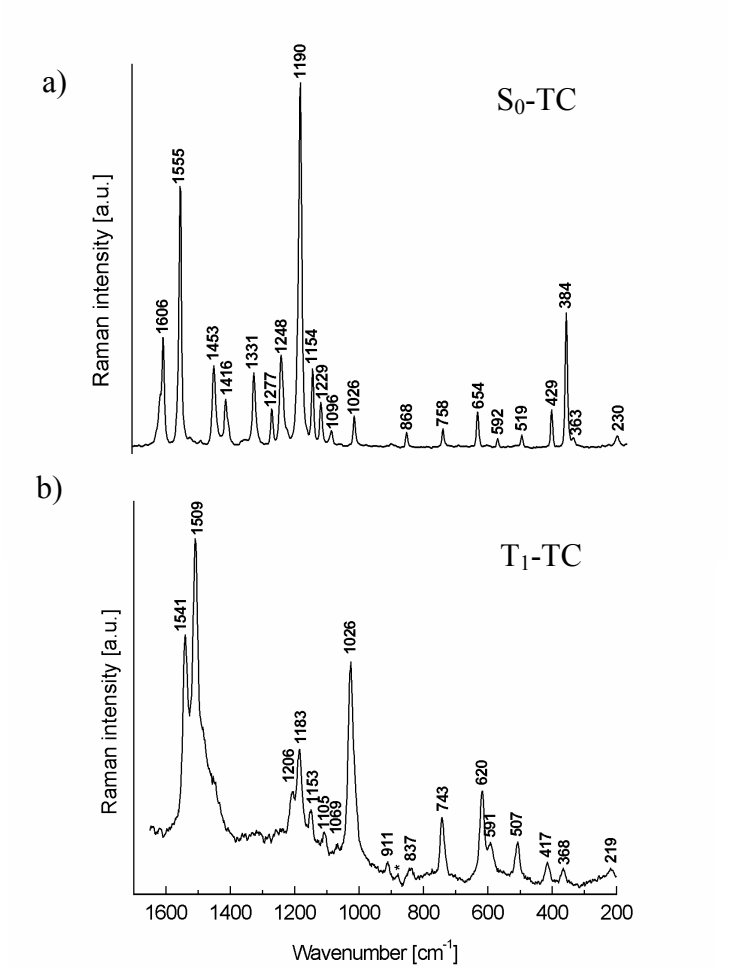

Figure 5.2. (a) Raman spectrum of S_0 thiocoumarin (1×10^{-1} M) in acetonitrile (solvent bands subtracted). (b) Transient resonance Raman spectra of the TC T_1 state in n-hexane recorded with 355 nm (1 mJ) pump pulses and 465 nm (1 mJ) probe pulses. The pump-probe delay was 20 ns. TC n-hexane solution (0.5×10^{-3} M) was deoxygenated. (*) due to subtraction of solvent bands.

The steady-state Raman spectrum recorded for TC in acetonitrile is presented in Fig.5.2a, which can be compared with that of the TC triplet T_1 Raman spectrum. These steady-state measurements were carried out using near IR FT-Raman spectrometry (*Bruker IFS 88* instrument). Vibrational assignments of the ground S_0 and triplet T_1 states Raman spectra were made on the basis of *ab inito* calculations (DFT and CIS).

5.3. *Ab initio* calculations of the structure of thiocoumarin in the ground state and in the first excited triplet state.

All structure calculations were performed with the Gaussian 98 program [13]. The ground state geometry of TC was optimised using the density functional theory (B3LYP) approach with the 6-31G* basis set [14]. It was also optimised at the Hartree–Fock (HF) level with the same basis set used as a starting point for the excited-state calculations. Configuration interaction singles (CIS) calculations were carried out in order to identify the molecular orbitals involved in the transition from the ground state to the lowest excited triplet state and also to optimise the geometry of this excited state. The optimised geometric parameters (bond lengths and angles), for the ground state S_0 and triplet state T_1 of TC were calculated by the mentioned methods and are listed in Table 5.1. The corresponding atom numbering corresponds to that given in Fig.5.3. Although some discrepancies are observed between the ground state structure of TC calculated using DFT and HF methods, the main geometric parameters of the optimised structure are similar. Consequently, in the following discussion, we will compare the geometric parameters of the triplet T_1 and ground S_0 states at the CIS and HF levels, respectively, because these results are obtained with the same calculation methodology.

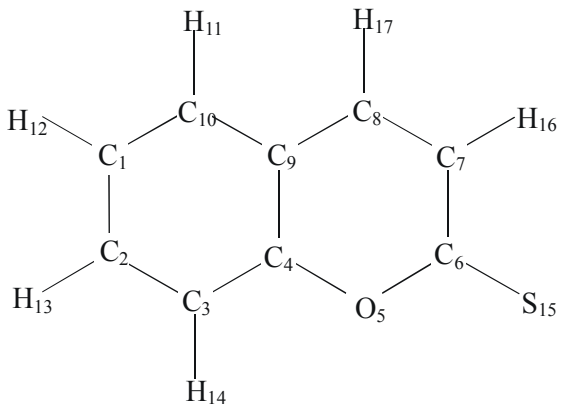

Figure 5.3. Thiocoumarin atom numbering.

The ground state of TC is characterised by a planar structure as attested by the values of the dihedral angles. This planar structure is consistent with the geometry obtained from a single crystal X ray study [15]. We can also notice for TC in the ground state, that the C-S and C_7-C_8 bonds possess a notable double bond character. In the case of T_1 state structure of TC, some important points can be underlined (see Fig.5.4):

- The molecule is planar according to the values of the dihedral angles listed in Table 5.1.
- The benzo moiety is only slightly modified (only a weak C_4-C_9 bond length variation) and keeps its aromatic character.
- Stronger distortions arise in the pyranthione moiety. The C_8-C_7 bond acquires a notable single bond character in the T_1 state because its length is increased by about 0.09 Å on going from the S_0 to the T_1 state. On the contrary, the C_7-C_6 bond length is decreased by about 0.06 Å. This confers a marked double bond character to this bond. A concomitant modification of about 3 degrees of the $C_6O_5C_4$, $C_7C_6O_5$ and $C_9C_8C_7$ angle values is also observed.
- The C=S double bond character is kept nearly unchanged upon photoexcitation to the triplet T_1 state (change by only 0.02 Å).

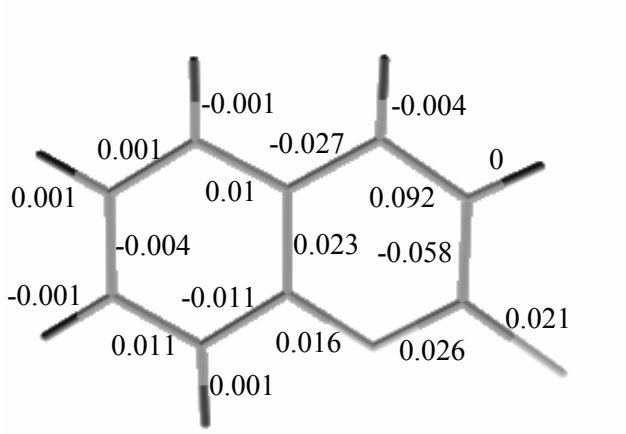

Figure 5.4. Changes of the bond lengths (in angstroms) resulting from the thiocoumarin $S_0 \rightarrow T_1$ transition. The corresponding optimised geometries have been calculated at the HF level for the ground state and at the CIS level for the triplet state.

Table 5.1. Optimised geometrical parameters of S_0 (DFT and HF) and T_1 (CIS) states of TC.

Geometrical parameters	S_0-TC B3LYP/6-31G*	S_0-TC HF/6-31G*	T_1-TC CIS/6-31G*
Bond lengths [Å]			
C1C10	1.388	1.375	1.376
C2C1	1.404	1.396	1.392
C3C2	1.391	1.378	1.389
C4C3	1.395	1.387	1.376
O5C4	1.368	1.354	1.370
C6O5	1.373	1.333	1.359
C7C6	1.444	1.451	1.393
C8C7	1.358	1.336	1.428
C9C8	1.438	1.447	1.420
C9C4	1.408	1.386	1.409
C10C9	1.408	1.398	1.408
H11C10	1.087	1.076	1.075
H12C1	1.086	1.074	1.075
H13C2	1.086	1.075	1.074
H14C3	1.085	1.073	1.074
S15C6	1.651	1.637	1.658
H16C7	1.083	1.071	1.071
H17C8	1.087	1.075	1.071
Bond angles [deg]			
C3C2C1	120.8	120.9	120.0
C4C3C2	118.8	118.6	119.7
O5C4C3	117.1	117.3	116.6
C6O5C4	123.0	124.2	121.0
C7C6O5	116.5	116.6	119.7
C8C7C6	121.8	121.0	121.6
C9C8C7	120.4	120.5	117.2
C10C9C8	124.6	124.6	123.9
H11C10C9	118.9	119.2	118.5
H12C1C2	120.0	120.0	120.0
H13C2C3	119.4	119.4	119.7
H14C3C4	119.1	119.3	118.9
S15C6C7	125.1	124.1	122.6
H16C7C8	121.9	122.5	121.1
H17C8C9	119.0	119.0	121.7
Dihedral angles [deg]			
C10C1C2H13	180.0	180.0	180.0
H12C1C2C3	180.0	180.0	180.0
H13C2C3H14	0.0	0.0	0.0
C2C3C4O5	180.0	180.0	180.0
C3C4C9C8	180.0	180.0	180.0
C4O5C6S15	180.0	180.0	180.0
O5C6C7C8	0.0	0.0	0.0
H16C7C8H17	0.0	0.0	0.0
C4C9C10H11	180.0	180.0	180.0

The last point implies that the T_1 state has pure $\pi\pi^*$ character, since a notably weaker C-S bond (almost a single bond) is expected in the case of an electron transition from a n to a π^* orbital. For instance, it has been observed that the C-O bond of benzophenone is considerably lengthened in the $T_1(n,\pi^*)$ triplet state [16]. Similarly, in the pyranthione T_1 state, which has $n\pi^*$ character, an increase of about 0.1 Å of the C-S bond length has been observed on going from the ground state to the triplet state [17]. We also determined the molecular orbitals that participate in the $S_0 \rightarrow T_1$ transition using the CIS method. It was found, that one pair of molecular orbitals has a predominant contribution while five other molecular orbital pairs partially participate (42→43 (81%), 39→44 (6%), 38→48 (4%), 39→43 (3%), 40→43 (3%), 42→45 (3%)). Fig.5.5 presents the two molecular orbitals that are dominantly involved in the $S_0 \rightarrow T_1$ transition. Fig.5.5 clearly shows the variation of bond order of the C_7-C_8 and C_7-C_6 bonds on going from the S_0 state to the T_1 state.

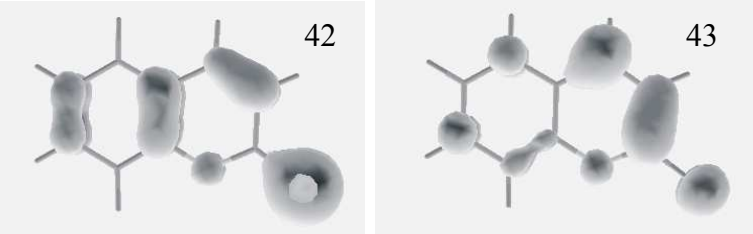

Figure 5.5. Orbitals 42 and 43 related to the ground and to the lowest excited triplet state of TC calculated by CIS method.

5.4. Vibrational assignments.

In order to validate the optimised structure of TC in the T_1 state and also to make a precise assignment of the Raman spectra of the ground state an triplet state of TC, we have calculated the vibrational frequencies from the potential energy surface of the optimised S_0 and T_1 states structure using Gaussian 98 program [13].

The calculated cartesian force constants, for the ground state and the triplet state of TC, were transformed into the force constants expressed in local symmetry coordinates for each vibration by using the REDONG program [18]. These nonredundant symmetry coordinates were defined in Table 5.2 as recommended by Pulay from the internal coordinates [19]. Note that Table 5.2 shows only the in-plane nonredundant coordinates, which are functions depending on the internal coordinates presented in Fig.5.6. The potential energy

distributions (PEDs) were calculated for each vibrational mode of thiocoumarin from the force constants expressed in local symmetry coordinates.

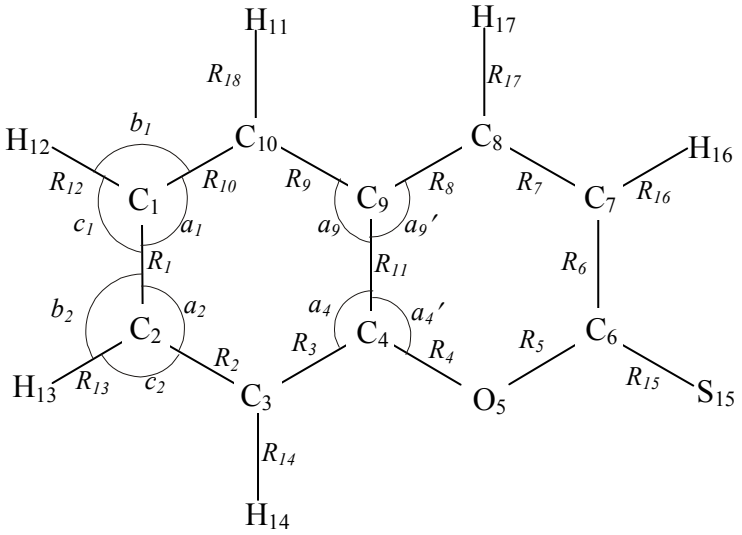

Figure 5.6. Internal coordinates of TC.

Table 5.2. Pulay in-plane internal coordinates of TC. The atomic numbering and the notations of internal coordinates are given in Fig.5.6.

Definition	Description
R_1, R_2, R_3, R_6, R_7, R_8, R_9, R_{10}, R_{11}	CC stretching
R_4, R_5	CO stretching
R_{12}, R_{13}, R_{14}, R_{16}, R_{17}, R_{18}	CH stretching
R_{15}	CS stretching
$\beta_6 = (1/\sqrt{2})(b_6 - c_6)$	CS in-plane bending
$\beta_i = (1/\sqrt{2})(b_i - c_i)$; i = 1, 2, 3, 7, 8, 10	CH in-plane bending
$S_{11} = a_1 - a_2 + a_3 - a_4 + a_9 - a_{10}$	Benzo moiety deformation
$S_{21} = a_5 - a_6 + a_7 - a_8 + a_9` - a_4`$	Pyranthione deformation
$S_{12} = 2a_1 - a_2 - a_3 + 2a_4 - a_9 - a_{10}$	Benzo moiety deformation
$S_{22} = 2a_5 - a_6 - a_7 + 2a_8 - a_9` - a_4`$	Pyranthione deformation
$S_{13} = a_2 - a_3 + a_9 - a_{10}$	Benzo moiety deformation
$S_{23} = a_6 - a_7 + a_9` - a_4`$	Pyranthione deformation

The 45 internal modes of vibration of TC are distributed between 31 in-plane modes and 14 out-of-plane modes. It was mentioned, that the experimental Raman spectra of the triplet state were obtained in resonance with a strongly allowed electronic transition. In this case, only the totally symmetric modes are expected to be active in the resonance Raman spectra. Since the only element symmetry of the molecule is the molecular plane, the totally symmetric modes compose all the in-plane vibrations. Accordingly, it was decided to only take into consideration these in-plane modes in the following discussion. The 6 C-H stretching in-plane vibrations, lying above 3000 cm^{-1}, are not expected to provide important information about the molecular structure. They are thus also excluded from the discussion. The vibrational analysis of the ground and triplet states of TC is thus restricted to the 25 in-plane modes expected in the 200 - 1650 cm^{-1} spectral range.

The ground state vibrational frequencies were calculated using the geometries obtained from HF and DFT calculations. However, frequencies calculated by DFT were found to be closer to the experimental frequencies than the HF ones. In consequence, we will only consider the former one in the rest of this discussion of the S_0 of TC.

The calculated frequency values were corrected by scaling factors of 0.98 (DFT-B3LYP) and 0.91 (CIS) for the S_0 and T_1 of TC respectively, which are comparable to those usually encountered for this type of molecule. For both states Table 5.3 represents the calculated and the experimental vibrational frequencies. A very good agreement is found between the computed values and the experimental frequencies. The root-mean square deviation values are 11 cm^{-1} and 10 cm^{-1}, for S_0 and T_1 states of TC, respectively. This definitively validates the calculated structures of TC in the S_0 and T_1 states. A description of vibrations by means of the potential energy distributions (PED) is shown in Table 5.3. To complete the description of all the totally symmetric modes of TC in the ground and triplet states, a graphical representation of the vibrations is also given (Fig.5.7 and 5.8). A high consistency between the observed and calculated vibrations can be seen in Table 5.3, an unambiguous assignment of the observed vibrational modes can be proposed. Many vibrational modes are common in both S_0 and T_1 states, but the frequencies are generally lower in the T_1 state than in the S_0 state. In particular, in the 200 - 1050 cm^{-1} spectral range, all the vibrational modes of the ground state of TC can be directly correlated to vibrational modes of T_1 state of TC. In the 1050 - 1650 cm^{-1} spectral range, some correspondences are also established, but most of the vibrations undergo a significant redistribution of the potential energy on going from S_0 to T_1.

Table 5.3. Observed and calculated frequencies of the totally symmetric modes of thiocoumarin in the ground S_0 and triplet T_1 states and Potential Energy Distributions (PED) [a]. The S_0 and T_1 states of TC were calculated by DFT-B3LYP/6-31G* and CIS/6-31G* methods respectively. Corresponding modes between the triplet and ground state are marked by (→).

S_0-TC			Related to:	T_1-TC		
Exp [cm^{-1}]	DFT	PED(%)[b]		Exp [cm^{-1}]	CIS	PED(%)[b]
230	224	β_6(66)	→	219	221	β_6(70)
384	380	R_{15}(20), S_{22}(14), S_{23}(42)	→	368	369	R_{15}(14), S_{22}(17), S_{23}(39)
429	426	β_6(44), S_{12}(15), S_{22}(12)	→	417	421	β_6(41), S_{12}(13), S_{22}(15)
519	517	S_{12}(37), S_{23}(28)	→	507	505	R_8(10), S_{12}(34), S_{23}(28)
592	594	S_{13}(43), S_{22}(34)	→	591	590	S_{13}(45), S_{22}(33)
654	652	R_6(11), R_{15}(26), S_{12}(11), S_{21}(20), S_{22}(11)	→	620	643	R_{15}(30), S_{12}(10), S_{21}(18), S_{22}(10)
758	756	R_8(15), R_9(11), R_{11}(19)	→	743	741	R_4(12), R_9(12), R_{11}(24)
868	865	R_4(10), R_{15}(11), S_{11}(43)	→	837	842	R_8(13), R_{15}(14), S_{11}(33), S_{12}(12)
	904	R_5(24), S_{21}(35)	→	911	899	R_5(25), R_7(10), S_{21}(36)
					958	R_6(15), R_7(43), β_8(11)
1026	1035	R_1(40), R_2(13), R_{10}(11), β_3(17), β_{10}(10)	→	1026	1019	R_1(40), R_2(14), β_3(15)
1096	1091	R_5(26), R_{15}(11), β_7(16), β_8(10), S_{11}(13)		1069	1082	R_1(21), R_2(22), R_3(13), R_9(10), R_{10}(12)
1129	1131	β_2(19), β_3(14)	→	1105	1103	R_{10}(17), β_1(12), S_{11}(19)
1154	1165	β_1(37), β_2(14), β_{10}(18)		1153	1161	R_{15}(22), β_7(16), β_{10}(16)
1190	1200	R_6(23), R_{15}(23), β_8(11)				
	1205	R_4(11), R_5(17), R_{15}(16), β_8(14)				
	1239	R_8(16), R_9(11), β_7(18), β_{10}(10)	→	1183	1174	R_8(24), R_9(13), β_8(13)
				1206	1205	R_{11}(10), β_1(20), β_2(24), β_3(10)
1248	1254	R_4(20), R_6(12), R_8(12), β_8(13), S_{11}(15)	→		1229	R_4(35), S_{11}(14)
1277	1281	β_2(11), β_3(26), β_{10}(26), S_{21}(12)	→		1281	β_2(10), β_3(24), β_{10}(15), S_{21}(13)
1331	1355	R_1(13), R_2(16), R_3(12), R_9(12), R_{10}(17), R_{11}(15)			1300	R_5(24), β_7(22)
1416	1429	R_6(11), β_7(23), β_8(22), β_1(14)	→		1392	R_8(19), β_7(18), β_8(46)
1453	1467	R_{10}(10), β_2(20), β_3(13)	↗↘		1451	R_9(10), β_1(26), β_{10}(27)
	1506	R_8(13), β_1(17), β_3(13), β_{10}(13)		1509	1484	R_{10}(13), R_{11}(10), β_2(16), β_3(18), β_{10}(15)
1555	1575	R_1(15), R_2(11), R_7(22), β_2(15)		1541	1553	R_6(29), R_7(19), β_7(20)
1606	1631	R_7(26), R_9(12), β_8(10)			1576	R_1(20), R_3(19), β_1(14)
	1635	R_3(17), R_{10}(21)			1585	R_2(17), R_9(12), R_{10}(13)

[a] Only in-plane vibrations are shown. [b] Values less than 10% are neglected.

The C=S stretching coordinate is distributed over many modes, in both the S_0 (380, 652, 865, 1091, 1200 cm^{-1}) and T_1 (369, 643, 842, 1161 cm^{-1}) states with contributions lower than 30 %. Note that in the triplet state, the C=S stretching motion contributes to slightly lower the frequency modes compared to that for the ground state of TC. This is consistent with the slightly longer C=S bond length of the TC T_1 state compared to that of the TC ground state (see Table 5.2). Considerations on the geometrical properties of TC led us to conclude that the

transition from the ground state to the triplet state results in: an increase of the C_7-C_8 bond length (single-bond character) and a decrease of the C_7-C_6 bond length (double-bond character). The Raman analysis supports this conclusion.

The most important contribution of the R_7 internal coordinate (corresponding to the C_7-C_8 bond) is for the 1631 cm^{-1} vibrational mode of the S_0 state (26 %) and for the 1553 cm^{-1} vibrational mode of the T_1 state (19 %). In parallel, the most important contribution of the R_6 internal coordinate (corresponding to the C_7-C_6 bond) is for the 1429 cm^{-1} vibrational mode of the S_0 state (11 %) and for the 1553 cm^{-1} vibrational mode of the T_1 state (29 %). This clearly reflects a lowering of the π electron density on the C_7-C_8 bond which is concomitant with an increase in the π density on the C_7-C_6 bond on going from the ground state to the triplet state of TC. Such observations are in agreement with the change in the electronic distribution shown in Fig.5.5.

It is worth noting that similar conclusions have been proposed for the keto-analogue coumarin (CM) [20]. An assignment of the coumarin triplet state Raman spectrum has been proposed on the basis of the frequency shifts observed upon isotopic (^{10}O, ^{13}C, deuterium) substitution [20]. A $\pi\pi^*$ character has been also reported for the T_1 triplet state of CM. The C_7-C_8 bond of the CM T_1 state has been found to be drastically lengthened and the C_9-C_8 and C_7-C_6 bonds shortened compared to that for the ground state of CM.

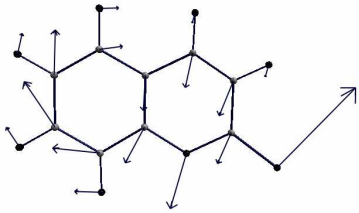

224 cm^{-1}

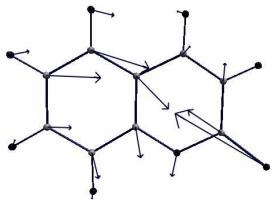

380 cm^{-1}

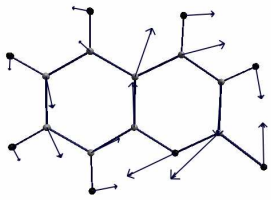

426 cm^{-1}

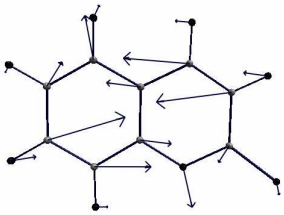

517 cm^{-1}

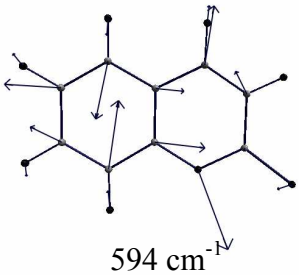

594 cm^{-1}

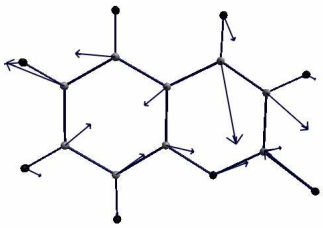

652 cm^{-1}

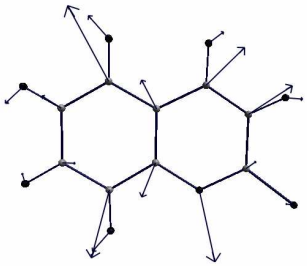

756 cm^{-1}

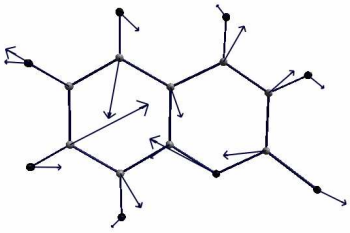

865 cm^{-1}

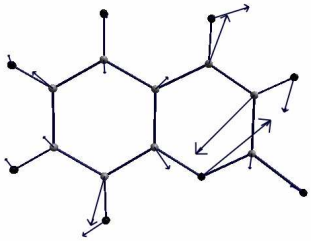

904 cm^{-1}

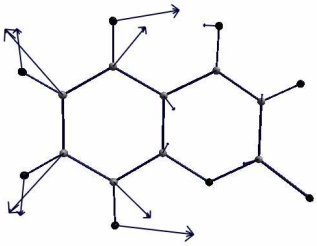

1035 cm^{-1}

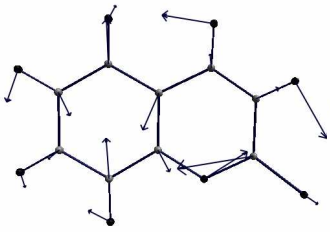

1091 cm^{-1}

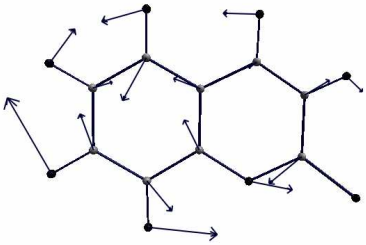

1131 cm^{-1}

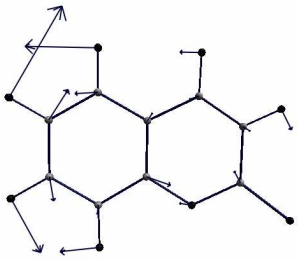

1165 cm^{-1}

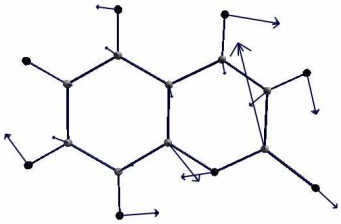

1200 cm^{-1}

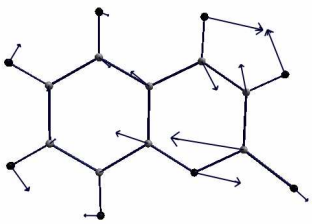

1205 cm^{-1}

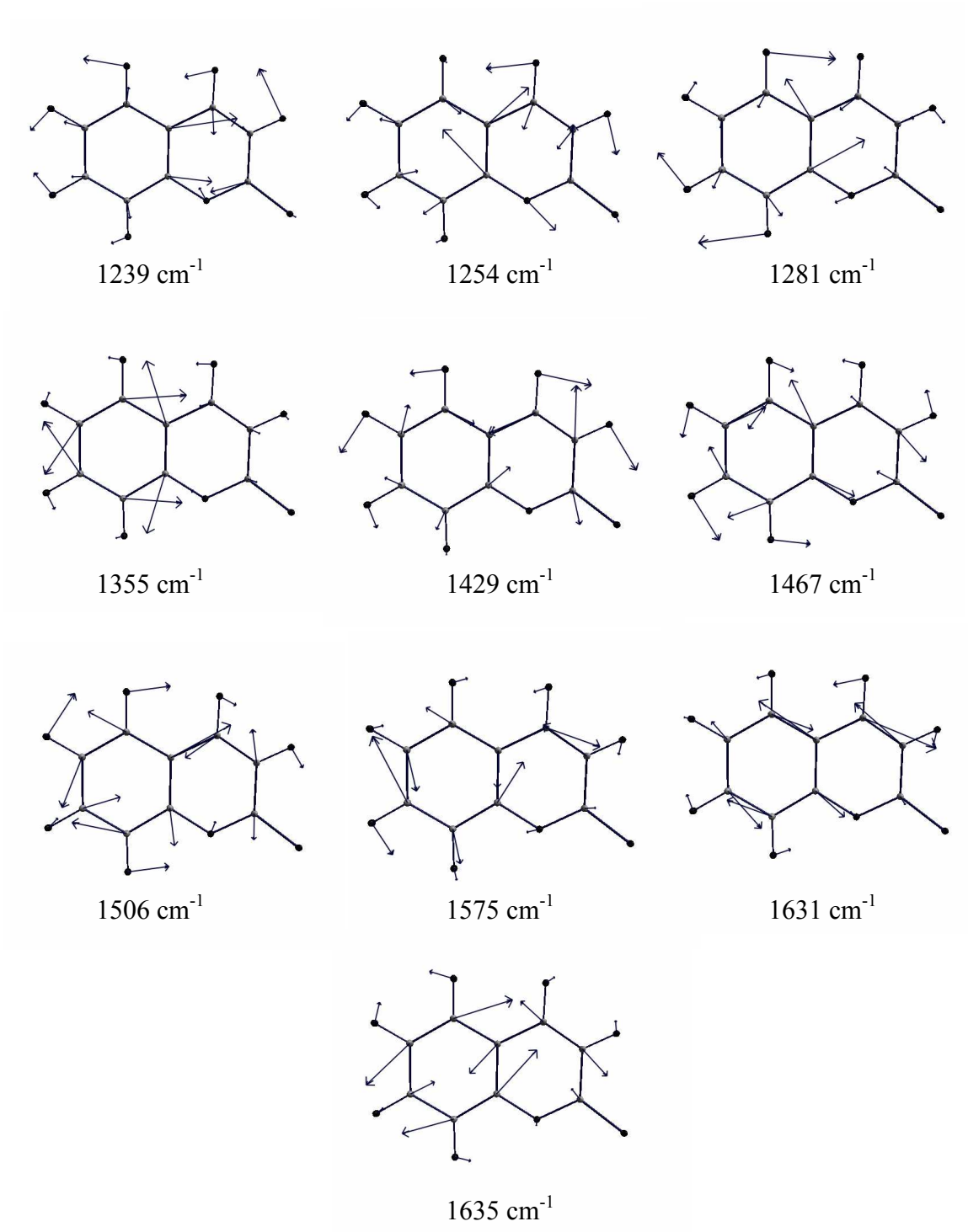

Figure. 5.7. Schematic representation of the totally symmetric modes of thiocoumarin in the ground state.

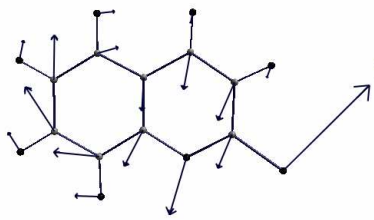

221 cm^{-1}

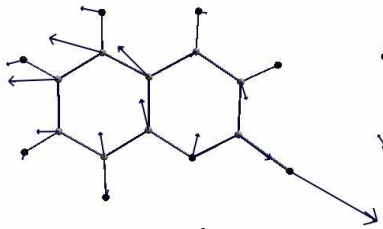

369 cm^{-1}

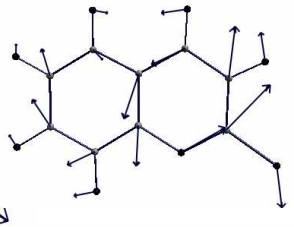

421 cm^{-1}

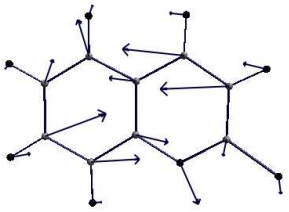

505 cm^{-1}

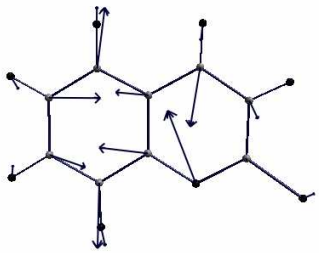

590 cm^{-1}

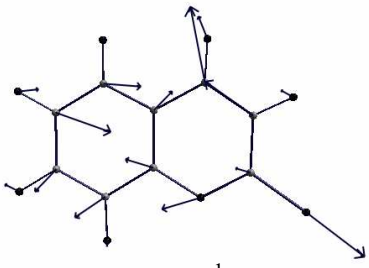

643 cm^{-1}

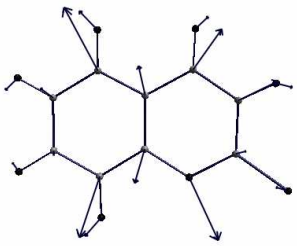

741 cm^{-1}

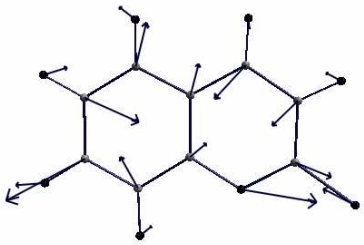

842 cm^{-1}

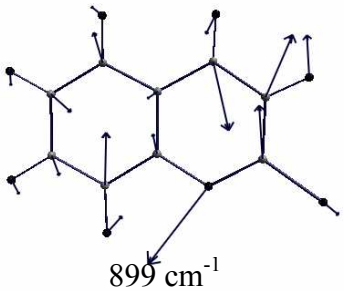

899 cm^{-1}

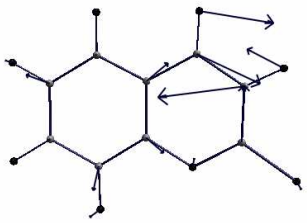

958 cm^{-1}

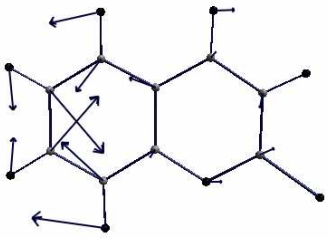

1019 cm^{-1}

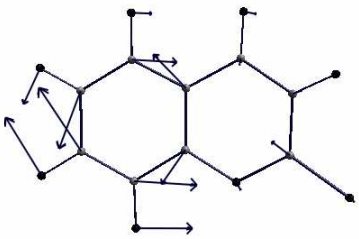

1082 cm^{-1}

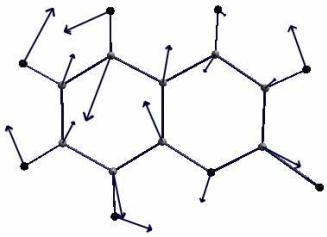

1103 cm^{-1}

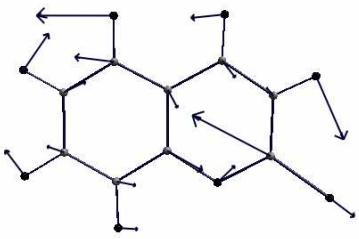

1161 cm^{-1}

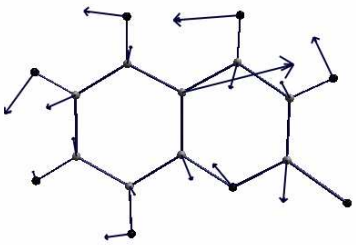

1174 cm^{-1}

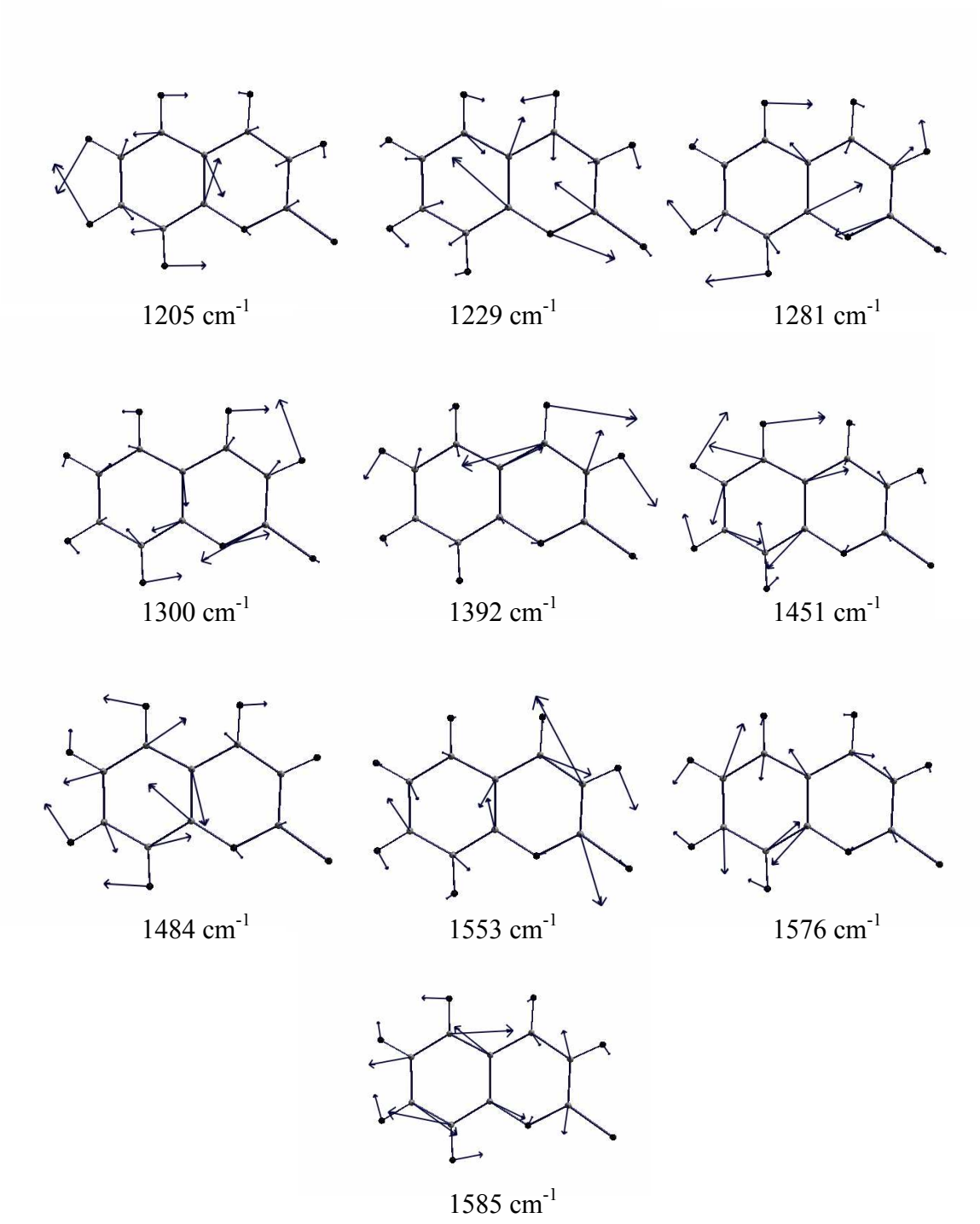

Figure 5.8. Schematic representation of the totally symmetric modes of thiocoumarin in the triplet $T_1(\pi,\pi^*)$ state.

5.5. References.

1. H. K. Sinha, L. Chantranupong, R. P. Steer, *J. Mol. Spectrosc.*, 169 (1995) 302.
2. H. K. Sinha, R. P. Steer, *J. Mol. Spectrosc.*, 181 (1997) 194.
3. Á. Somogyi, G. Jalsovszky, C. Fulop, J. Stark, J. E. Boggs, *Spectrochim. Acta*, 45A (1989) 679.
4. A. A. Ruth, F. J. O'Keeffe, M. W. D. Mansfield, R. P. Brint, *J. Phys. Chem. A*, 101 (1997) 7735.
5. A. A. Ruth, F. J. O'Keeffe, R. P. Brint, M. W. D. Mansfield, *Chem. Phys.*, 217 (1997) 83.
6. A. A. Ruth, F. J. O'Keeffe, M. W. D. Mansfield, R. P. Brint, *Chem. Phys. Lett.*, 264 (1997) 605.
7. A. A. Ruth, W. G. Doherty, R. P. Brint, *Chem. Phys. Lett.*, 352 (2002) 191.
8. A. A. Ruth, T. Fernholz, R. P. Brint, M. W. D. Mansfield, *Chem. Phys. Lett.*, 287 (1998) 403.
9. A. A. Ruth, T. Fernholz, R. P. Brint, M. W. D. Mansfield, *J. Mol. Spectrosc*., 214 (2002) 80.
10. R. P. Brint, W. G. Doherty, A. A. Ruth, *J. Mol. Spectrosc.*, 216 (2002) 151.
11. M. Szymanski, A. Maciejewski, J. Kozlowski, J. Koput, *J. Phys. Chem. A*, 102 (1998) 677.
12. K. Bhattacharyya, P. K. Das, V. Ramamurthy, V. Pushkara Rao, *J. Chem. Soc., Faraday Trans. 2*, 82 (1986) 135.
13. M. J. Frisch, G. W. Trucks, H. B. Schlegel, G. E. Scuseria, M. A. Robb, J. R. Cheeseman, V. G. Zakrzewski, J. A. Montgomery, R. E. Stratmann, J. C. Burant, S. Dapprich, J. M. Millam, A. D. Daniels, K. N. Kudin, M. C. Strain, O. Farkas, J. Tomasi, V. Barone, M. Cossi, R. Cammi, B. Mennucci, C. Pomelli, C. Adamo, S. Clifford, J. Ochterski, G. A. Petersson, P. Y. Ayala, Q. Cui, K. Morokuma, D. K. Malick, A. D. Rabuck, K. Raghavachari, J. B. Foresman, J. Cioslowski, J. V. Ortiz, A. G. Baboul, B. B. Stefanov, G. Liu, A. Liashenko, P. Piskorz, I. Komaromi, R. Gomperts, R. L. Martin, D. J. Fox, T. Keith, M. A. Al-Laham, C. Y. Peng, A. Nanayakkara, M. Challacombe, P. M. W. Gill, B. Johnson, W. Chen, M. W. Wong, J. L. Andres, C. Gonzalez, M. Head-Gordon, E. S. Replogle and J. A. Pople, *GAUSSIAN 98*, Revision A.9, Gaussian, Inc., Pittsburgh, PA, 1998.
14. B. Miehlich, A. Savin, H. Stoll and H. Preuss, *Chem. Phys. Lett.*, 157 (1989) 200.

15. P. Munshi, T. N. Guru Row, *Acta Cryst.*, E57 (2001) 1175.
16. T. Tahara, H. Hamaguchi, M. Tasumi, *J. Phys. Chem.*, *91* (1987) 5875.
17. J. Tatchen, M. Waletzke, C. M. Marian S. Grimme, *Chem. Phys*., 264 (2001) 245.
18. A. Allouch, REDONG (QCPEG28).
19. P. Pulay, G. Fogarasi, F. Pang and J. E. Boggs., *J. Am. Chem. Soc.*, 101 (1979) 2550.
20. Y. Uesugi, M. Mizuno, A. Shimojima, H. Takashi, *J. Phys. Chem. A*, 101 (1997) 268.

CONCLUSIONS AND PERSPECTIVES.

In this investigation, the photophysical properties of benzopyranthione (BPT) have been examined by transient absorption and emission spectroscopies in various solvents such as hydrocarbons, acetonitrile and water. In addition, the first excited triplet state of thiocoumarin (TC) has been studied by transient absorption and resonance Raman scattering in n-hexane. The new information obtained during this thesis is summarised below.

S_2 state.

The S_2 state of BPT has been characterised by both transient absorption and emission spectroscopies. The $S_2 \rightarrow S_0$ fluorescence decay has been monitored at different wavelengths within the emission band. The S_2 state lifetime has been determined in acetonitrile (15 ps), in hydrocarbons (13.0 ps in cyclohexane) and in H_2O (1.0 ps). The absorption spectrum of the S_2 state of BPT has been obtained for the first time. Its assignment has been made by comparison with the dynamics with that of $S_2 \rightarrow S_0$ fluorescence (including that of stimulated emission). It is characterised by a broad band located in the 560 - 750 nm spectral range with a maximal extinction coefficient ε_{S2}^{max} of 3400 $M^{-1}cm^{-1}$ at 630 nm. The BPT S_2 state vibrational relaxation and orientational anisotropy decay have also been studied. In n-hexane, the intramolecular vibrational redistribution process has been found to be very fast (less than 150 fs), while the vibrational cooling process is characterised by a 2.5 ps time constant irrespective of the excess of vibrational energy carried to the BPT S_2 state (1500 - 5000 cm^{-1}). The decay of orientational anisotropy has been observed for the first time for a molecule in the S_2 state. The anisotropy decay has been found to be monoexponential ($r(t)=r(t_0)exp(-t/\tau_{or})+C$) in different linear hydrocarbon solvents (n-hexane, n-heptane, n-octane, n-decane and n-dodecane) and in cyclohexane. The initial value $r(t_0)$ obtained for the anisotropy is located in the 0.29 to 0.35 range. The dependence of the rotational time-constant τ_{or} on the solvent viscosity has been approximated by a linear function with a slope of 2.6 ± 1 ps/cP. The rotation dynamics have been explained in terms of the Stokes-Einstein-Debye hydrodynamics theory for a slip condition assuming a symmetric oblate shape of BPT in the S_2 state.

S_1 state.

Since no spectral signature of the S_1 state has been found in all the investigated solvents by femtosecond transient absorption method, we have concluded that the

instantaneous concentration of BPT molecules in the S_1 state is very low due to its very short lifetime (not longer than 0.5 ps in water).

T_1 state.

The first excited triplet state T_1 of BPT has been observed by transient absorption spectroscopy. The triplet state absorption spectrum has been characterised by a main band situated in the 410 - 520 nm spectral region with maximal extinction coefficient ε_{T1}^{max} of 1600 $M^{-1}cm^{-1}$ at 470 nm. Weak characteristic absorption maxima have also been found at 580, 630 and 690 nm. In water and acetonitrile the absorption band has a different shape compared with that in hydrocarbons. This is possibly due to the fact that in polar solvents, the T_1 state is π,π^*, while in non-polar solvents the T_1 state is n,π^*. In the case of TC, a high ε_{T1}^{max} value of about 14000 $M^{-1}cm^{-1}$ at 470 nm has been estimated. Structural information on the TC T_1 state has been found by resonance Raman scattering measurements and *ab initio* calculations. Both S_0 and T_1 states have been found to be planar. The benzo moiety of the T_1 state is only slightly modified compared to the ground state and keeps its aromatic character. However, stronger distortions arise in the pyranthione moiety. A lowering of the π electron density on the C_7-C_8 bond, concomitant with an increase in the π density on the C_7-C_6 bond on going from the ground state to the triplet state has been found. The $\pi\pi^*$ character of the T_1 state has been confirmed. A good agreement has been found between the observed and calculated frequencies. The S_0 and T_1 states totally symmetric vibrational modes have been described in terms of Potential Energy Distributions. The C=S stretching coordinate is distributed over many modes, in both the S_0 (380, 652, 865, 1091, 1200 cm^{-1}) and T_1 (369, 643, 842, 1161 cm^{-1}) states with individual contributions lower than 30 %.

S_2 quenching process.

The mechanism of the BPT S_2 state quenching by the solvent has been investigated for hydrocarbons, acetonitrile and water. The quenching process leads to the BPT S_1 state followed by the intersystem crossing to the T_1 state. However, the nature of the reaction coordinate involved in the quenching reaction depends on the solvent.

In hydrocarbons, the reaction coordinate involves the S_2 state of BPT and a hydrogen atom donor (solvent molecule). Three observations support the idea of an intermolecular hydrogen atom abstraction quenching process: (1) a shortening by about one order of magnitude of the S_2 state lifetime of BPT in hydrocarbons relative to that in perfluorohydrocarbons, (2) a notable kinetic isotope effect on the rate of the quenching process upon deuteration of the hydrocarbon molecule (k_H/k_D=3.2), and (3) a dependence of

the S_2 state quenching rate constant on the mean energy of the hydrocarbon C-H bonds. The determined values of the quenching rate constants by the hydrogen atom on the primary and secondary carbon sites are of $k_H(I) = 1.8\times10^{10}\ s^{-1}$ and $k_H(II)= 6.4\times10^{10}\ s^{-1}$ respectively. We have found that, the growth of the triplet T_1 state absorption band parallels the decay of the S_2 state one. The failure to observe the expected radical products, has been explained either by assuming that an ultrafast back hydrogen transfer occurs within the solvent cage, or by considering that the reaction is aborted well before the hydrocarbon C-H bond is broken and the BPT-$H^{\bullet}$ bond formation is completed. In the latter case, we assume that a progress along the reaction pathway towards a conical intersection leading to the electronic deactivation of S_2 state to the S_1 state takes place.

In acetonitrile, two reaction coordinates have been tentatively proposed: an aborted formation of a S_2 state exciplex and an aborted hydrogen atom abstraction. These two quenching mechanisms have been taken into account in order to explain why as many as 78 % of BPT in the S_2 state are quenched by interaction with acetonitrile molecules and to rationalise a notable kinetic isotope effect upon deuteration of the acetonitrile molecule. As in hydrocarbons, the growth of the triplet state T_1 absorption band parallels the decay of the S_2 state. No intermediates between the S_2 and T_1 states have been observed.

In water, we have suggested that an aborted formation of a hydrogen-bonded complex between BPT S_2 state and water molecule may occur. A notable kinetic isotope effect has been observed upon deuteration of the water molecule, possibly due to the weaker hydrogen bond network of H_2O compared to D_2O and to the mass difference between H^+ and D^+.

We have shown within this thesis that the photophysical properties of thioketones are very sensitive to the environment. In this respect, in the future, we could use them as probes in micro-organised (micellar) solution studies. We believe that time-resolved measurements could provide real time information on the thioketone environment within a micelle containing a hydrophilic surface and a hydrophobic core (for instance, SDS, anionic sodium dodecylsulphate surfactant added to water). In the case of BPT, the low solubility in water compared to that in the micellar solution ensures that the BPT is located within the SDS micelle. Moreover, the small BPT molecular volume ensures that the micelle structure will not be distorted.

In this thesis, we have addressed the problem of the study of the S_2 state quenching process of thioketones as a function of the solvent properties. A possible complementary approach to this problem would be to study the mechanism and the dynamics of the intermolecular deactivation processes of the S_2 state for other aromatic thioketones exhibiting

different excited states energy levels (E_{S2} and S_2-S_1 energy gap), different electron density on the thiocarbonyl group, different positions of the C=S group in the molecule and different accessibility of this group to the solvent. It would be also very interesting to study the deactivation process of the S_2 state in inert perfluorohydrocarbon solvents with an addition of various concentrations of quencher molecules (hydrocarbons for instance). This investigation could provide information on the influence of the local solvation of the aromatic thioketone (first solvent shell) on the quenching process.

Finally, the study of the quenching mechanism of the S_2 state of aromatic thioketones could also be extended to other molecules that present a thiocarbonyl group for which the observation of a highly reactive S_2 state has already been reported (for instance thiouracil [1]).

1. K. Taras-Goslinska, G. Wenska, B. Skalski, A. Maciejewski, G. Burdzinski, J. Karolczak, *Photochem. Photobiol.*, 75 (2002) 448.